



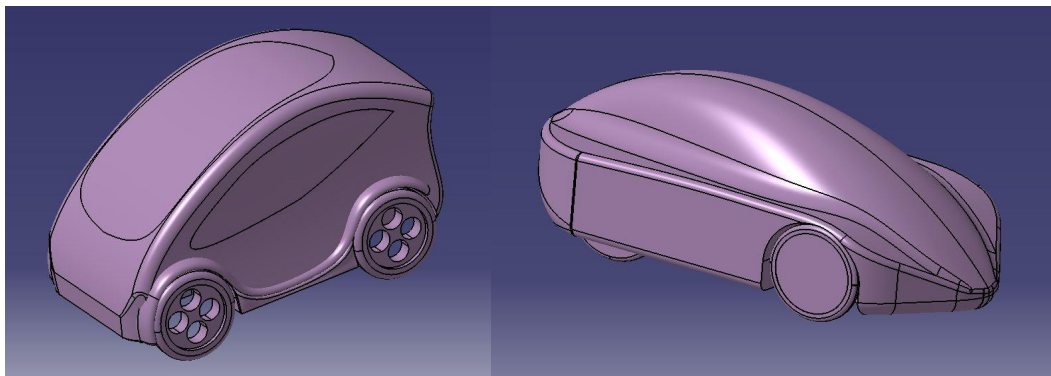
Technical University of Crete

Department of Production Engineering and Management

Conceptual and aerodynamic design of an urban vehicle

Thesis submitted in partial fulfillment of the requirements for the

Diploma Degree in Production Engineering & Management



by **TZANAKIS ATHANASIOS**

Supervised by: Dr. Ioannis K. Nikolos, Ass. Professor

Chania, GREECE, 2012

Abstract

The preliminary design of a vehicle, taking into account the majority of constraints, the usage and the type of the vehicle etc. and finally the shaping of a functional one is characterized as its conceptual design. The aim of this thesis is, firstly, to propose an alternative, environmentally friendly, urban vehicle and describe its conceptual design procedure. Following the trends of urban transportation and considering the necessity for less crude oil dependence, an extended range electrical vehicle is designed.

Secondly, the aerodynamic design and evaluation of a real racing vehicle, which participates to a fuel consumption competition is described in detail, in the second part of this thesis. In both procedures CATIA V5R19 and ANSYS-CFX v.11 were used for the geometric design and aerodynamic simulation respectively.

The extended-range electric vehicle is a new approach of an idea, which may be soon adopted by automotive industries due to its close relation with the current hybrid-car technology. On the other side, the aerodynamically-optimized racing vehicle proved its design goals by achieving the fourth place in the European Shell Eco Marathon 2012, the best ranking for the racing team of the Technical University of Crete ever achieved so far.

To Anna

Acknowledgements

First of all, I wish to express my thanks to my advisor, Ass. Prof. Ioannis K. Nikolos, for his guidance. He offered me his knowledge, enhancing and encouraging me to fight for the best, as much on studies as in life. Moreover, he provided me with countless suggestions and constructive criticism, which in many ways helped my work.

Many thanks to Prof. Tsourveloudis Nikolaos. He provided me with the opportunity to be a member of the "Technical University of Crete Eco Racing Team" (TUCer); with his advices he played decisive role to completing my present thesis.

I would like to thank the leader of TUCer Team, Spanoudakis Polychronis for his continuing support. Having a two years collaboration, he has broadened my horizons in the automotive world. I am really thankful to him as he trusted me to design the aerodynamic shape of the new vehicle of the team.

Finally, I am grateful so much to my family for supporting me (in many ways) for a long time.

Table of Contents

| | |
|--|-----|
| 1. Introduction..... | 14 |
| 1.1 Statement of work..... | 14 |
| 1.2 Introduction..... | 14 |
| Part A..... | 16 |
| 2. Social and economic factors in urban transportation | 17 |
| 2.1 Urbanization | 17 |
| 2.2 Urban transportation | 18 |
| 2.3 Current trends in urban transportation | 19 |
| 2.4 Vehicle miles traveled and vehicle occupancy | 20 |
| 2.5 Parking demands | 22 |
| 2.6 Trends in annual vehicle sales | 23 |
| 2.7 Future fuels and electric vehicles | 25 |
| 2.7.1 Future transport fuels | 25 |
| 2.7.2 Focus on road transportation..... | 25 |
| 2.7.3 Electrical vehicles ideally suited for urban areas | 29 |
| 2.7.4 Types of electric propulsion vehicles..... | 29 |
| 2.8 Environmental and noise impacts of ICE vehicles | 30 |
| 2.8.1 Greenhouse gas emissions in European Union | 30 |
| 2.8.2 Noise in urban areas..... | 31 |
| 2.8.3 Life-cycle analysis of new automobile technologies | 35 |
| 3. Extended Range Electrical Vehicle (EREV)..... | 42 |
| 3.1 Vehicle performance - Tractive effort | 422 |
| 3.2 Energy requirements..... | 45 |

| | | |
|-------|--|-----|
| 3.3 | Assumptions for modeling | 46 |
| 3.4 | Wheel hub/In-Wheel motor | 47 |
| 3.5 | Power inverter | 49 |
| 3.6 | Battery range and size | 49 |
| 3.7 | On-board battery charger | 50 |
| 3.8 | Engine/Generator size | 51 |
| 3.9 | Fuel tank | 53 |
| 3.10 | Wheelbase | 53 |
| 3.11 | Seat | 54 |
| 4. | Preliminary design of the proposed EREV | 55 |
| | Part B | 59 |
| 5. | Eco Racer Vehicle 2012..... | 60 |
| 5.1 | Methodology | 60 |
| 5.2 | ER11 analysis | 60 |
| 5.3 | Boundaries Conditions | 73 |
| 5.4 | Results | 79 |
| 5.5 | Design specifications | 86 |
| 5.5.1 | Rules | 86 |
| 5.5.2 | Vehicle Design | 86 |
| 5.5.3 | Visibility | 86 |
| 5.5.4 | Vehicle Access | 87 |
| 5.5.5 | Dimensions | 87 |
| 5.5.6 | Wheels..... | 87 |
| 6. | Design and CFD Simulation..... | 88 |
| 6.1 | TUCER ER12 1 st Model | 88 |
| 6.1.1 | Design | 88 |
| 6.1.2 | CFD Simulation Results for the 1st model | 95 |
| 6.2 | TUCER ER12 2 nd Model | 100 |

| | | |
|-------|--|-----|
| 6.2.1 | Design | 100 |
| 6.3 | TUCER ER12 3 rd Model..... | 104 |
| 6.3.1 | Design | 104 |
| 6.3.2 | CFD Simulation Results for the 3rd model | 107 |
| 6.4 | TUCER ER12 4th Model..... | 112 |
| 6.4.1 | Design | 112 |
| 6.4.2 | CFD Simulation Results..... | 116 |
| 7. | Final Decision..... | 122 |
| | References..... | 127 |

List of Figures

| | |
|--|----|
| Figure 2.1: : Mode of transport in Europe [21]. | 18 |
| Figure 2.2: The context of urban travel [2] | 20 |
| Figure 2.3: Average Daily Miles Driven (per Driver) [3]. | 21 |
| Figure 2.4: Average vehicle occupancy by trip purpose [3] | 21 |
| Figure 2.5: Investigation result of curb parking purpose [4]. | 23 |
| Figure 2.6: Medium scenario-global annual new vehicle sales [5] | 24 |
| Figure 2.7: High scenario-global annual new vehicle sales [5]. | 24 |
| Figure 2.8: U.S. Light Vehicle Sales and Fleet Composition Under Baseline Scenario [18] | 25 |
| Figure 2.9: Energy pathways in transport and other sectors [6]. | 27 |
| Figure 2.10: GHG emissions in the EU-27 [7] | 31 |
| Figure 2.11: Noise map for the City of Bremerhaven, Germany (Noise exposure from road traffic in Lden) [20]. | 33 |
| Figure 2.12: Overall noise annoyance at home [8] | 34 |
| Figure 2.13: Noise annoyance in European built up areas [8] | 34 |
| Figure 2.14: Energy Use (MJ/km) [10] | 36 |
| Figure 2.15: Range (km) [10] | 37 |
| Figure 2.16: Tank-to-Wheel Efficiency (%) [10]. | 38 |
| Figure 2.17: Cycle Carbon Emission (g C/km) [10] | 39 |
| Figure 2.18: Comparison of US Operating Costs in \$(1997)/km for Selected New Vehicle Options in 2020 [10]. | 40 |
| Figure 2.19: Battery Cost for High Power Applications [12] | 41 |
| Figure 2.20: FC System Cost [12] | |
| Figure 2.21: Electric Machine Cost [12] | 41 |
| Figure 2.22: Electric Machine Peak Efficiency [12] | |
| Figure 3.1: Forces acting on a vehicle | 42 |
| Figure 3.2: Energy flow [14] | 45 |
| Figure 3.3: Installation of the unit [15] | 48 |
| Figure 3.4: Mounted unit [15]. | |
| Figure 3.5: Schematic of axle unit [15] | 48 |
| Figure 3.6: Efficiency of reducer [15] | |
| Figure 3.7: Electric vehicle batteries [27] | 50 |
| Figure 3.8: On-board battery charger [24] | 51 |

| | |
|--|----|
| Figure 3.9: Engine power vs. vehicle constant speed on a flat road and at 5% grade road [13] | 52 |
| | |
| Figure 3.10: Polaris Generator [16] | 52 |
| Figure 3.11: Parameters which determine passenger car driver seat location [17] | 54 |
| Figure 4.1: Basic line | 55 |
| Figure 4.2: Main surface of the vehicle | 55 |
| Figure 4.3: Side view of EREV | 56 |
| Figure 4.4: Front view of EREV | 56 |
| Figure 4.5: Rear side view of EREV | 57 |
| Figure 4.6: Volumes of parts for EREV | 57 |
| Figure 4.7: 2D drawing of EREV | 58 |
| Figure 5.1: View of the vehicle before the simplifications | 61 |
| Figure 5.2: View of the vehicle after the simplifications | 61 |
| Figure 5.3: Points which define the size of the control volume | 62 |
| Figure 5.4: Control volume of the flow domain | 62 |
| Figure 5.5: Air volume which includes the vehicle | 63 |
| Figure 5.6: The cavity formed by the vehicle inside the flow domain | 63 |
| Figure 5.7: Default 2D region (the surface of the vehicle) | 64 |
| Figure 5.8: "Top" surface | 64 |
| Figure 5.9: The "Bottom" surface (ground) | 65 |
| Figure 5.10: The "Inlet" surface of the flow domain | 65 |
| Figure 5.11: The "Outlet" surface of the flow domain | 66 |
| Figure 5.12: The "Symmetry" plane of the flow domain | 66 |
| Figure 5.13: The "Side" surface of the flow domain | 67 |
| Figure 5.14: Face spacing definition | 67 |
| Figure 5.15: Face Spacing on a 1 m cube, with a Constant Edge Length of 0.05 m, Radius of Influence 0.2 m, and Expansion Factor 1.2 [25] | 69 |
| Figure 5.16: Inflated mesh region and the transition between the inflation mesh and the tetrahedral mesh [25]. | 69 |
| Figure 5.17: Reference area for "Inflated Boundary" | 70 |
| Figure 5.18: Inflation parameters used in this project | 71 |
| Figure 5.19: Final mesh for the ER11 vehicle | 71 |
| Figure 5.20: close-up of the final mesh at the vehicle region (ER11) | 72 |
| Figure 5.21: Detail of the inflation layer at the solid boundary | 72 |

| | |
|--|----|
| Figure 5.22: View of the ANSYS CFX-Pre and the meshed flow domain with the corresponding boundary conditions | 73 |
| Figure 5.23: General options for the flow domain (Default Domain) | 74 |
| Figure 5.24: Fluid Model parameters of the Default Domain | 75 |
| Figure 5.25: The tree of parameters in ANSYS CFX-Pre..... | 76 |
| Figure 5.26: Basic Settings on Default Domain Default (vehicle)..... | 76 |
| Figure 5.27: Boundary Details of Default Domain Default (vehicle) | 77 |
| Figure 5.28: The surface that consists the Default Domain Default (vehicle)..... | 77 |
| Figure 5.29: Basic setting for the solver control (ANSYS-CFX)..... | 78 |
| Figure 5.30: Surface pressure contours - front view | 80 |
| Figure 5.31: Surface pressure contours - side view..... | 80 |
| Figure 5.32: Surface pressure contours - rear view | 81 |
| Figure 5.33: Pressure contours at the symmetry plane | 81 |
| Figure 5.34: Streamlines at the symmetry plane | 82 |
| Figure 5.35: Streamlines at a plane 0.35m away from the symmetry plane | 82 |
| Figure 5.36: Equal-velocity surface for 0.5m/s..... | 83 |
| Figure 5.37: Equal-velocity surface for 1m/s..... | 83 |
| Figure 5.38: Equal-velocity surface for 2 m/s..... | 84 |
| Figure 5.39: Equal-velocity surface for 3 m/s..... | 84 |
| Figure 5.40: Equal-velocity surface for 4 m/s..... | 85 |
| Figure 6.1: Six sections produced from the 3D model of the old vehicle (ER11) | 89 |
| Figure 6.2: The wireframes resulted from the sections | 89 |
| Figure 6.3: Reshaping the vehicle using the wireframes..... | 90 |
| Figure 6.4: The final shape of the 1st model using wireframes | 90 |
| Figure 6.5: The final surface for the 1st model | 91 |
| Figure 6.6: Front - side view of the 1st model..... | 91 |
| Figure 6.7: Side view of the 1st model | 92 |
| Figure 6.8: Front view of the 1st model | 92 |
| Figure 6.9: Back-side view of the 1st model..... | 93 |
| Figure 6.10: 2D drawings of the 1st model | 94 |
| Figure 6.11: Surface pressure contours - front view | 95 |
| Figure 6.12: Surface pressure contours - side view..... | 95 |
| Figure 6.13: Surface Pressure contours - rear view..... | 96 |
| Figure 6.14: Pressure contours at the symmetry plane | 96 |

| | |
|---|-----|
| Figure 6.15: Streamlines on the symmetry plane | 97 |
| Figure 6.16: Streamlines on a plane 0.35m away from the symmetry plane | 97 |
| Figure 6.17: Equal-velocity surface for 0.5m/s..... | 98 |
| Figure 6.18: Equal-velocity surface for 1m/s..... | 98 |
| Figure 6.19: Equal-velocity surface for 2m/s..... | 99 |
| Figure 6.20: Equal-velocity surface for 3m/s..... | 99 |
| Figure 6.21: Equal-velocity surface for 4m/s..... | 100 |
| Figure 6.22: Side view of the 2nd model..... | 101 |
| Figure 6.23: Rear-side view of the 2nd model | 102 |
| Figure 6.24: Front View of the 2nd model | 102 |
| Figure 6.25: 2D drawings of the 2nd model | 103 |
| Figure 6.26: Side view of the 3rd model..... | 104 |
| Figure 6.27: Front-side view of the 3rd model..... | 104 |
| Figure 6.28: Rear-side view of the 3rd model | 105 |
| Figure 6.29: Front view of the 3rd model..... | 105 |
| Figure 6.30: 2D drawings of the 3rd model..... | 106 |
| Figure 6.31: Surface Pressure contours - front view - 3rd model | 107 |
| Figure 6.32: Surface Pressure contours - side view - 3rd model..... | 107 |
| Figure 6.33: Surface pressure contours - Rear View - 3rd model..... | 108 |
| Figure 6.34: Streamlines - symmetry plain - 3rd model..... | 108 |
| Figure 6.35: Streamlines at a plane 0.35m away from the symmetry plain - 3rd model..... | 109 |
| Figure 6.36: Equal-velocity surface for 0.5m/s - 3rd model | 109 |
| Figure 6.37: Equal-velocity surface for 1 m/s - 3rd model | 110 |
| Figure 6.38: Equal-velocity surface for 2 m/s - 3rd model | 110 |
| Figure 6.39: Equal-velocity surface for 3 m/s - 3rd model | 111 |
| Figure 6.40: Equal-velocity surface for 4 m/s - 3rd model | 111 |
| Figure 6.41: Side view of the 4th model..... | 112 |
| Figure 6.42: Front-side view of the 4th model..... | 113 |
| Figure 6.43: Front View of the 4th model | 113 |
| Figure 6.44: Rear Side - 4th model | 114 |
| Figure 6.45: 2D drawing of the 4th model | 115 |
| Figure 6.46: Surface pressure contours - Front View - 4th model | 116 |
| Figure 6.47: Surface pressure contours - Side View - 4th model | 116 |
| Figure 6.48: Surface pressure contours - Rear View - 4th model..... | 117 |

| | |
|---|-----|
| Figure 6.49: Streamlines at symmetry plane - 4th model..... | 117 |
| Figure 6.50: Streamlines at a plane 0.35m away from symmetry plane - 4th model..... | 118 |
| Figure 6.51: Equal-velocity surface for 0.5m/s - 4th model..... | 118 |
| Figure 6.52: Equal-velocity surface for 1 m/s - 4th model..... | 119 |
| Figure 6.53: Equal-velocity surface for 2 m/s - 4th model..... | 119 |
| Figure 6.54: Equal-velocity surface for 3m/s - 4th model..... | 120 |
| Figure 6.55: Equal-velocity surface for 4 m/s - 4th model..... | 120 |
| Figure 7.1: Using the old vehicle to construct the initial mockup..... | 123 |
| Figure 7.2: The Final male-mold..... | 123 |
| Figure 7.3: The constructed female-mold..... | 124 |
| Figure 7.4: The rear side of the female-mold..... | 124 |
| Figure 7.5: The rear carbon-fiber surface..... | 125 |
| Figure 7.6: The final carbon-fiber surface of ER12 (4th model)..... | 125 |
| Figure 7.7: ER12 at European Shell Eco Marathon 2012..... | 126 |
| Figure 7.8: Technical University of Crete Eco Racing Team in front of ER12..... | 126 |

List of Tables

| | |
|---|-----|
| Table 2.1: Commuting Flows in U.S. Metropolitan Areas [2] | 19 |
| Table 2.2: Changping town, parking demand forecasting [4] | 22 |
| Table 2.3: Coverage of transport modes and travel range by different alternative [6]..... | 30 |
| Table 3.1: Specifications of in-wheel motor [15] | 49 |
| Table 3.2: Specifications of the inverter [15] | 49 |
| Table 3.3: Specifications of the on board battery charger [24] | 51 |
| Table 3.4: Polaris Engine Specifications [16] | 53 |
| Table 7.1: Comparison of the alternative designs..... | 122 |

1. Introduction

1.1 Statement of work

The goals of the present work are, firstly, to propose an extended range electric vehicle (EREV) and secondly, the design and aerodynamic analysis of a new vehicle (ER12) configuration, in order to participate to the European Shell Eco Marathon. To achieve the first goal, the social and environmental impacts of transportation in domestic areas were analyzed, considering the trends in auto-motion. For the second goal the results of aerodynamic simulation consisted the base for the final choice among the various alternative configurations tested. Decisive role in designing of ER12 played the Computational Fluid Dynamics (CFD) analysis in ANSYS-CFX commercial software, simulating the flow field around the vehicle in predefined conditions.

1.2 Introduction

People all over the world are migrating to cities in search of jobs and cultural advantages. Their demands in energy consumption are really high, the majority of them are mainly covered by the crude oil products, causing unsustainable urban environments. In the coming decades, oil and other fossil fuels are expected to become more expensive, as demand increases and low cost sources dry up. The negative impact on the environment will be greater, as conventional resources are replaced by more polluting supplies. Meanwhile, the need to move to a low-carbon economy and the growing concerns about energy security will bring about a greater need for low-cost renewable energy resources, made much cheaper by technological progress and massive production.

Road transportation is one of the main sectors which contribute to a more unsustainable environment, increasing rapidly both the Nitro oxide and Carbon monoxide levels in domestic areas. For example, in the EU, compared with 1990 levels, in no other sector has been the growth rate of greenhouse gas (GHG) emissions as high as in transport [7]. This

sector, besides the air pollution, affects negatively urban environments due to the high noise levels, which may have a considerable impact on people's quality of life. Despite the reflections in health, which are caused by both air and noise polluted city environments, it is remarkable the social costs of road traffic noise. For instance, in the European Union, that cost is estimated to be in the range of 30 to 46 billion Euros per year, approximately the 0.4% of the GDP in the European Union [8].

The necessity of improving the quality of life into urban environments and simultaneously the necessity to increase the independence from crude oils products has created a new trend in auto mobility which is focused in new propulsion systems, fostering the companies to launch either hybrid or pure electric vehicles. By now, better gas emissions have been achieved, consisting new cars more ecological friendly. Moreover, the usage of the electric motors instead of internal combustion engines during short routes around the city, has played a decisive role in ordering noise levels to be reduced in domestic areas .

Taking into account the new demands for a more sustainable transport both parts of that thesis have been focused on the design of low consumption vehicles. In the first part there is an extended research about the new types of fuels and propulsion systems, the average amount of passengers who usually travel in a car during a day, an analysis of automotive market place and other aspects and facts, which define the constrains for approaching the conceptual modeling of an urban vehicle. Actually, it is a two-seat electrical extended range vehicle, using a 320 c.c. engine in order batteries to be recharged, supplying with electricity the four in-wheel-motors. The second part deals with the exterior design and the aerodynamic analysis of a one-seat low-consumption vehicle, designed and constructed by the Technical University of Crete Eco Racing Team, which participates in the European Shell Eco Marathon competition for the last five years. Three totally different versions have been launched since the first participation of the team, showing a gradual evolution. The model designed during this work achieved an improved aerodynamic efficiency by 50% (in terms of drag coefficient) and a weight reduction by 30%, in comparison with the previous version of the racing vehicle. CATIA V5R19 and ANSYS CFX 11 were used for the geometrical design and aerodynamic simulation respectively.

Part A

2. Social and economic factors in urban transportation

2.1 Urbanization

Urbanization is a phenomenon which appeared during the last century and is expected to continue. The percentage of Europeans who live in urban areas will have been raised by 12%, between 2007 and 2050, reaching the 85% [1]. The multicultural environment and the chances for a better life is a major source of advantages that drive urbanization. On the other hand, during the last 50 years there was a high growth of urban areas in contrast with the resident population, consisting a new challenge for urban transportation. Thus, the necessity for individual transport modes forced the generation of congestion and environmental problems [1].

Congestion is appearing mainly in agglomerations and in their access routes, causing large costs due to delays and higher fuel consumption. As most freight and passenger transport starts or ends in urban areas, urban congestion also negatively impacts on inter-urban travel. The densely populated cities provide better mass transport services, however, the lack of land and society acceptance are the main factors which negatively influence the construction of new infrastructures for public or alternative means of transport [1].

According to the recent European Commission's Green Paper "Towards a new culture for urban mobility" [1]:

- 60% of the Europeans live in domestic areas,
- 85% of European gross domestic product (GDP) is produced in urban areas,
- every year €100 billion, or 1% of the EU GDP, are lost to the European economy as a result of delays and pollution related to urban traffic,
- urban traffic is responsible for 40% of CO₂ emissions and 70% of other pollutants arising from road transport.

2.2 Urban transportation

Transportation has undoubtedly played a decisive role in urban life; without it activities in cities grind to a halt. On the contrary it is the main factor of many seemingly intractable urban problems, congestion, pollution, inequality, and reliance on fossil fuels. The issues which are relative with urban transportation are not only congestion problems but wide range of matters such as environmental management, historic preservation, and citizen participation. Through transportation is given the chance to carry out the diverse range of activities that make up daily life. It is necessary to travel around the city in order to satisfy the daily needs for goods and services, for example to visit food stores, Laundromats, banks, drugstores, hospitals, libraries, schools, post offices (Figure 2.1) [21]. Moreover, home and work are in the same location for only a few people (about 3.3% of the U.S. workforce in 2000), so that to earn an income as well as to spend it one must travel. Generally all movements incur a cost of some sort, separately time and monetary cost or a combination of them. Trips by auto, bus, or train, have both time and monetary costs, in comparison with those made on foot, involve an outlay primarily of time, so travelers often trade off time versus money costs, as the more costly travel modes are usually the faster ones. A trade-off is also involved in the decision to make a trip: the traveler weighs the expected benefits to be gained at the destination against the expected costs of getting there [2].

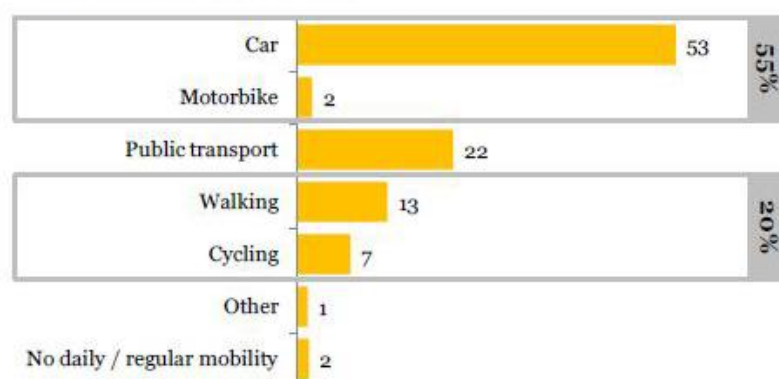


Figure 2.1: : Mode of transport in Europe [21].

2.3 Current trends in urban transportation

The main section that urban transportation planning has been focused are the work trips. Among all the trips in domestic areas (including work, socializing, recreation, shopping, and personal business), work used to account for the largest proportion of trips. In addition, work trips are strongly connected with traffic jams on rush hours, because most people have to be at work between 7:00 A.M. and 9:00 A.M. and leave 8 hours later. The peak load associated with the work trip has placed the greatest demands on the transportation system [2].

The commuting flows have become complex the last decades, the route suburb-to-central-city has not been the dominant work trip type since at least as long ago as 1970 [2]. In 2000, excluding the trips around of nonmetropolitan areas, and focusing on metropolitan, the national pattern of commuting flows looks quite intricate (Table 2.1) [2]. It is remarkable that the dominant route is the within-suburb, accounting for about two-fifths of all metropolitan work trips.

| | | |
|---|-------------------|--------------|
| Suburbs to central city | 18,175,489 | 17.4% |
| Within suburbs | 40,745,878 | 39.0% |
| From suburbs to outside home MSA¹ | 7,650,705 | 7.3% |
| Central city to suburbs | 7,984,014 | 7.6% |
| Within central city | 27,425,079 | 26.3% |
| From central city to outside home MSA | 2,402,466 | 2.3% |

Table 2.1: Commuting Flows in U.S. Metropolitan Areas [2]

Due to the complexity of the flow patterns illustrated in Table 2.1, it is expected that the figures of work trips made by auto have raised while the figures made on public transport have continued to drop (Figure 2.2) [2]. It is significant that only the 5%, in 2000, of work trips were made on public transport in contrast with the figures of people driving alone to

¹ MSA metropolitan statistical area (a city and its surrounding suburbs)

work (being increased to about 80%). On the other side, carpooling figures dropped by 8% the last two decades [2].

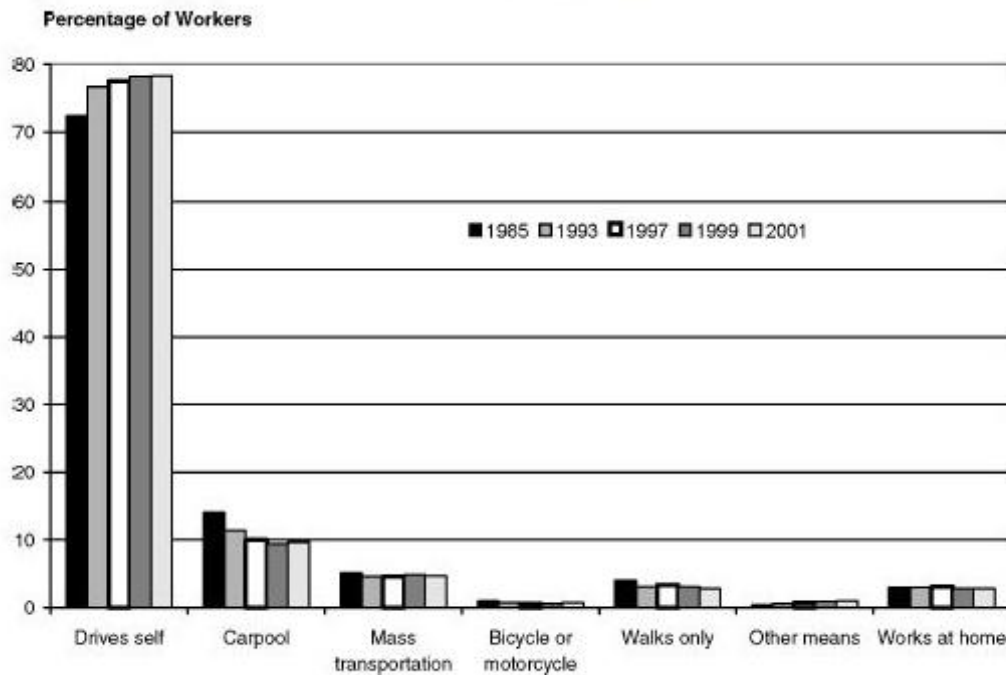


Figure 2.2: The context of urban travel [2]

2.4 Vehicle miles traveled and vehicle occupancy

United States have the highest rate of private vehicle ownership, the highest level in daily miles traveled, and the lowest rates of trip making by modes other than the auto [3]. Even if there are comparable per capita income and geography differences between Canada and United States, the transit mode share in Canada is far larger than that of the United States. It is estimated that in countries of northern Europe, which also have comparable per capita income but lower rate of vehicles per person, miles traveled (VMT) per capita is on average half of that in the United States (Figure 2.3) [3].

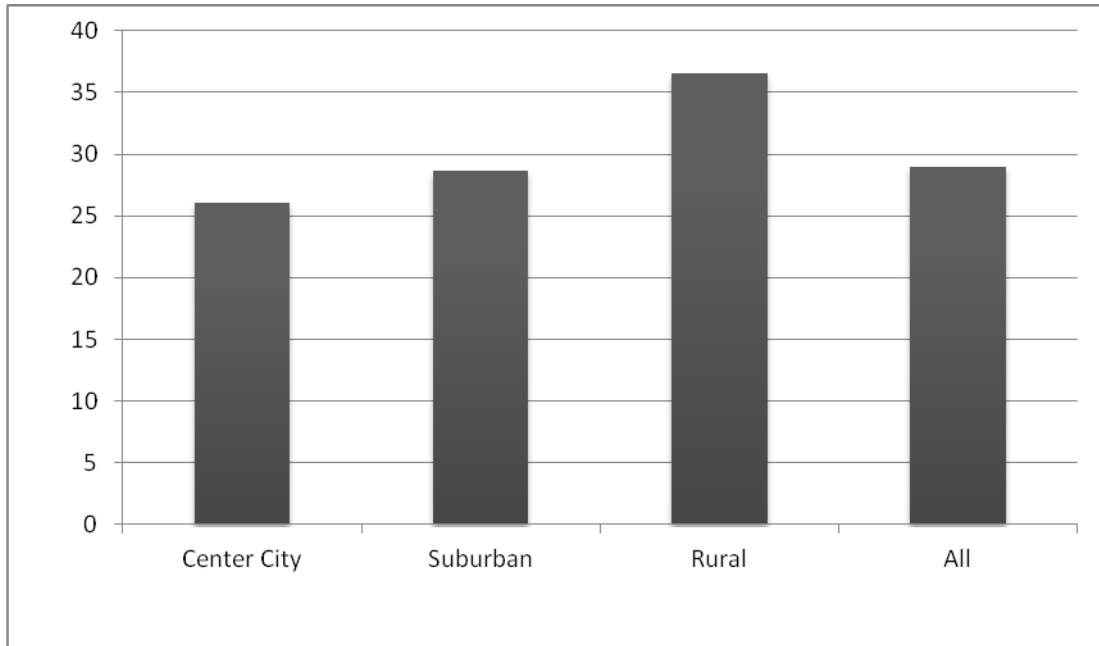


Figure 2.3: Average Daily Miles Driven (per Driver) [3]

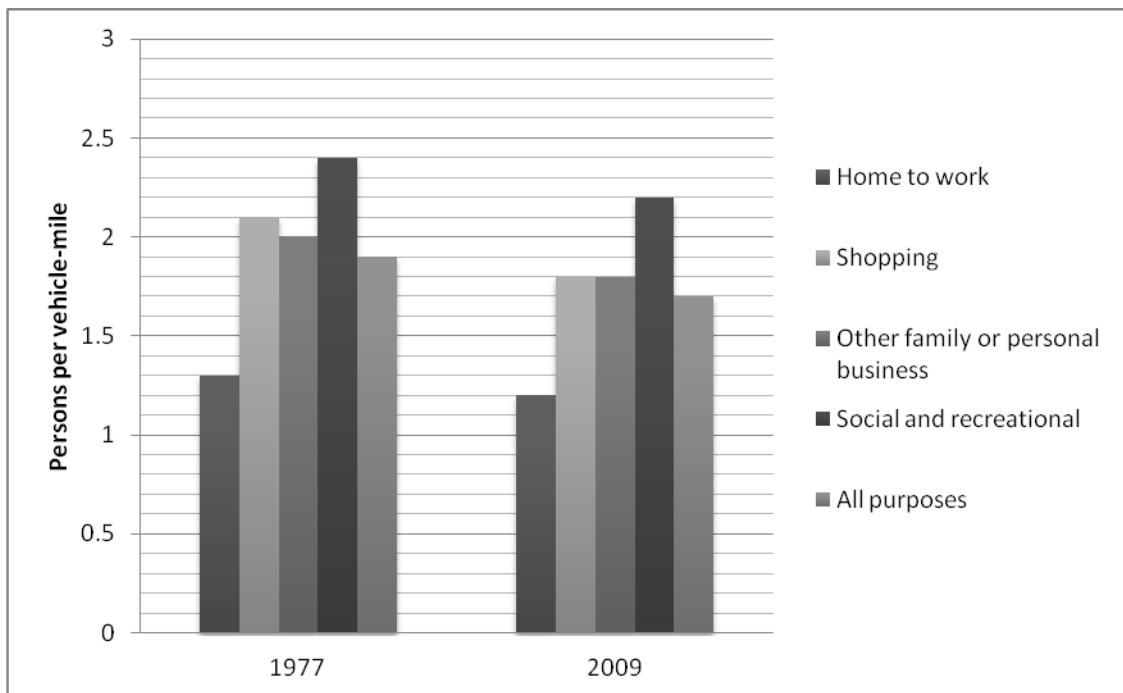


Figure 2.4: Average vehicle occupancy by trip purpose [3]

The average vehicle occupancy is higher for social and recreational purposes. The highest vehicle occupancy levels for all purposes were in 1977 (Figure 2.4). The increase in number

of vehicles per household and the decrease in average household size could have contributed to the decline since then [3].

2.5 Parking demands

The gradual increase of parking demands is higher than the growth speed of parking facilities in cities, having as a result the increase of parking problems mainly in the domestic areas (Table 2.2).

| Year | Car population | Car parking demand | Motorcycle population | Motorbike parking demand |
|------|----------------|--------------------|-----------------------|--------------------------|
| 2010 | 16390 | 2933 | 30437 | 8170 |
| 2011 | 17697 | 3167 | 32866 | 8822 |
| 2012 | 19072 | 3413 | 35420 | 9507 |
| 2013 | 20525 | 3673 | 38119 | 10232 |
| 2014 | 22067 | 3949 | 40982 | 11000 |
| 2015 | 23710 | 4243 | 44033 | 11819 |

Table 2.2: Changping town, parking demand forecasting [4]

A great example to investigate parking issues is Changping. The Changping town is a railway terminal of Pearl River Delta, and it is the economic and culture center of Dongguan. There are 23 off-side parking lots, 1,800 natural berths and 10,000 curb parking natural berths in the center area of Changping town. For the off-side parking lots, the summit parking indexes are relatively high, which display the parking facilities are fully utilized in rush hours [4].

The average berth utilization rate in rush hours is 0.39, and the minimum value is 0.1, the maximum value being 0.9. There is a great difference in parking demands between rush hours and the rest of them. For the curb parking lots the summit parking indexes are higher than 0.75, even 1.0. The average parking time is 28 minutes, while the parking purposes include business, shopping, and loading or unloading cargo (Figure 2.5) [4].

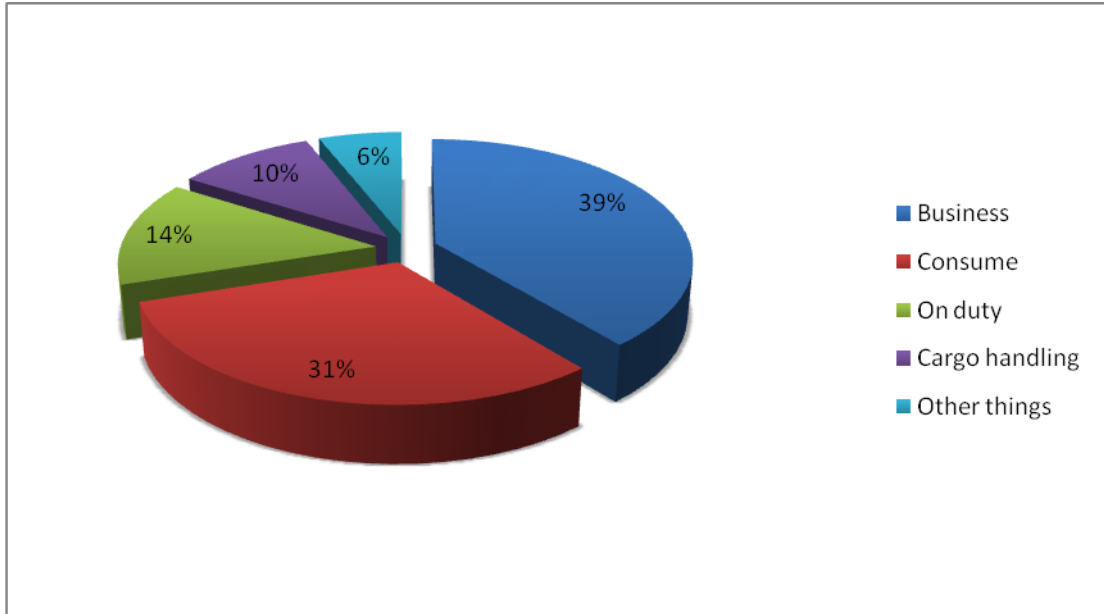


Figure 2.5: Investigation result of curb parking purpose [4]

2.6 Trends in annual vehicle sales

Road transport has negatively influenced the environment, considered as the biggest contributor to greenhouse gas (GHG) emissions [5]. The adoption of new policy measures and the technological improvements have been already focused on the future reduction of GHG emissions, relative to the road transport. The continuing development in automotive industry has already achieved a large reduction of gas emissions on the existing ICE vehicles. At the same time, several automotive manufacturers have announced the launch of battery electric vehicles (BEV) and plug-in hybrid vehicles (PHEV) for the coming years, contributing to a more green society. At graphs below two predictions for the future annual vehicle sales are demonstrated (Figures 2.6 - 2.7) [5].

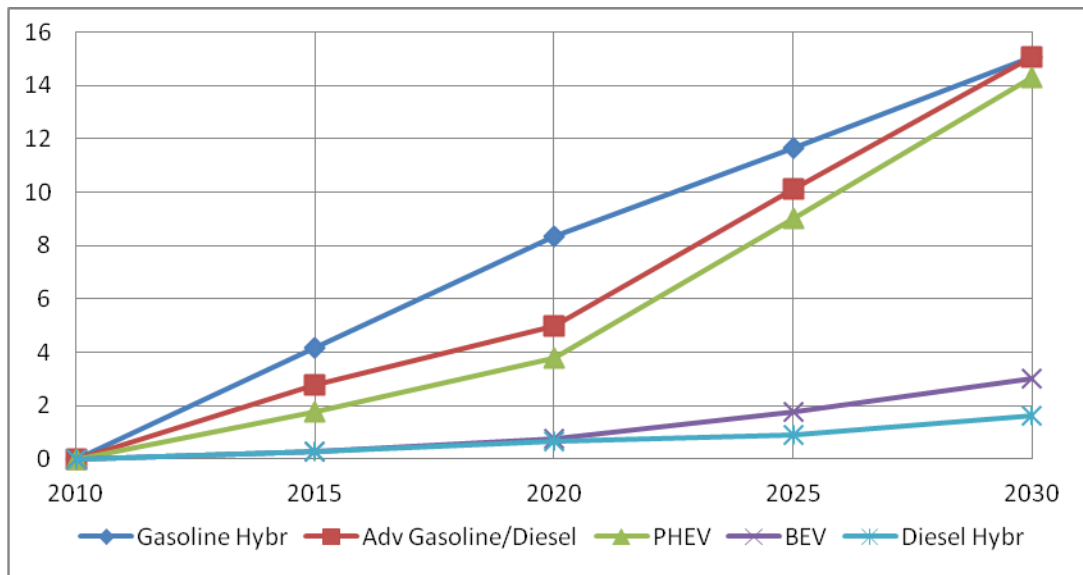


Figure 2.6: Medium scenario-global annual new vehicle sales [5]

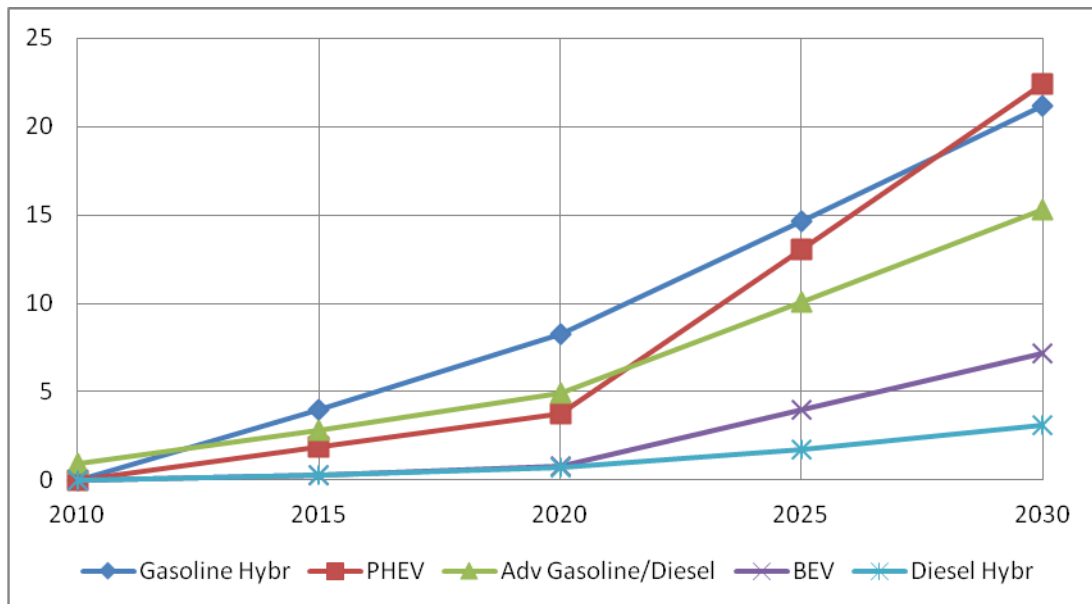


Figure 2.7: High scenario-global annual new vehicle sales [5]

In both cases, the most significant evident is the sharply growth of PHEV sales which is a totally new category. A PHEV shares the characteristics of both conventional hybrid electric vehicle (having an electric motor and an internal combustion engine - ICE), and of an all-electric vehicle, having a plug to connect to the electrical grid. In the following Figure (2.8) the left columns and axis represent forecasts for the composition of U.S. light vehicle sales under the baseline oil price scenario from the EIA. The right columns and axis represent the corresponding mix of vehicles in the U.S. [18].

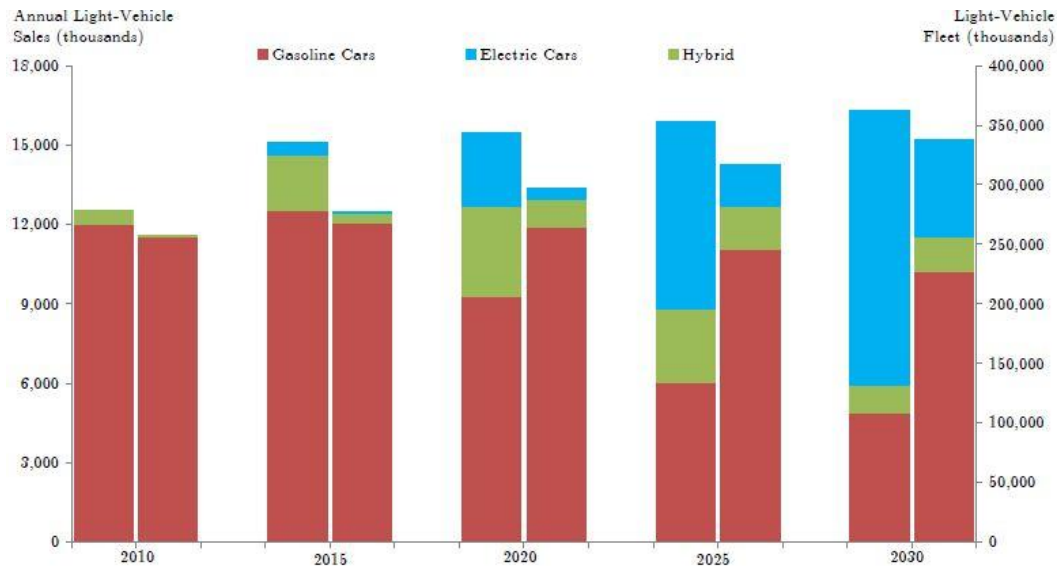


Figure 2.8: U.S. Light Vehicle Sales and Fleet Composition Under Baseline Scenario [18]

2.7 Future fuels and electric vehicles

2.7.1 Future transport fuels

The EU objective is an overall reduction of CO₂ emissions of 80%-95% by the year 2050, with respect to the 1990 level [6]. This could happen through decarbonisation of transport and the substitution of oil as transport fuel. The almost total dependence of road transportation on crude oil so far has led to the improvement of transport efficiency and management of transport volumes, aiming to the reduction of CO₂ emissions. In addition, the use of finite renewable resources will contribute to meet the full energy demand from transport in the long term [6].

Alternative fuel options for substituting oil as energy source for propulsion in transport are [6]:

- Electricity / hydrogen, and biofuels (liquids) as the main options.
- Synthetic fuels as a technology bridge from fossil to biomass based fuels.
- Methane (natural gas and biomethane) as complementary fuels.
- LPG as supplement.

Electricity and **hydrogen** are universal energy carriers and can be produced from all primary energy sources. The main advantage of both pathways is the zero emission of CO₂. Propulsion on these vehicles is achieved with the use of electric motors. The energy can be supplied via three main pathways [6]:

- **Battery-electric**, with electricity from the grid stored on-board vehicles in batteries. The disadvantage of that technology is the short range that could be covered due to the low energy density batteries. Moreover a great issue is the lack of battery recharging infrastructure and power management [6].
- **Fuel cells powered by hydrogen**, used for on-board electricity production. This technology faces more issues due to new infrastructures, which are required to support hydrogen production, distribution, and storage. By now hydrogen technology is really expensive for automotive manufactures but lower cost on basic parts (fuel cell) are expected in the future [6].
- **Overhead Line / Third Rail** for tram, metro, trains and trolley-buses, with electricity taken directly from the grid without the need of intermediate storage [6].

Biofuels could technically substitute oil in all transport modes, with existing power train technologies and existing re-fuelling infrastructures. There are two generation of biofuels, the first one was based on traditional crops, animal fats, or used cooking oils and the second generation is produced from ligno-cellulosic feedstock and wastes. Generally in both generations there was limited production due to the lack of land, water or energy and the limited availability from wastes. A supportive policy framework at the EU level and harmonized standards for biofuels across the EU are key elements for the future uptake of sustainable biofuels [6].

Methane can be sourced from fossil natural gas or from biomass and wastes as biomethane [6]. The advantage of methane fuel is the usage of internal combustion engines for propulsion, similar to those for liquid hydrocarbon fuels. However, refueling infrastructures should be built, supporting a widespread supply and feeding methane powered vehicles from a single grid and not from general gas grid.

LPG (Liquefied Petroleum Gas) is a by-product of the hydrocarbon fuel chain, currently resulting from oil and natural gas, in future possibly also from biomass. Almost 3% of the European vehicles uses LPG, being the most widely used alternative fuel in Europe. The core infrastructure is established, with over 27,000 public filling stations [6].

The different transport modes require different options of alternative fuels [6]:

- **Road transport** could be powered by electricity for short distances, hydrogen and methane up to medium distance, and biofuels and LPG up to long distance.
- **Railways** should be electrified wherever feasible, otherwise use biofuels.
- **Aviation** should be supplied from biomass derived kerosene.

Energy supply for transport could take a large number of different pathways as shown above (Figure 2.9).

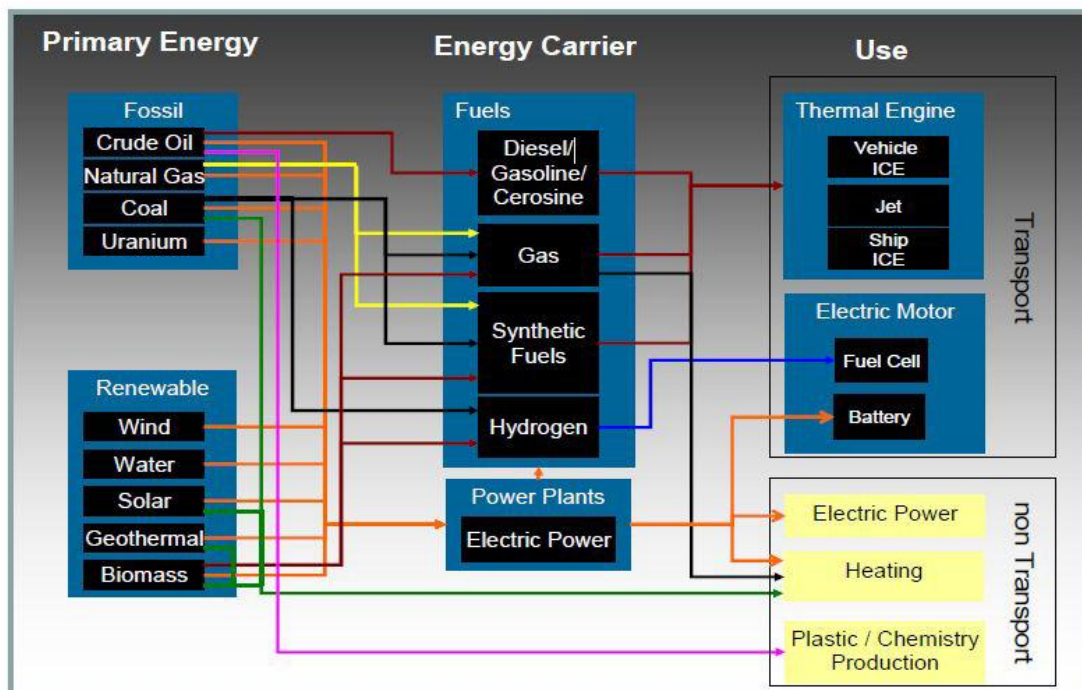


Figure 2.9: Energy pathways in transport and other sectors [6]

2.7.2 Electrical vehicles ideally suited for urban areas

For urban transportation purposes either electricity or hydrogen/fuel cell vehicles could be used, producing zero gas emissions. Additionally, road transportation in domestic areas could be powered by neat synthetic or paraffinic fuels, methane, or LPG. At the same time, competition between fuels needs to be avoided due to the possible economical impacts [6].

A great benefit of electric propulsion is the low levels of gas emissions, making electric vehicles an ideal solution for densely populated urban areas where air quality issues are appeared. Furthermore, the range of an electrical vehicle could be extended either using intermediate storage on board, or producing electricity on board [6].

Intermediate storage technology was firstly appeared in the second half of 19th century, when externally chargeable batteries were launched on board road transport vehicles. However, the performance of these vehicles was restricted by the low energy density of batteries. In the beginning of the 20th century electric vehicles were outperformed in the market by internal combustion engine vehicles using high energy density, cheap and plenty liquid fuels. The last decades battery technologies have been improved, giving a new chance in electric mobility. On the other side the autonomy/range of electric vehicles is still strongly limited with today's technology, but large efforts and investments are being made to improve the performance and reduce costs for future electric vehicles [6].

On-board generation of electricity for propulsion has been applied in ships powered by diesel and electro motors. The same technology was adopted in automotion, creating the extended range electrical vehicles. The electricity on that vehicles is generated on board by an internal combustion engine supplying the batteries and the motors with electricity. Moreover an on board battery charger allows external electricity supply, by plugging to the grid [6].

Another alternative solution, long under development, is the use of a fuel cell as energy converter. It produces electricity as output from the chemical reaction of hydrogen and oxygen, recombining to water. The electricity then drives directly an electric motor, or is stored in a battery [6].

2.7.3 Types of electric propulsion vehicles

Electric propulsion of road vehicles is used in different configurations [6]:

- Hybrid Electric Vehicle (HEV). A combination of an ICE and an electric motor. The internal combustion engine is the external energy supplier, while batteries are being charged by braking energy recuperation.
- Plug-in Hybrid Electric Vehicle (PHEV). A similar power train as in HEV, giving the chance, at the same time, of charging the battery also by plugging to the electricity grid.
- Range-extender vehicle (REV). It is another type of HEV. Using an electric motor as propulsion system while batteries are being recharged mainly by a small ICE working as generator or plug in to the electricity grid.
- Battery Electric Vehicle (BEV). Based on electric propulsion only, charging batteries through electricity grid.
- Hydrogen/Fuel Cell Vehicle (HFCV). Based on electric propulsion only, recharging batteries through fuel cell system.

The first hybrid configurations do not contribute to oil substitution but have already improved the overall energy efficiency of a vehicle, saving oil and reducing CO₂ emissions. On the other hand configurations with additional external energy input in form of electricity (PHEV, Plug-in REV, and BEV) or hydrogen (HFCV) could contribute to oil substitution and full decarbonisation. Even though, battery and fuel cell technology could play a decisive role to a more sustainable mobility; the low energy density and their cost are the difficulties which postpone the prevalence of that vehicles [6]. “As long as batteries alone cannot meet the customers’ expectations for range, reliability and price, hybrid solutions, including range extenders, could be adequate bridging technologies from ICE to battery driven power trains” [6]. In the following Table 2.3 the coverage of transport modes and travel range by different alternative are illustrated [6].

| | | Road/passengers | | | Road/freight | | | Rail | Water | | | Air |
|-------------------|------|-----------------|-----|------|--------------|-----|------|------|--------|--------------------|----------|-----|
| | | short | med | long | short | med | long | | inland | short-sea shipping | maritime | |
| Electric | BEV | ■ | | | ■ | | | ■ | | | | |
| | HFC | ■ | ■ | | | | | | ■ | | | |
| | Grid | ■ | | | ■ | | | ■ | | | | |
| Biofuels (liquid) | | ■ | ■ | ■ | ■ | ■ | ■ | ■ | ■ | ■ | ■ | ■ |
| Synthetic fuels | | ■ | ■ | ■ | ■ | ■ | ■ | ■ | ■ | ■ | ■ | ■ |
| Methane | CNG | ■ | ■ | ■ | ■ | ■ | | | | | | |
| | CBG | ■ | ■ | ■ | ■ | ■ | | | | | | |
| | LNG | ■ | ■ | ■ | ■ | ■ | ■ | ■ | ■ | ■ | ■ | |
| LPG | | ■ | ■ | ■ | ■ | ■ | | ■ | ■ | ■ | | |

Table 2.3: Coverage of transport modes and travel range by different alternative [6]

2.8 Environmental and noise impacts of ICE vehicles

2.8.1 Greenhouse gas emissions in European Union

Setting strict emission standards, air quality in European cities has been improved but more needs to be done, focusing on the decrease of NOx emissions in urban environments, as well as ensuring that real world emissions are adequately controlled [7].

Transport is the sector with the highest level on green gas (GHG) emissions in the European Union, having a gradually increase the last decades (Figure 2.10). The three main components which produce GHG emissions are the following: the amount of the activity that generates the emissions; the energy intensity of that activity; and the GHG intensity of the energy that is being used. Analyzing the past developments in transport, it was determined that in spite of the transport factor has been greatly increased, there was not any activity to reduce its energy and GHG intensity [7].

Even though the energy efficiency of transport has been increasing, the results on decrease of overall fuel consumption have not depicted yet. It is remarkable that transportation dependence on fossil fuels is reaching the 97 %, which has negative implications for the security of energy supply. The growth of transport activity raises concerns for its environmental sustainability. Transport was responsible for the 23.8% and 27.9% of total

GHG and CO₂ emission in the EU-27 in 2006, according to data from the European Environment Agency (Figure 2.10) [7].

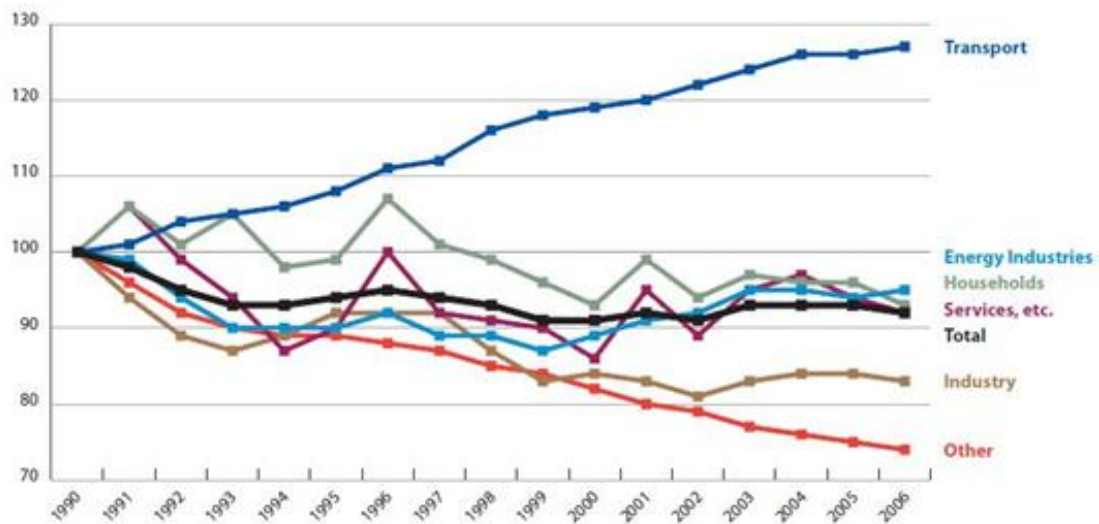


Figure 2.10: GHG emissions in the EU-27 [7]

2.8.2 Noise in urban areas

Quality of life is affected by numerous parameters. Particularly in the urban environment noise can significantly affect the life of the citizens. According to the WHO's Guidelines for Community Noise [26], 50% of the population of Europe (EU 15) are considered to live in areas exposed to high acoustic levels. It is estimated that during daytime, about 40% of the EU citizens are exposed to road traffic noise that exceeds 55 dB, while 20% is above 65 dB. Furthermore, at night, about 30% of the population is exposed to sound levels above 55 dB that can affect sleeping. Despite the fact that the exact relation between noise and health risks have not been scientifically established, recent studies have shown that exposure to increased noise levels can affect high blood pressure that lead to heart attacks. According to these studies, night time exposure to noise levels above 50 db could be associated to high blood pressure. During daytime, men that are exposed to road traffic noise above 65 db are more probable by 20% to suffer from heart attacks. In Germany, about 3% of myocardial infarctions are attributed to road traffic noise, accounting for approximately 4,300 cases annually and causing more than 2,800 deaths per year [8].

Among the main considerations about the costs of the design and execution of action plans about noise, it is a fact that noise itself creates costs. For example, the costs are related to medical treatments, as well as low residence and rental values. Furthermore, road traffic noise in Europe is considered to generate a cost of about 40 billion euros annually, accounting for the 0.4% of the GDP in the EU22. Considering that, it is obvious that reducing noise levels will not only have significant social and health benefits, but could also positively affect the economy. According to a Dutch study about the development of noise abatement measures for the Netherlands [8], the benefits of the reduction of road and rail noise could be up to 10.8 billion euros in market value of residences and land. Similar studies in other countries [8] relate a decrease of 20 euro in an average monthly letting value of 350 euro for every dB above the level of 50 dB. Moreover, since the renting values are connected to taxes, this could also affect the tax revenues of the authorities. To conclude, the numbers above confirm that noise reduction measures can have multiple benefits not only for the citizens but also for the authorities, thus, high cost can be justified.

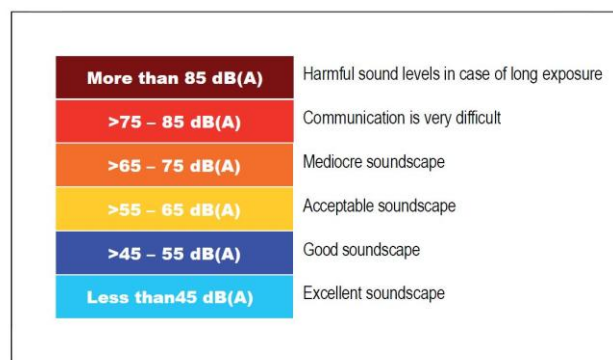
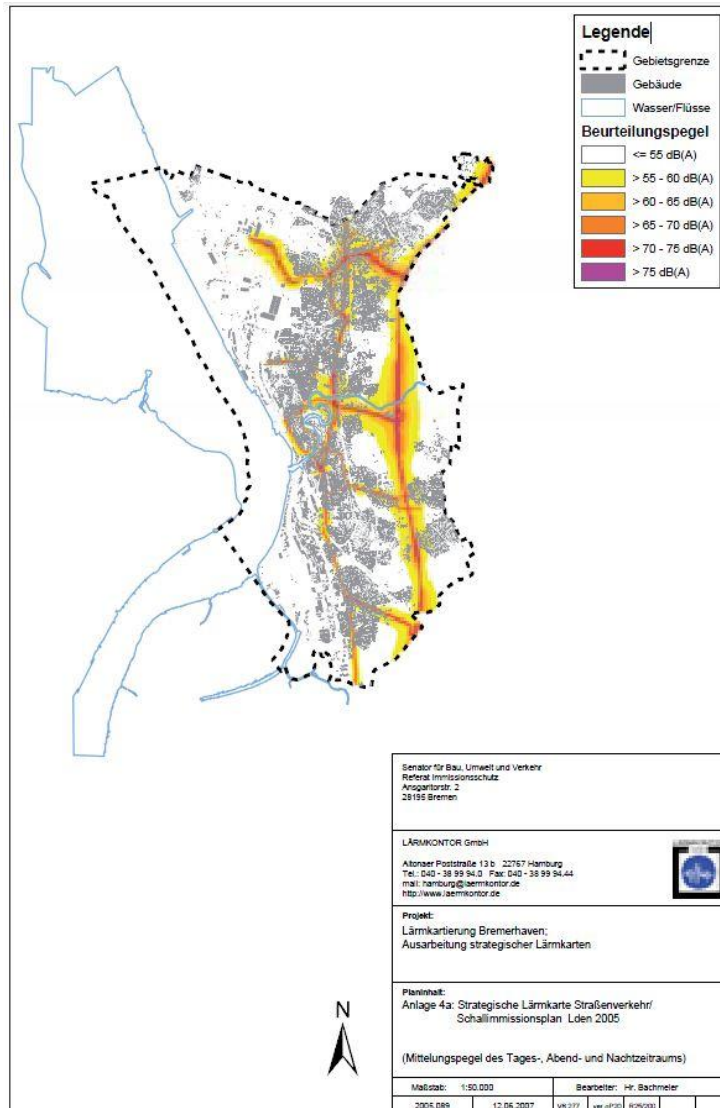


Figure 2.11: Noise map for the City of Bremerhaven, Germany (Noise exposure from road traffic in Lden) [20]

According to a survey, in which took part 2046 persons from 14 European countries, most of them (74%) have lived close to noisy areas for an average duration of about 11 years and no hearing problems were appeared in 88% of them. A remarkable point is the high levels of noise annoyance of Germany and Poland citizens in contrast with those from Italy and other countries (Figure 2.12). Mainly, due to the fact that 53% of the German and 49% of the Polish participants live in noisy areas, while less than 44% of the rest participants stay in similar areas [8].

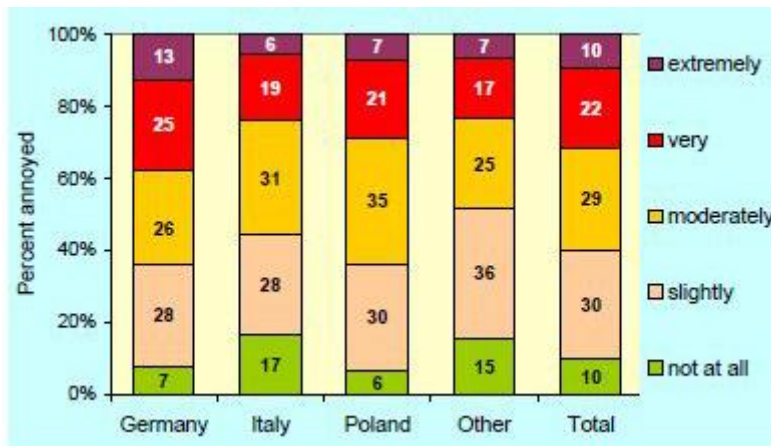


Figure 2.12: Overall noise annoyance at home [8]

Road traffic is the most annoying noise source. More than half participants referred that were moderately annoyed by it but only 16% by railway noise. It is significant the difference between 28% and 7% of participants who judged road traffic and railway as noisy, respectively (Figure 2.13) [8].

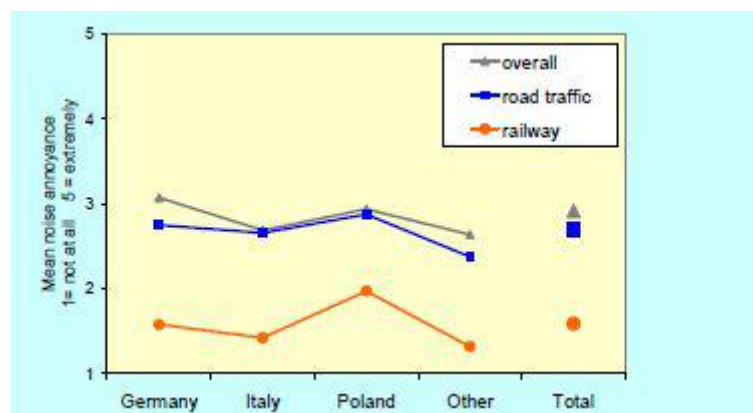


Figure 2.13: Noise annoyance in European built up areas [8]

2.8.3 Life-cycle analysis of new automobile technologies

Many transportation fuel-cycle analyses have been conducted since the 1980s, estimating the energy and environmental impacts of fuel/vehicle system. In the past fuel cycle analyses were concentrated mainly on battery-powered electric vehicles (EVs), but the current transportation fuel-cycle analyses are focused on fuel-cell vehicles (FCVs) due to the zero emissions [9]. In order energy and environmental effects to be compared between fuel cell vehicles and the relative with internal combustion engine technology requires a full fuel-cycle analysis. These analyses are named as “life-cycle” or “cradle-to-grave” but mainly in the transportation field is referred as a “well-to-wheels” (WTW) analysis. However, WTW analyses do not determine the energy and emissions which are demanded by the fuel production process, unlike with life-cycle analyses [9].

In the following charts the results of the analysis are presented. All categories of future technologies are compared to an “evolved baseline”. As baseline is chosen a mid-size passenger car, relative with consumer characteristics to a 1996 “reference car”, considering that fuel consumption and GHG emissions have been decreased by about a third by 2020 [9]. In order to compare all categories, the analysis is settled on an equal Power Weight ratio (75 W/kg) [10].

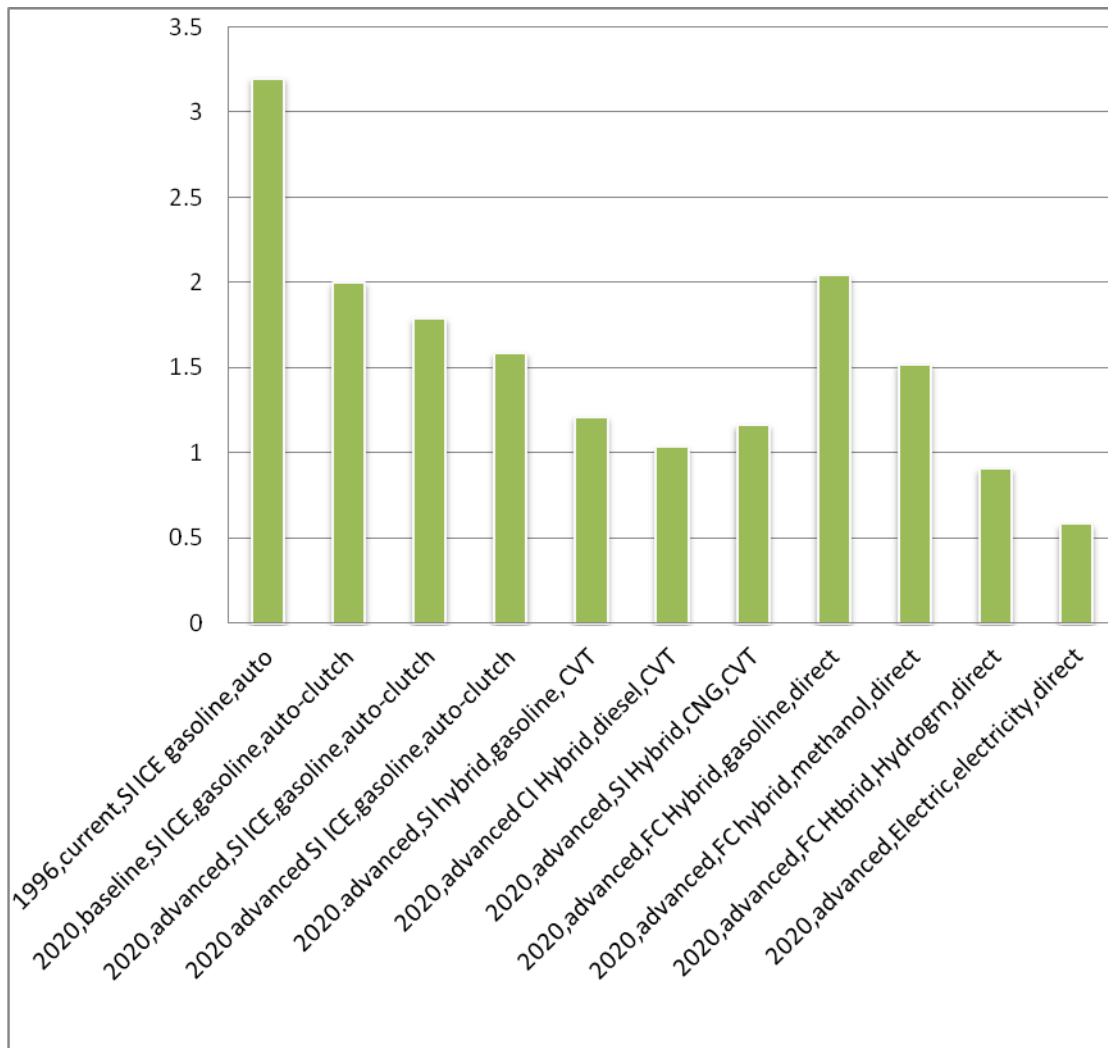


Figure 2.14: Energy Use (MJ/km) [10]

The previous chart (Figure 2.14) illustrates the energy demands per kilometer in an urban environment. Generally, all the future predictions are less intensive on energy in comparison with 1996 baseline technology. The highest energy consumptions is appearing in both FC, Hybrid, gasoline, with direct transmission and SI ICE, gasoline, auto-clutch. A remarkable point is the consumption of the "electric, electricity, with direct transmission" type, which is almost 0.5 MJ/km.

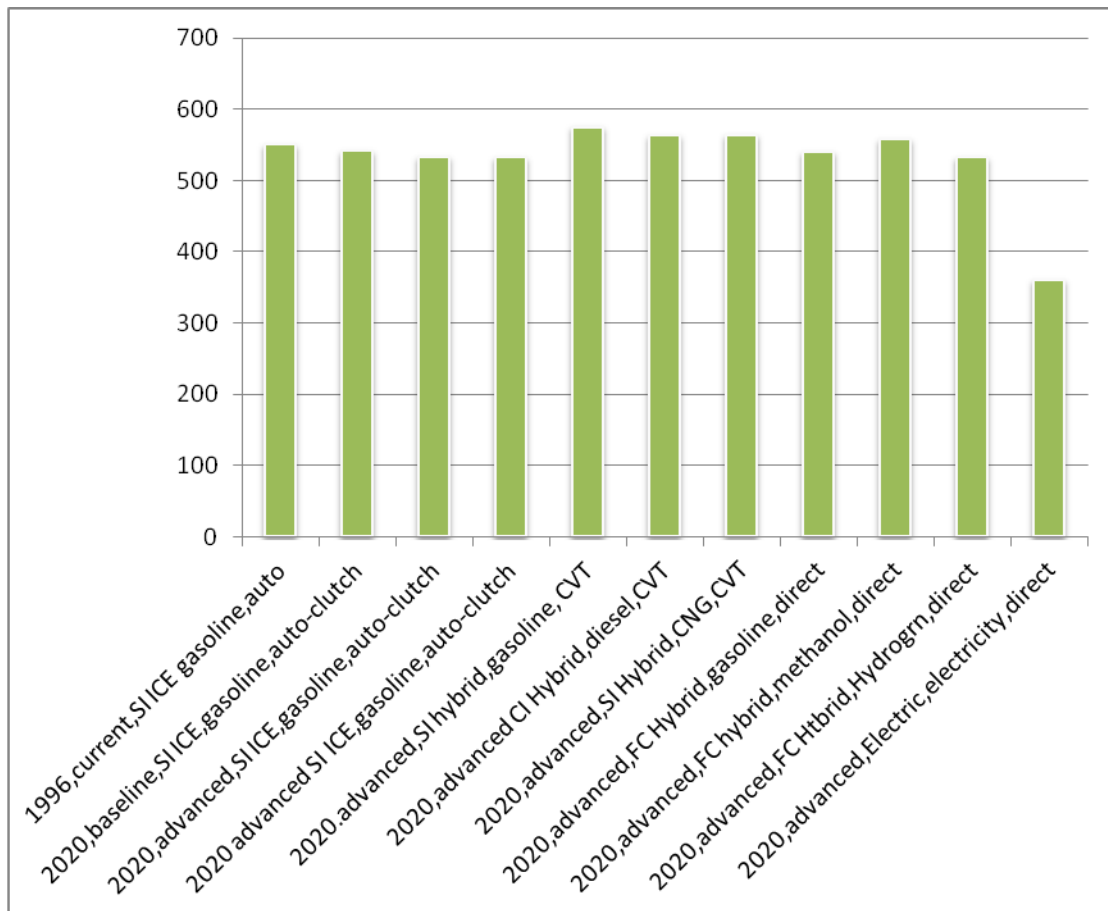


Figure 2.15: Range (km) [10]

Range is a significant factor in order to compare the future vehicle technologies. The chart in Figure (2.15) shows a slight fluctuation among different technologies (SI Hybrid gasoline CVT has the longest range, over 570km) but "Electric, electricity with direct transmission" type differs, covering only the two third of kilometers than the rest vehicles do so. In the other hand, it is the most efficient technology (more than 60 per cent) according to the chart below (Figure 2.16), almost twice more than the second one ("FC, Hybrid, Hydrogen with direct transmission" type).

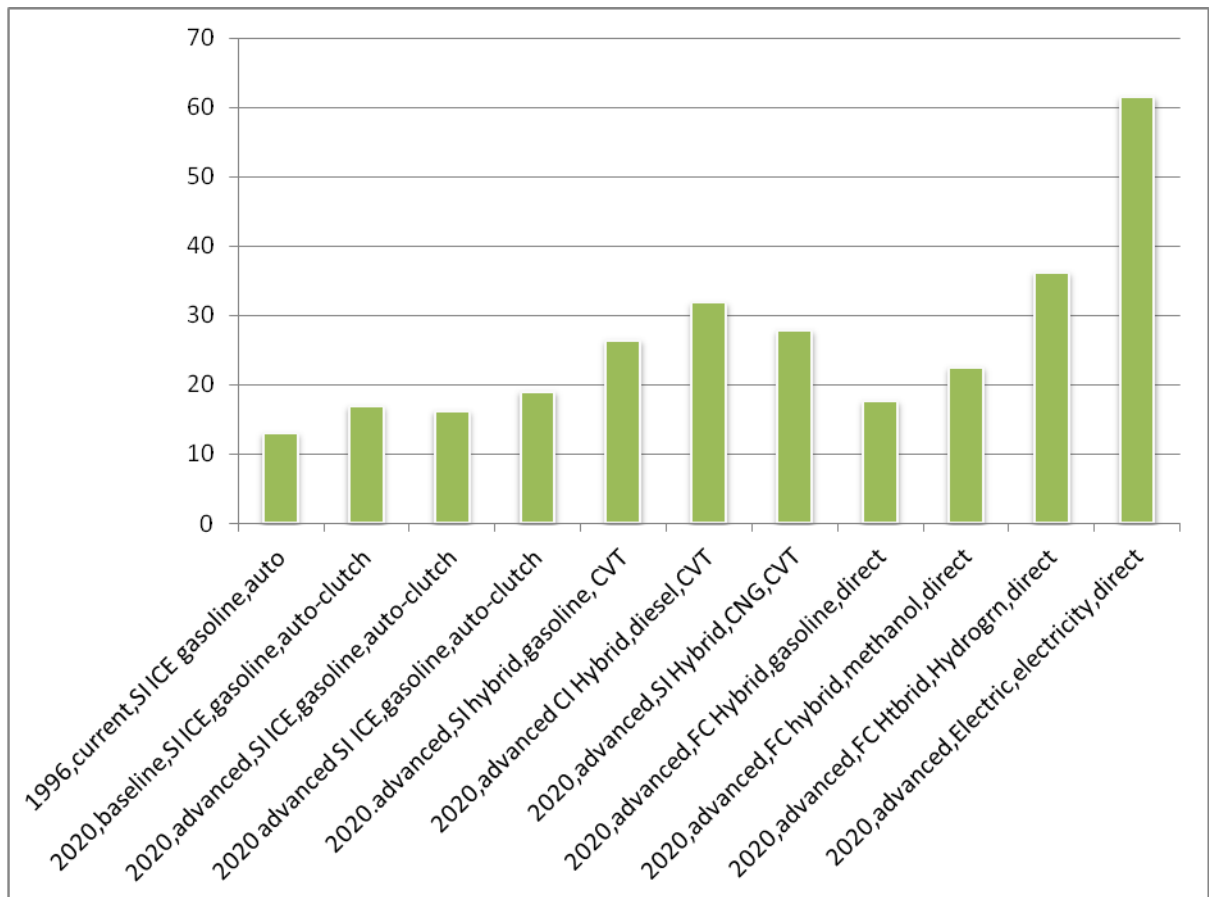


Figure 2.16: Tank-to-Wheel Efficiency (%) [10]

A main advantage of electric vehicles is the high tank to wheel efficiency in comparison to the rest categories. The second most competitive category is the "advanced Fuel cell vehicles"; it is significant that its efficiency is reduced almost by 50% compared to battery vehicles. This difference is due to the high efficiency of electric motors. Moreover, new technologies such as in-wheel motors have been already developed, offering the same advantages as an ordinary motor, covering less space.

The European Commission will assess the feasibility of the Cycle Carbon Emission target suggested by the European Parliament of reaching **70 gCO₂/km by 2025** [11]. The chart below (Figure 2.17) illustrates the future emissions in all categories by 2020, which is less than 70gC/km as the European Commission suggests. A significant point is the zero carbon emissions of both Hydrogen and Electric vehicles.

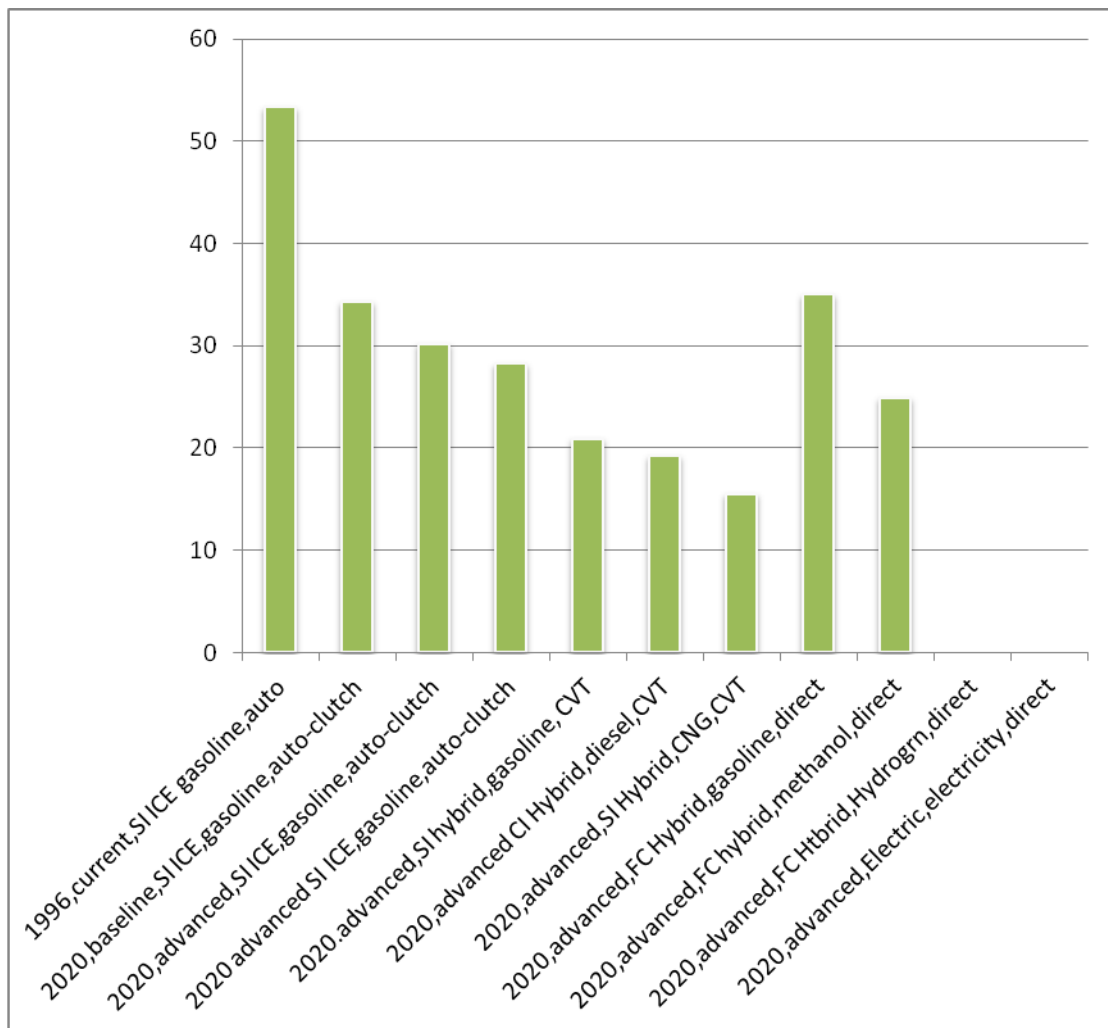


Figure 2.17: Cycle Carbon Emission (g C/km) [10]

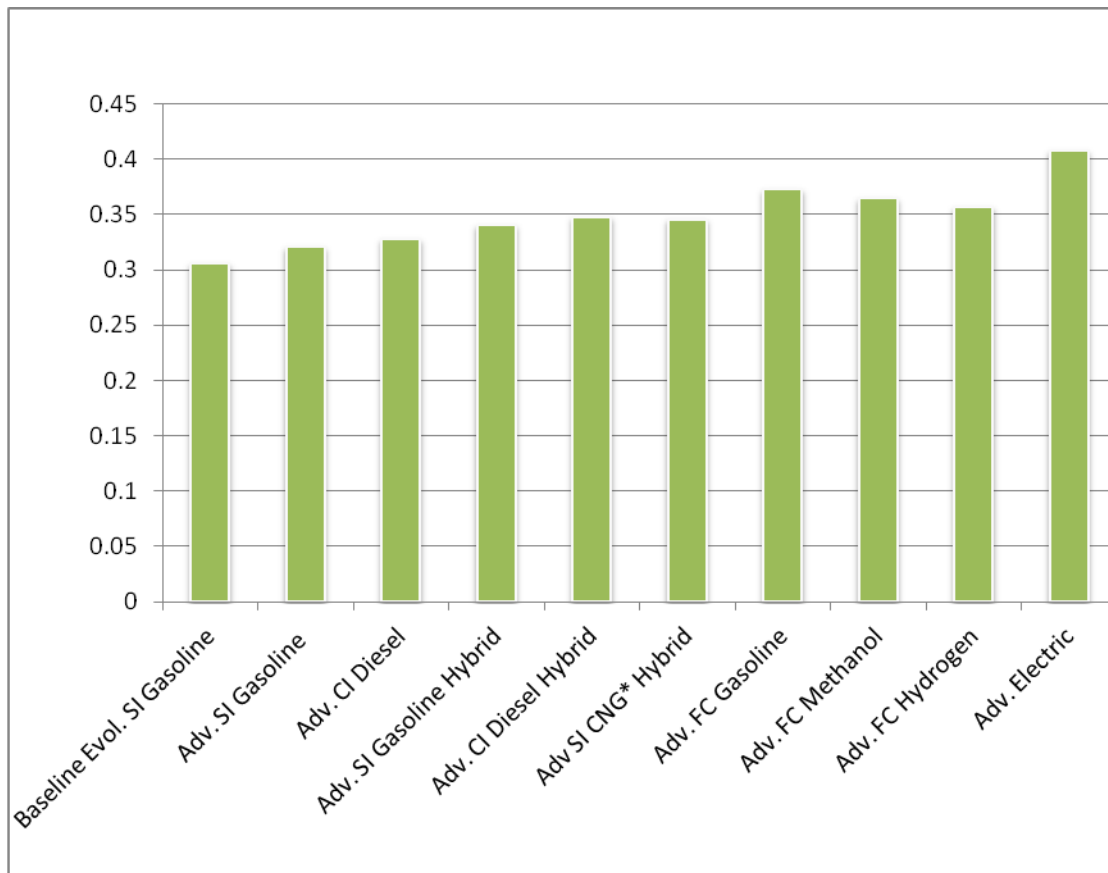


Figure 2.18: Comparison of US Operating Costs in \$(1997)/km for Selected New Vehicle Options in 2020 [10]

Even though electric vehicles have negligible emissions, a high cost per kilometer is appeared, as it is shown in Figure (2.18). Estimates indicate that the more efficient vehicles, from an energy consumption standpoint, are more expensive, and the charges associated with increased price more than offset any fuel savings at 1997 US tax rates. Moreover high cost appears in the group of "Fuel cell Hybrid Vehicle", due to the high cost of FC module.

Summing up, both electric vehicles and Fuel cell powered vehicles are the least energy demanding vehicles, produce zero CO₂ emissions and provide the highest tank to wheel efficiency. The disadvantages are focused on the low range that could be covered and to the high cost per kilometer. But according to Cost Benefit Analysis of Advanced Power trains from 2010 to 2045 [22], battery , FC, and Electric machine cost per KW are sharply reducing, in contrast to electric machine peak efficiency which shows a significant rise [12] (Figures 2.19 - 2.22).

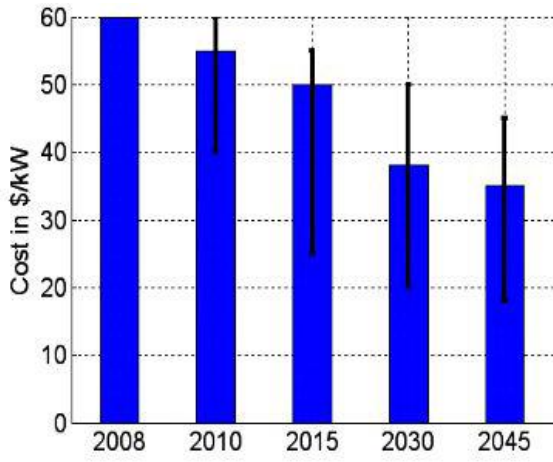


Figure 2.19: Battery Cost for High Power Applications [12]

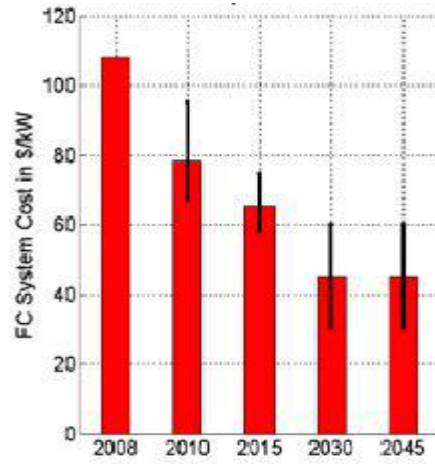


Figure 2.20: FC System Cost [12]

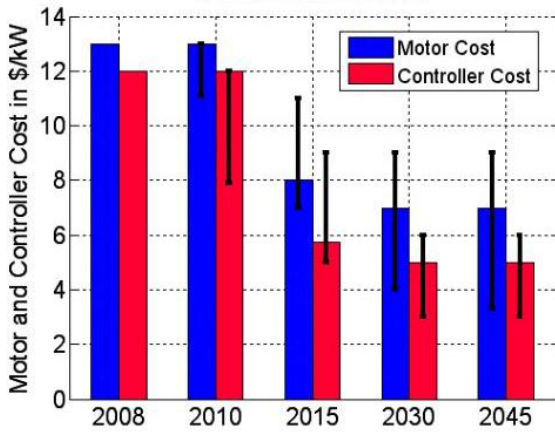


Figure 2.21: Electric Machine Cost [12]

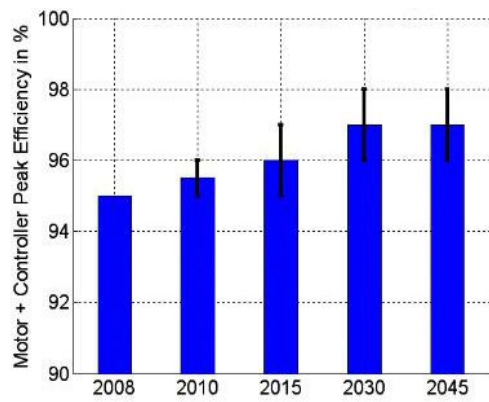


Figure 2.22: Electric Machine Peak Efficiency [12]

3. Extended Range Electrical Vehicle (EREV)

Analyzing the transportation impacts, as much in environment as in the society, investigating the habits of customers, finally was chosen the concept of a two seat Extended Range Electrical Vehicle as a proposal for a more green transportation. In this chapter the modeling of an EREV is presented, by building an approach on the vehicle's performance evaluation and showing the main differences with respect to an ordinary ICE vehicle.

3.1 Vehicle performance - Tractive effort

The production of the tractive effort equation is the initial step in vehicle performance modeling, calculating the force which is propelling the vehicle forward, transmitted to the ground through the drive wheels. The total tractive effort is the sum of rolling resistance force, aerodynamic drag, the hill climbing force, and the acceleration force. In the picture below (Figure 3.1) the main forces are plotted, which a vehicle has to overcome in order to move forward.

- F_{rr} is the rolling resistance force
- F_{ad} is the aerodynamic drag
- F_{hc} is the hill climbing force

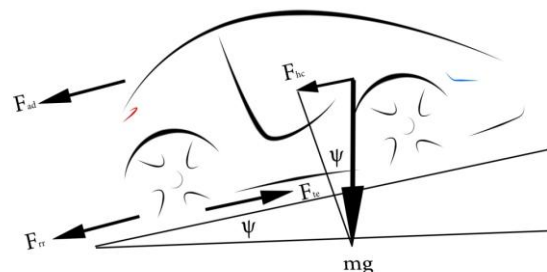


Figure 3.1: Forces acting on a vehicle

Rolling resistance force

The rolling resistance is due to the friction of the vehicle on the road. It is almost constant and is connected more to vehicle weight than vehicle speed. It is computed as:

$$F_{rr} = \mu_{rr} mg \quad 3.1$$

where μ_{rr} is the coefficient of rolling resistance, which has a range between 0.015 and 0.005, depending on the type of the tire and the tire pressure. The lowest figure of rolling resistance coefficient is usually met on electric vehicles tires [13].

Aerodynamic drag

The force which is being resisted on the motion of vehicle while it is traveling at a particular speed is called drag force. This is due to friction of the vehicle body moving through the air. It depends on the frontal area, the shape and velocity as in the following equation (Figure 3.1):

$$F_{ad} = \frac{1}{2} \rho A C_d v^2 \quad 3.2$$

where ρ is the density of the air, A is the frontal area, v is the velocity, C_d is a constant called the drag coefficient. The shape of the vehicle influences the value of the drag coefficient C_d and can be reduced by proper vehicle design. Generally, the C_d for a commercial vehicle is about 0.3, but some electric vehicle designs have achieved values as low as 0.19. For an electric vehicle a better value of C_d could be achieved due to the flexibility in the location of the major components, in addition with less need for cooling air ducting [13].

Hill climbing force

When a vehicle travels up or down a slope, a force due to vehicle's weight produces a component, which is always directed to the downward direction. It is computed as (Figure 3.1) [13]:

$$F_{hc} = mg \sin \psi \quad 3.3$$

Acceleration force

The force which is required to provide a linear acceleration while vehicle velocity is changing is called as acceleration force. This force is given by equation derived from the Newton's second law:

$$F_{la} = ma \quad 3.4$$

However, in order to produce linear acceleration a force for rotational acceleration is required, making the rotating parts to turn faster. That force is computed by the following equation [14]:

$$F_{\omega\alpha} = I \frac{G^2}{r^2 n_g} \quad 3.5$$

where G is the gear ratio of the system connecting the motor to the axle, I is the moment of inertia of the rotor of the motor, r is the tire radius and n_g is the efficiency of the gear system.

In case of lack in some information during the modeling of a vehicle, such as the moment of inertia of the motor, a reasonable approximation is to increase the mass by 5% in equation (3.4), and to ignore the $F_{\omega\alpha}$ term [14].

Total tractive effort

$$F_{te} = F_{rr} + F_{ad} + F_{hc} + F_{la} + F_{\omega\alpha} \quad 3.6$$

3.2 Energy requirements

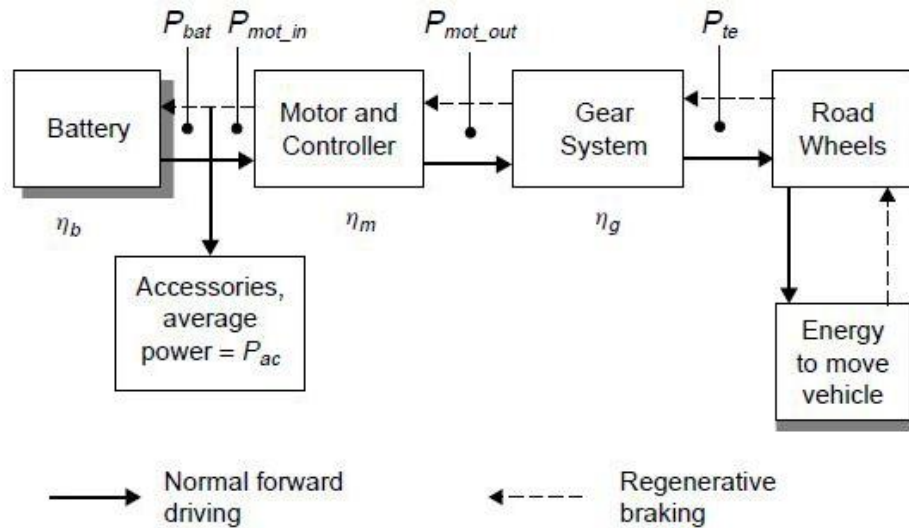


Figure 3.2: Energy flow [14]

The energy required to move the vehicle per second (the power) is equal to the tractive effort multiplied by the velocity:

$$\text{Energy required per second} = P_{te} = F_{te} \times u$$

Generally the electrical power required by the motor is greater than the mechanical output power due to the inefficiencies of the motor, the controller and the gear system. The following equations describes this proportion [14]:

$$P_{mot_in} = \frac{P_{mot_out}}{\eta_m} \quad P_{mot_out} = \frac{P_{te}}{\eta_g} \quad 3.7 \text{ \& } 3.8$$

3.3 Assumptions for modeling

The following assumptions were used as a starting point for our design:

- ✓ Vehicle total mass: 1140 kg (70kg+70kg for passengers)
- ✓ Rolling Resistance coefficient: 0.015
- ✓ Aerodynamic drag coefficient: 0.3
- ✓ Motor efficiency: 0.93
- ✓ Front area: 1.8 m^2
- ✓ Transmission efficiency (single gear) n_g : 0.9
- ✓ Acceleration time: 10sec
- ✓ Tire radius: 0.381m
- ✓ Velocity: 13.8 m/sec

Calculation

Using the previous assumptions the following calculations can be made:

- Rolling Resistance: $F_{rr} = \mu_{rr} mg = 0.015 \times 1140 \text{ kg} \times 9.81 \frac{\text{m}}{\text{s}^2}$

$$F_{rr} = 55.9 \text{ N}$$

- Aerodynamic Drag: $F_{ad} = \frac{1}{2} \rho A C_d v^2 = 0.5 \times 1.25 \text{ kg} \cdot \text{m}^3 \times 1.8 \text{ m}^2 \times 0.3 \times 13.8^2 \frac{\text{m}}{\text{s}^2}$

$$F_{ad} = 64.3 \text{ N}$$

- Acceleration Force: $F_{la} = ma = 1197 \text{ kg} \times 1.38 \frac{\text{m}}{\text{s}^2}$

$$F_{la} = 1651.8 \text{ N}$$

- Hill climbing: $F_{hc} = mg \sin \psi = 1140 \text{ kg} \times 9.81 \frac{\text{m}}{\text{s}^2} \times \sin 10^\circ$

$$F_{hc} = 1941.9 \text{ N}$$

Thus, according to equation 3.6 $F_{te} = 3713.9 \text{ N}$

$$P_{te} = F_{te} v = 3713.9\text{N} \times 13.8 \frac{\text{m}}{\text{s}}$$

$$P_{te} = 51.25 \text{ kW}$$

$$P_{\text{mot_out}} = \frac{51.25 \text{ kW}}{0.9} = 56.94 \text{ kW}$$

$$P_{\text{mot_in}} = \frac{56.94}{0.92} = 61.89 \text{ kW}$$

By separating the power to the four wheels of the vehicle, a 15.47 kW motor is required for each wheel.

3.4 Wheel hub/In-Wheel motor

Using a single central motor, the gearless wheel motor drive systems for pure electric or hybrid vehicles have many advantages; mounting the motors directly to the wheels simplifies the mechanical layout. In that way, the overall reliability and efficiency is improved, reducing the drive line components. Another important advantage of that technology is the overall decrease of vehicle weight due to the fact that mechanical differential and gear reduction are not used. However, the total torque is produced directly into the wheel by motors, increasing both the size and weight of them [15].

For this work an in-wheel motor was chosen constructed by the NTN company. NTN has been developing the in-wheel type integrated motor axle unit for electric vehicles. The unit accomplishes compact size and light weight by integrating a hub bearing, a cycloid reducer and a high-speed motor, realizing least increase in the unsprung mass of in-wheel motor vehicles (Figures 3.3, 3.4). Moreover NTN has developed a new reducer that can decrease the required maximum torque for the motor so that a lighter motor can be used [15].

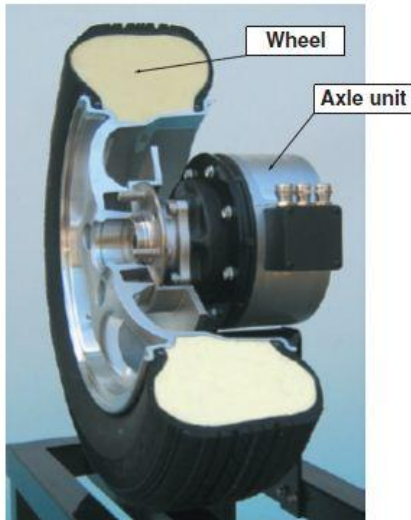


Figure 3.3: Installation of the unit [15]

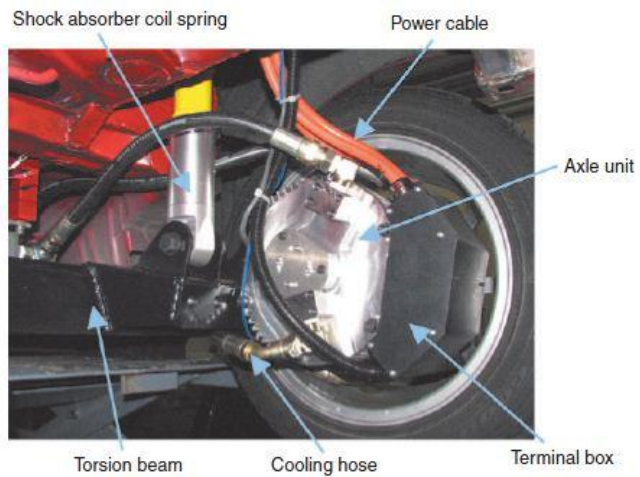


Figure 3.4: Mounted unit [15]

NTN in-wheel motor axle unit schematic is illustrated in Figure 3.5. The basic components of this design consist of a hub, a reducer, and a motor. It is achieving a 94% transmission efficiency using a rolling contact type reducer (Figure 3.6). The specifications of the motor are illustrated in Table 3.1 below [15].

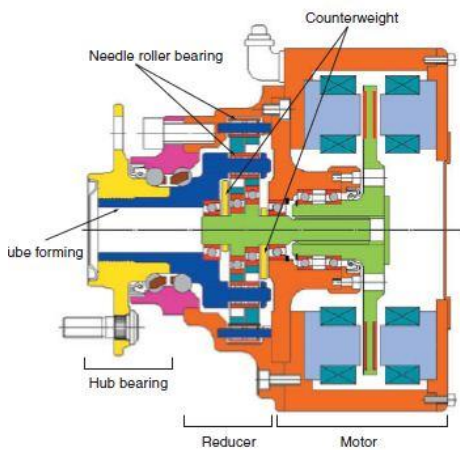


Figure 3.5: Schematic of axle unit [15]

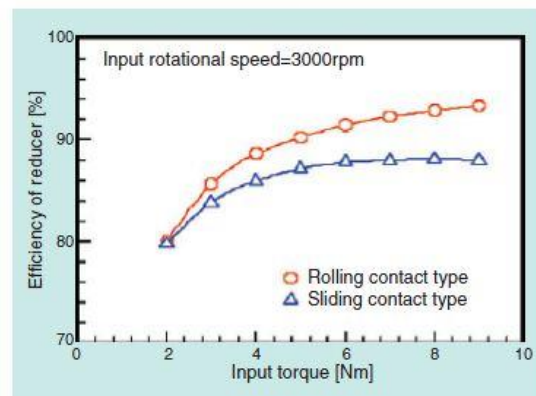


Figure 3.6: Efficiency of reducer [15]

| | |
|-------------------------|---|
| Max. output | 20kW |
| Max. torque | 490Nm |
| Mass | Approx. 25 kg |
| Reducer type | Cycloid reducing system |
| Reduction ratio | 1/11 |
| Motor type | Axial gap type permanent magnet synchronous motor |
| Max. motor speed | 15000min-1 |

Table 3.1: Specifications of in-wheel motor [15]

3.5 Power inverter

A power inverter, or inverter, is an electrical device that changes direct current (DC) to alternating current (AC); the converted AC can be at any required voltage and frequency with the use of appropriate transformers, switching, and control circuits. Solid-state inverters have no moving parts and are used in a wide range of applications, from small switching power supplies in computers, to large electric utility high-voltage direct current applications that transport bulk power. Inverters are commonly used to supply AC power from DC sources such as solar panels or batteries (Table 3.2) [15].

| | |
|--------------------------|---|
| Supply voltage | Max. 450 V |
| Output | 30kW |
| Dimensions | W400×D500×H248mm |
| Carrier frequency | 20kHz |
| Drive system | Rectangular wave PWM system |
| Cooling system | Forced cooling |
| Powering system | 120–180°degrees switchoverr powering system |

Table 3.2: Specifications of the inverter [15]

3.6 Battery range and size

We compare with a similar gasoline vehicle with a fuel consumption of 6.5lt/100 Km. The specific energy of gasoline fuel is approximately 13kWh/kg and the conversion efficiency of the engine and transmission is approximately 10%, resulting in 1.3 kWh of energy per liter of fuel stored delivered at the wheels. In order to travel 150 km the vehicle will consume 10 liters of fuel, which weights approximately 7.6 kg allowing for fuel density. This fuel has an energy value of 98.8, and the energy delivered to the wheels will be 9.8 kWh allowing for the 10% efficiency. This can be divided by the electric motor and transmission efficiency, typically about 0.7 (70%), to give the energy needed from the battery, i.e. **14.11 kWh**. Hence if a lithium ion battery is used (specific energy 90Wh/kg) and energy density 200Wh/L [23] the battery mass will be **70 kg**, occupying **23lt (0.23m³)** respectively [14].



figure 3.7: Electric vehicle batteries [27]

3.7 On-board battery charger

Battery charging from a normal domestic electricity supply is achieved via an on-board charger which converts main AC voltage to a suitable charging voltage for the traction battery. It is compatible with all international power grids and is designed to charge a vehicle battery pack quickly. A full charge from at or near empty can be achieved in around 4.5 hours (Table 3.3) [24].



Figure 3.8: On-board battery charger [24]

| | |
|------------------|---|
| Input | Input Voltage Range: 85 to 265 VAC Input Frequency Range: 45 to 70 Hz Input Current: 16 ARMS max |
| Output | Output Voltage Range: 170 to 440 VDC Output Power: 3.3kW max Output Current: 12 ADC max |
| Packaging | Volume: < 5.6L Weight: < 5kg |

Table 3.3: Specifications of the on board battery charger [24]

3.8 Engine/Generator size

The power rating of the engine/generator is designed to be capable of supporting the vehicle at a regular urban speed (100 km/h) on a flat road. Figure 3.9 shows that the engine power needed at 100 km/h is 22 kW, in which energy losses in transmission (90% of efficiency), motor drive (85% of efficiency), and generator (90% of efficiency) are involved. [13].

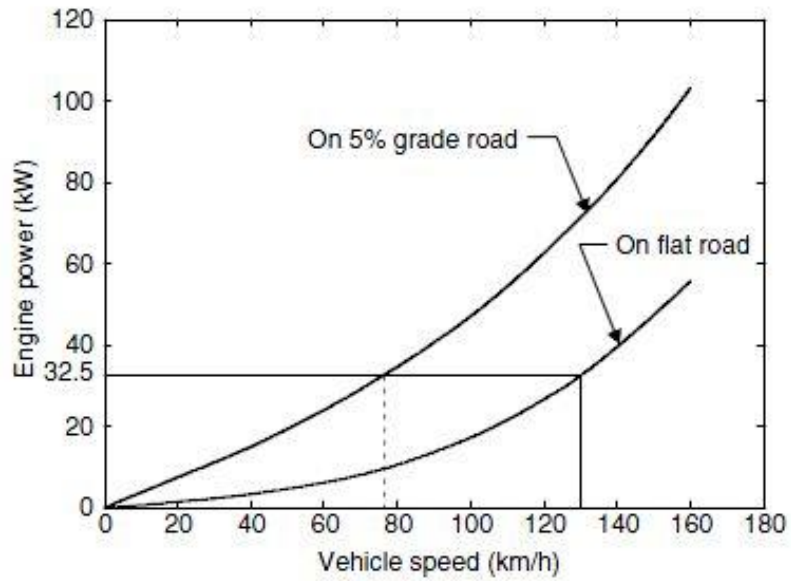


Figure 3.9: Engine power vs. vehicle constant speed on a flat road and at 5% grade road [13]

Polaris Industries Inc. in collaboration with Wenko AG Swissauto, have already constructed a gasoline engine generator. It is a one-cylinder 325cc ICE, which supplies 26 kW of power to Brusa generator with 22kW electrical output. Generator acts as flywheel, dynamic balancer and starter as well (Figure 3.10 - Table 3.4) [16].

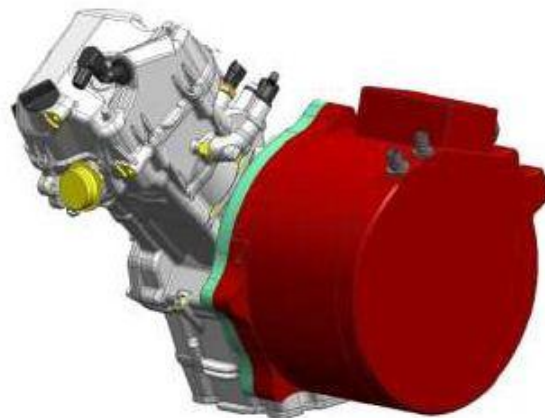


Figure 3.10: Polaris Generator [16]

| Displacement | One-cylinder 325cc ICE |
|-------------------------|------------------------|
| Power | 26kW |
| Electrical output power | 22kW |
| Weight | 38kg |
| BSFC ² | 240 g/kWh |

Table 3.4: Polaris Engine Specifications [16]

3.9 Fuel tank

Considering that the vehicle is traveling on a flat road with constant velocity of 50km/h the energy which is required is approximately 2kW (equations 3.1 & 3.2). The energy that battery supplies to the in-wheel motors is 14.11 kWh; with constant energy demanding in 3,5 hours the battery would have the half power, having 7kWh. The Brake Specific Fuel Consumption of the engine is 240g/kWh. In order to the ICE motor to recharge the battery needs 1680gr of gasoline. The density of gasoline is 719.7 gr/L so the ICE needs 1lt of gasoline to recharge the battery when 75km of distance have been already covered.

3.10 Wheelbase

The wheelbase l , is an important factor in the vehicles ride and handling properties and it is measured from the centre of the front to the centre of the rear axle. In case of a long wheelbase relative to the overall length of the vehicle, it is offered as much more spare space for passenger as decrease on the influence of the load on the axle load distribution.

² **Brake Specific Fuel Consumption (BSFC)** is a measure of fuel efficiency within a shaft reciprocating engine. It is the rate of fuel consumption divided by the power produced. It may also be thought of as power-specific fuel consumption, for this reason. BSFC allows the fuel efficiency of different reciprocating engines to be directly compared.

On the other hand the short body overhangs to high level of ride comfort due to the front and rear reduce the tendency to pitch oscillations; moreover, a short wheelbase makes cornering easier, giving a smaller swept turning circle [13]. The following ratio can be used as reference for a right wheel base (on small cars it is up to 0.72 [13])

$$i = \frac{\text{wheel base}}{\text{vehicle length}}$$

In the current project we set the following value: $i = \frac{1800\text{mm}}{2931\text{mm}} = 0.61$

3.11 Seat

The seating reference point, heel point, vertical and horizontal distance between these two points, and body angles specified by the vehicle manufacturer form the basis for determining the dimensions of the driver's seating position (Figure 3.11) [17].

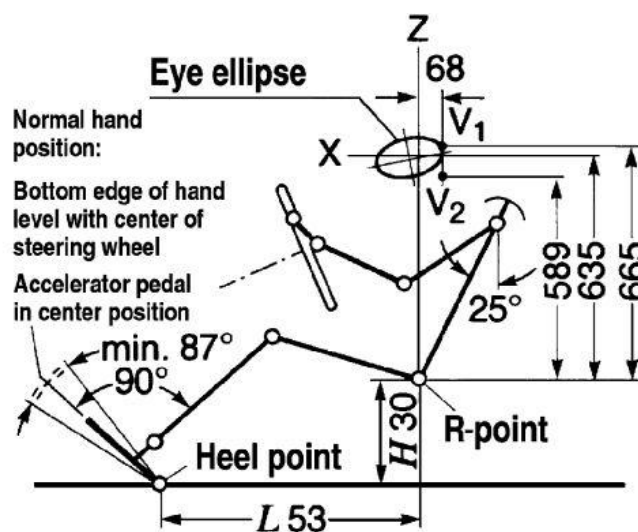


Figure 3.11: Parameters which determine passenger car driver seat location [17]

4. Preliminary design of the proposed EREV

According to the constraints which have been analyzed before, an urban vehicle was designed on CATIA V5R19. A small, two seat, extended range electric vehicle is the proposal of that thesis in order the environmental and social impacts of transportation to be faced.

The design started drawing the base lines of the vehicle using the spline mode as illustrated in Figure 4.1.

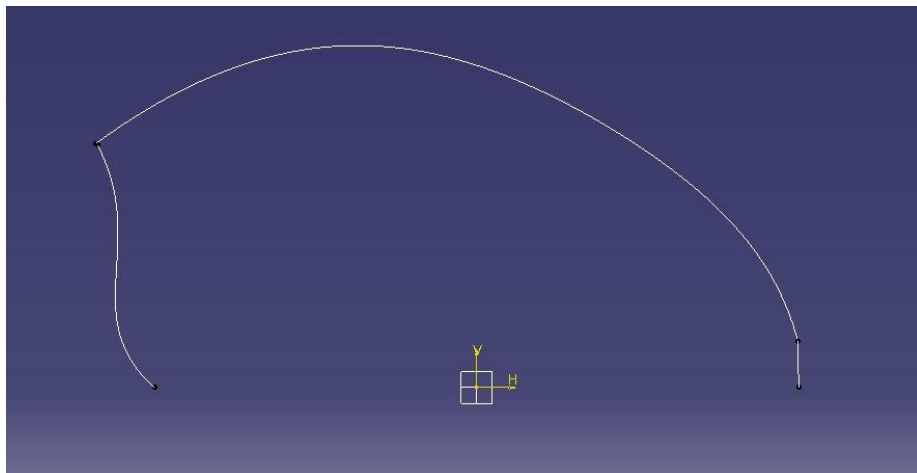


Figure 4.1: Basic line

The main surface was created afterwards, shaping the vehicle.



Figure 4.2: Main surface of the vehicle

Joining all the surfaces (command: Join) the volume of vehicle was created. Rounding the edges (command: Edge fillet), drawing windows (command: Split) and finally adding the wheels, a preliminary drawing of the urban vehicle was constructed, presented in the following Figures 4.3 to 4.7.

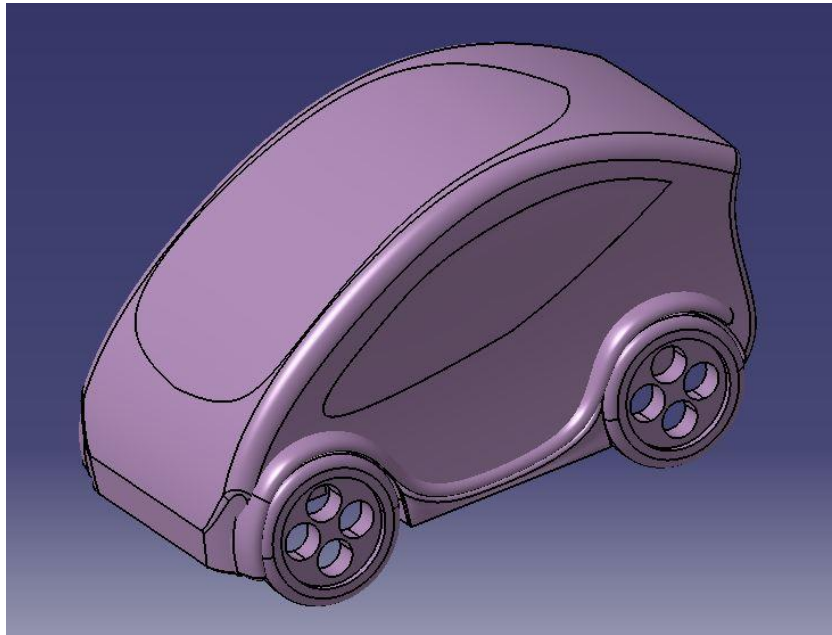


Figure 4.3: Side view of EREV

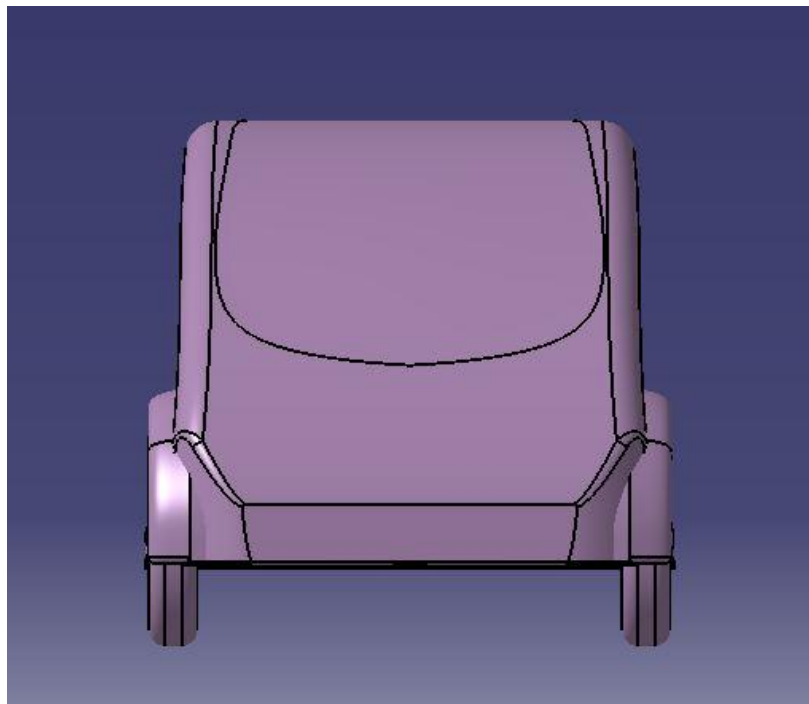


Figure 4.4: Front view of EREV

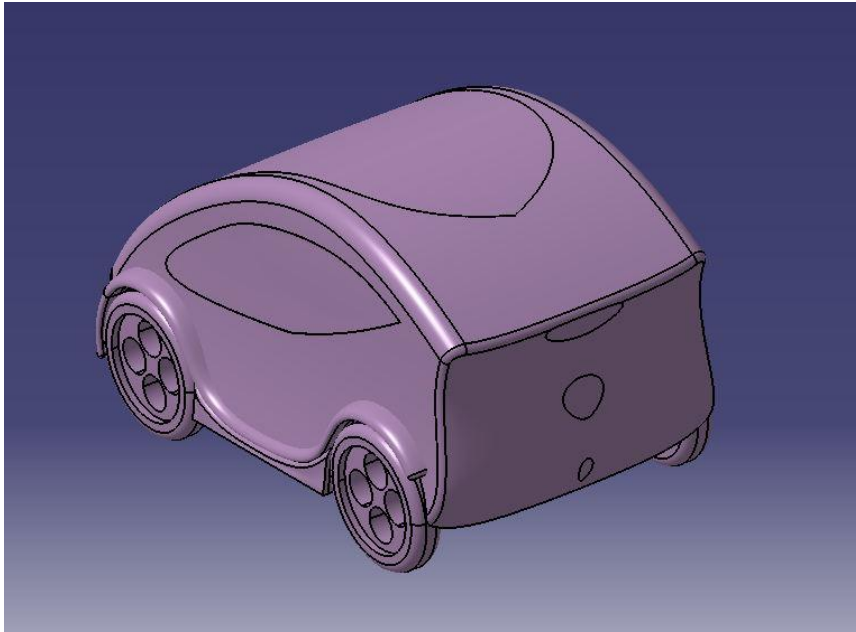


Figure 4.5: Rear side view of EREV

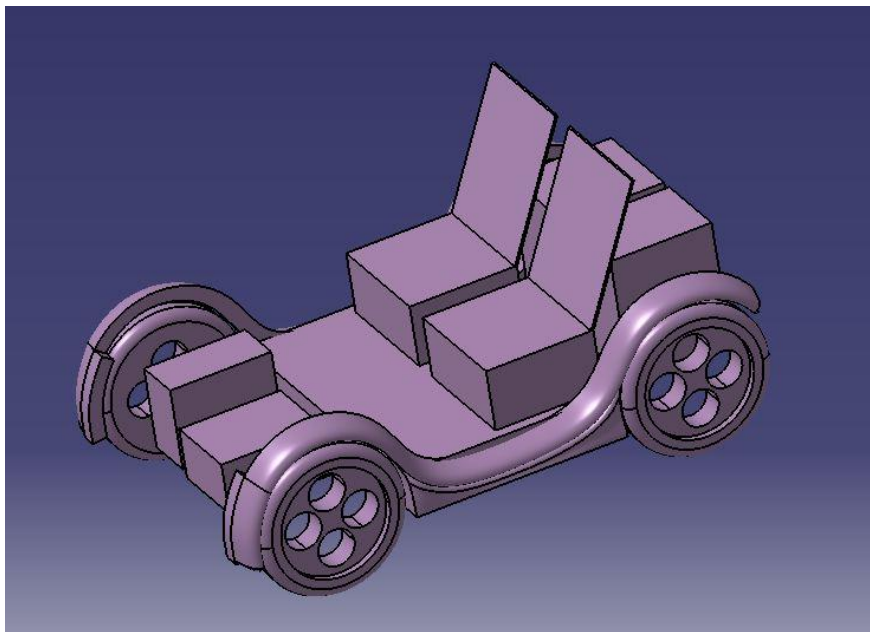


Figure 4.6: Volumes of parts for EREV

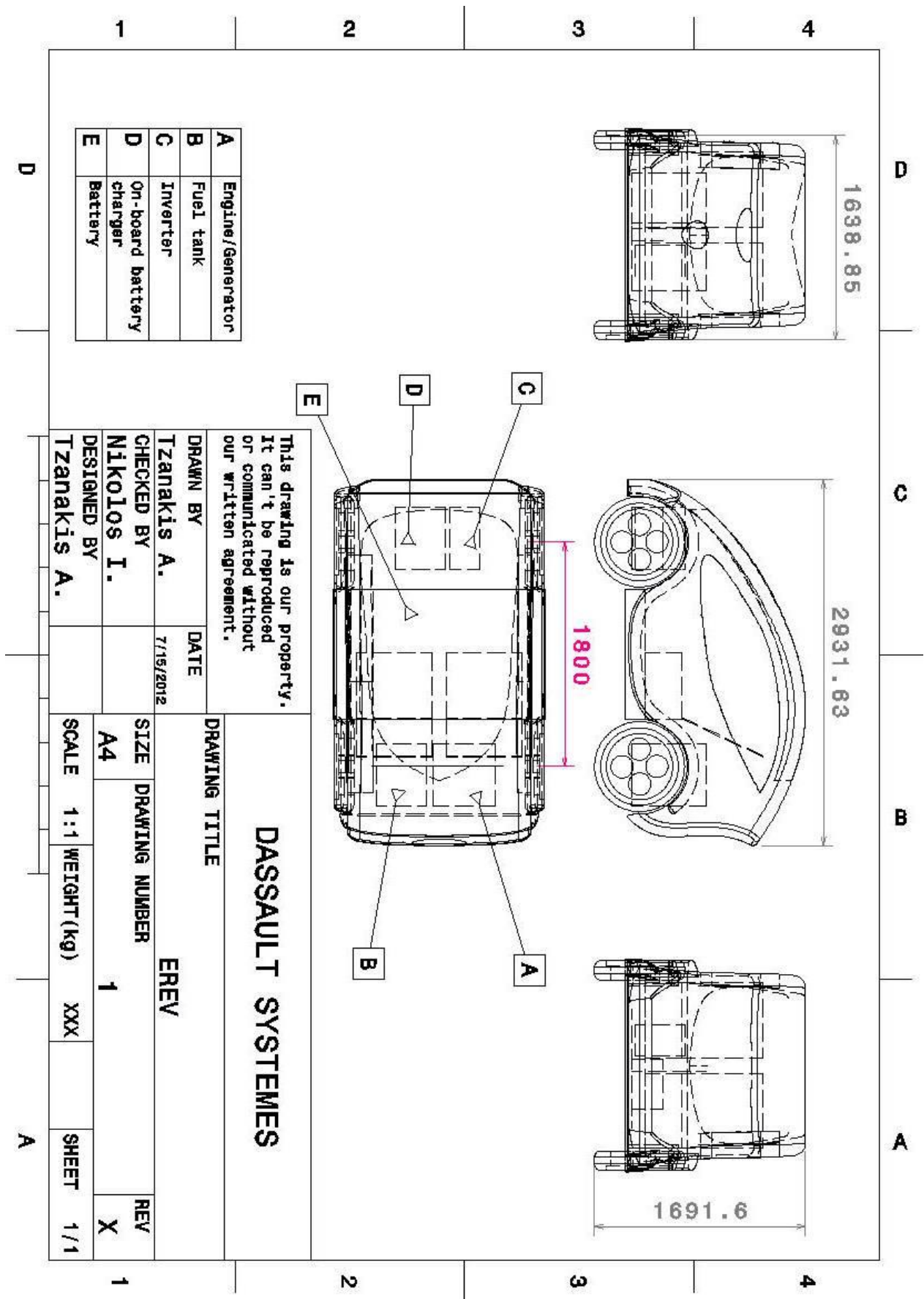


Figure 4.7: 2D drawing of EREV

Part B

5. Eco Racer Vehicle 2012

5.1 Methodology

The second part of this thesis aims at contributing to the design of a racing vehicle, with better aerodynamic efficiency than the previous models. The first phase was the aerodynamic analysis of the last model (ER11) of the vehicle in order a basis of comparison to be created. The construction of the 3D model on CATIA V5R19 and its aerodynamic simulation using ANSYS CFX v.11 consist the first step of the second phase, which was completed with the final choice among three alternative designs of the new vehicle. After the selection of the final design the construction of the vehicle took place, and the differences between the 3D model and the actual shape were identified.

5.2 ER11 analysis

Prior to the design of the new shape the aerodynamic efficiency of the previous model (ER11) of the vehicle should be computed in order to form a basis of comparison with the new designs. ANSYS CFX v.11 was used for the analysis of the flow around the vehicle; it is a widespread commercial Computational Fluid Dynamics (CFD) code, with the ability for mesh generation and post-processing of the solver results.

In order to simulate the flow around the previous (ER11) model of the vehicle some simplifications were adopted, to support the mesh generation around the vehicle and render the flow simulation easier:

- The bottom of the vehicle was closed with a planar surface.
- The frontal areas of wheel rims were set as closed surfaces.
- All the parts of the vehicle were considered as a single solid part.
- The wheels were considered as stationary.
- A very small clearance between the wheels and the ground was implemented to simplify the mesh generation at those regions.

Figures 5.1 and 5.2 illustrate some of these simplifications.

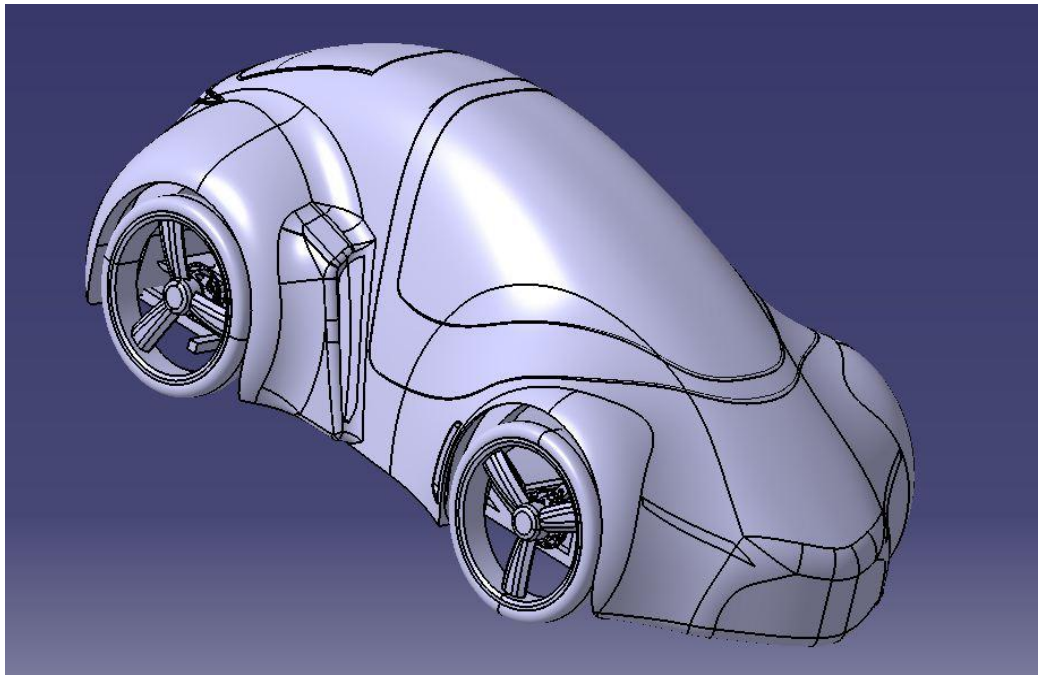


Figure 5.1: View of the vehicle before the simplifications

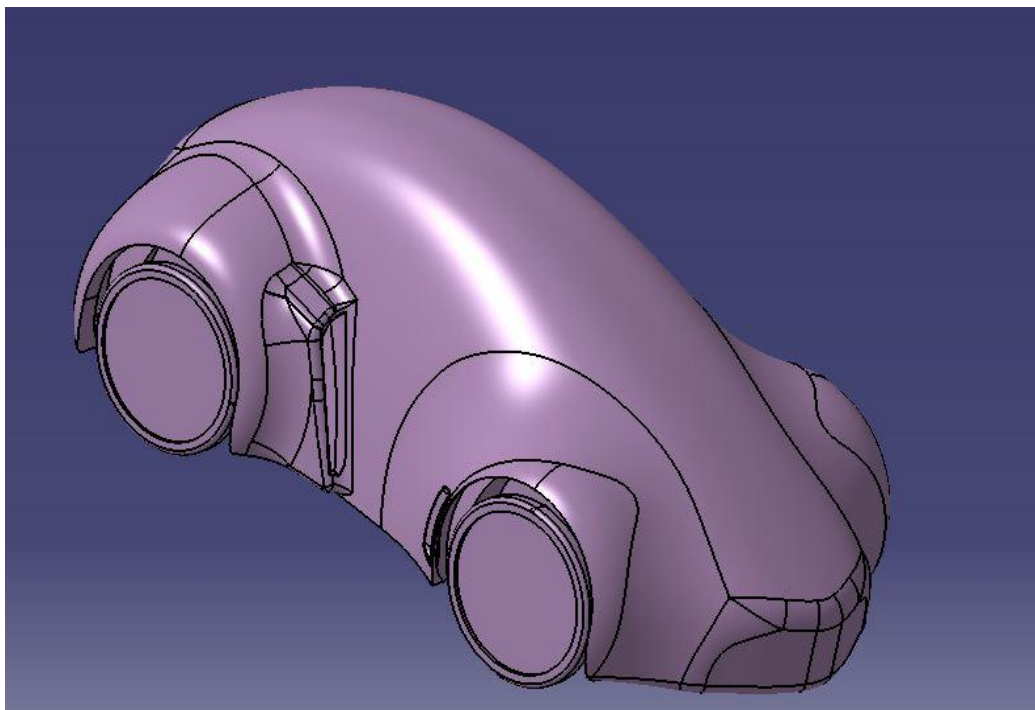


Figure 5.2: View of the vehicle after the simplifications

In order to construct the flow domain a rectangle containing the solid vehicle was constructed, taking into account its symmetry. The completion of this process is described in the following steps:

1. Definition of the frontal surface of the control volume (Figure 5.3).

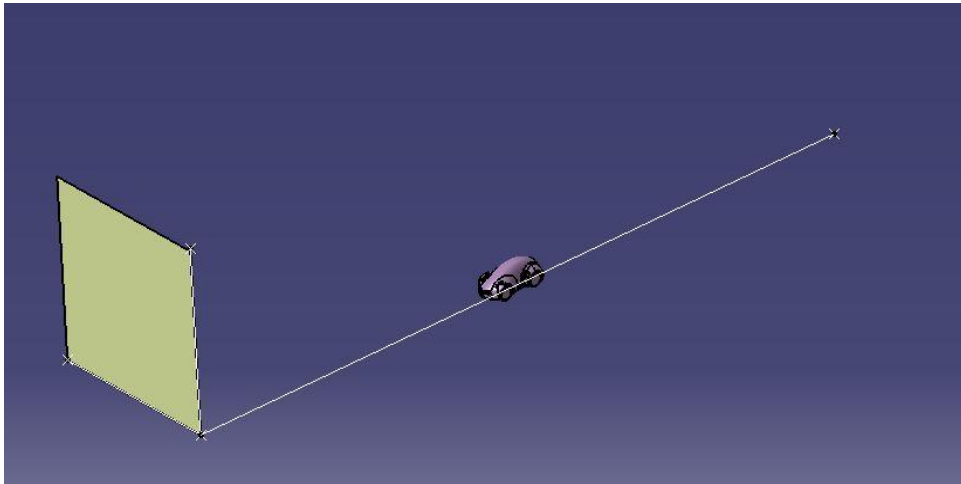


Figure 5.3: Points which define the size of the control volume

2. Definition of the control volume (Extrude) (Figure 5.4) Volume dimensions are $10L \times 10W \times 5H$ (with L , W and H the maximum vehicle dimensions in the corresponding directions).

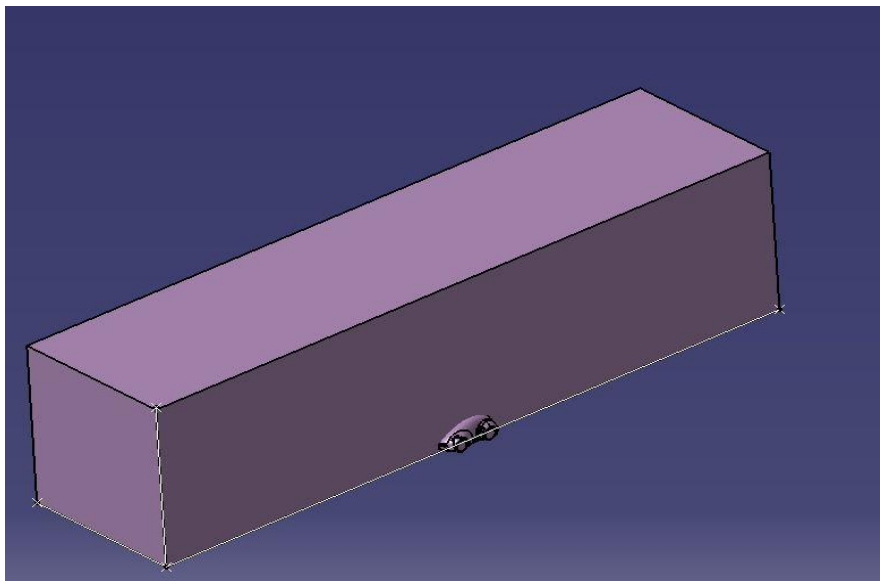


Figure 5.4: Control volume of the flow domain

3. Removing the vehicle from the rectangular volume to form the final fluid flow domain (Figures 5.5 - 5.6). Due to the symmetrical shape of the vehicle, only half of the flow domain was simulated, to decrease the computational power.

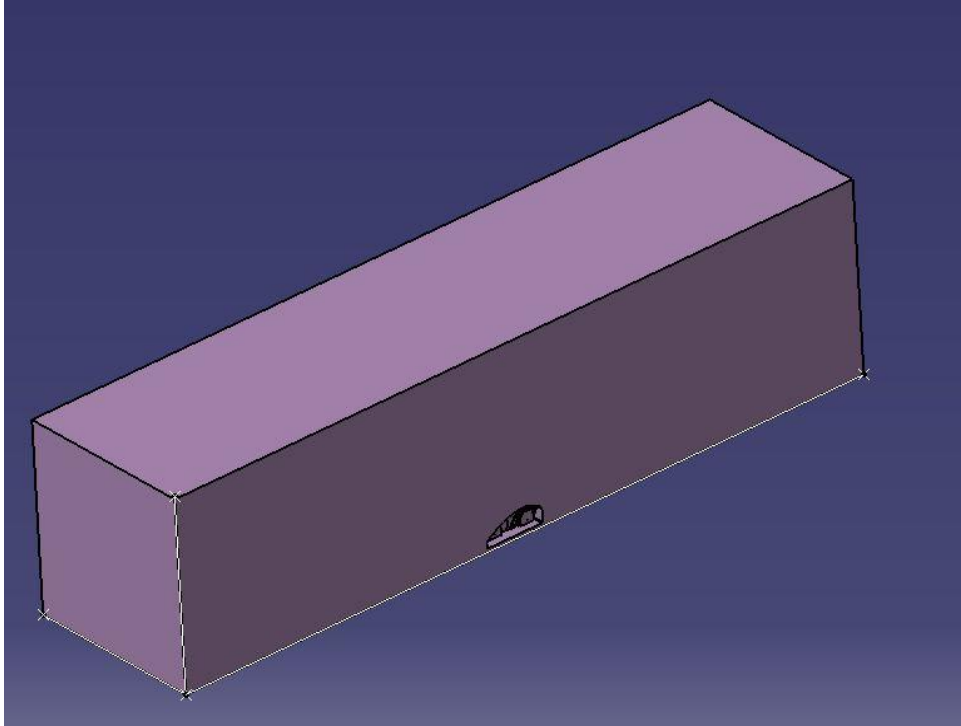


Figure 5.5: Air volume which includes the vehicle

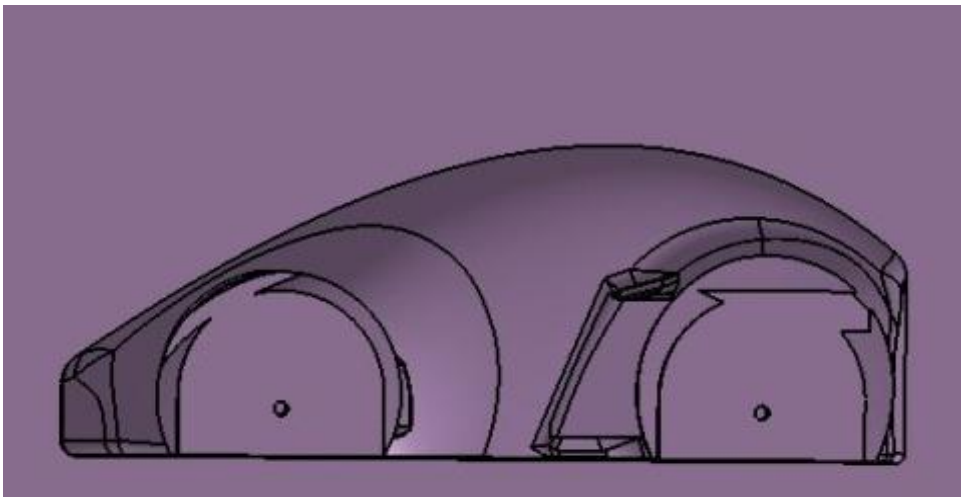


Figure 5.6: The cavity formed by the vehicle inside the flow domain

The final geometry was imported to ANSYS CFX 11.0 in which the final parameters were defined for the mesh generation.

Regions

The surface of the computational domain was divided in different regions to simplify the definition of the mesh generation parameters and better control mesh characteristics. The discrete regions used are described below.

- Default 2D Region: The vehicle (Figure 5.7).

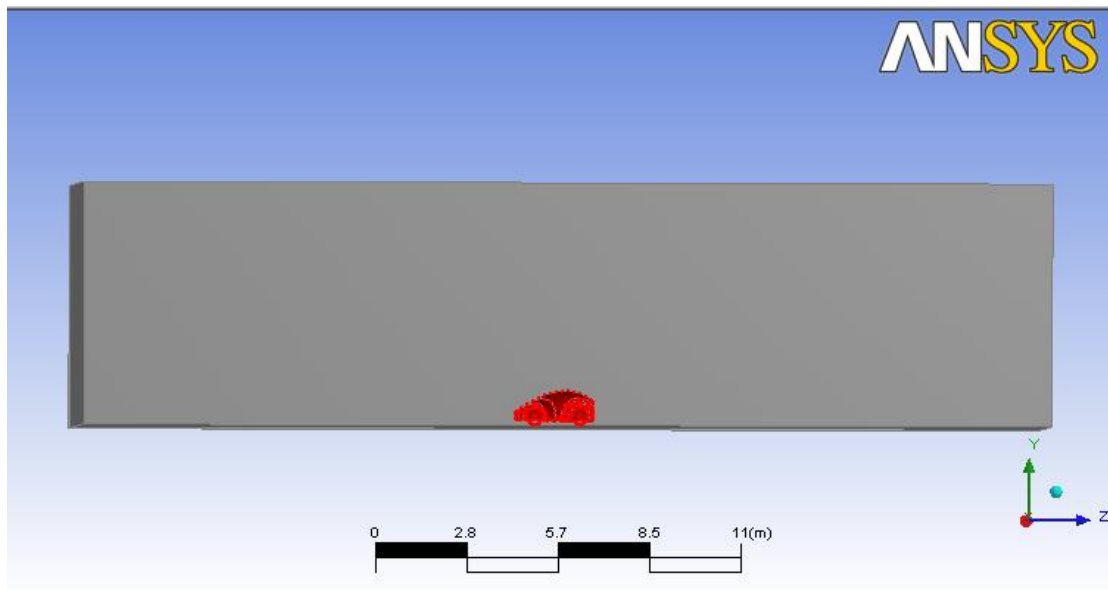


Figure 5.7: Default 2D region (the surface of the vehicle)

- Top: The upper surface of the control volume

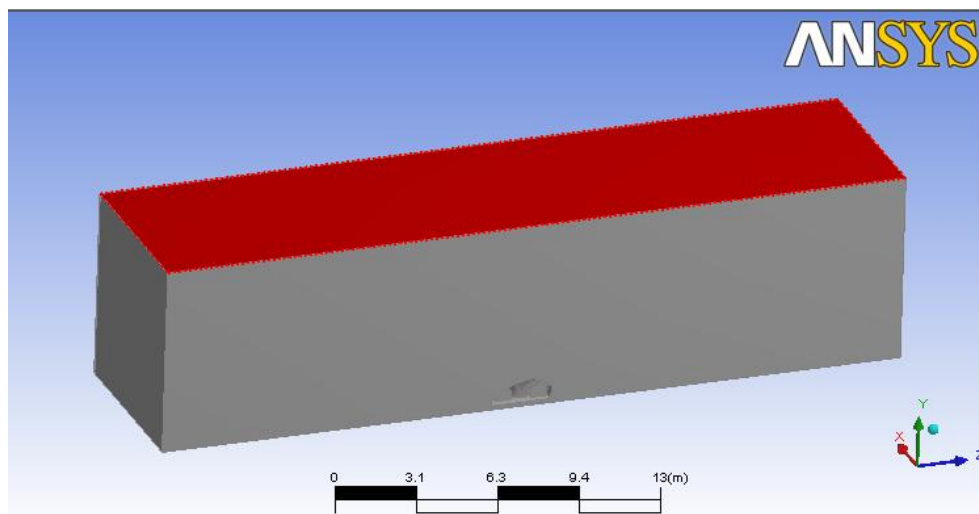


Figure 5.8: "Top" surface

- Bottom: the lower surface of the flow domain (representing the solid ground - Figure 5.9).

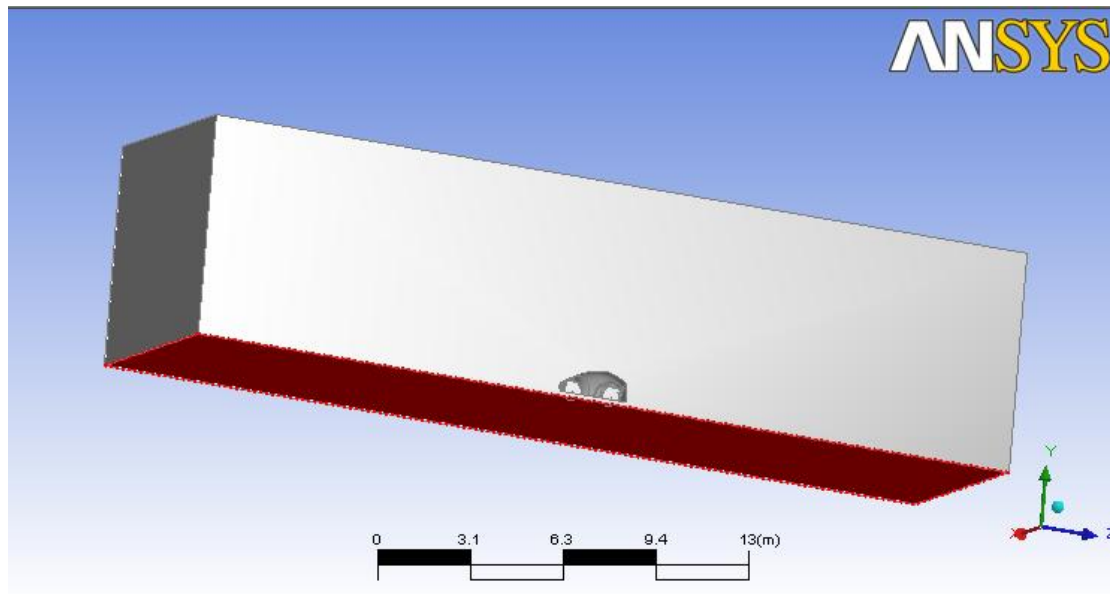


Figure 5.9: The "Bottom" surface (ground)

- Inlet: the inlet region where the inlet boundary conditions will be applied (Figure 5.10).

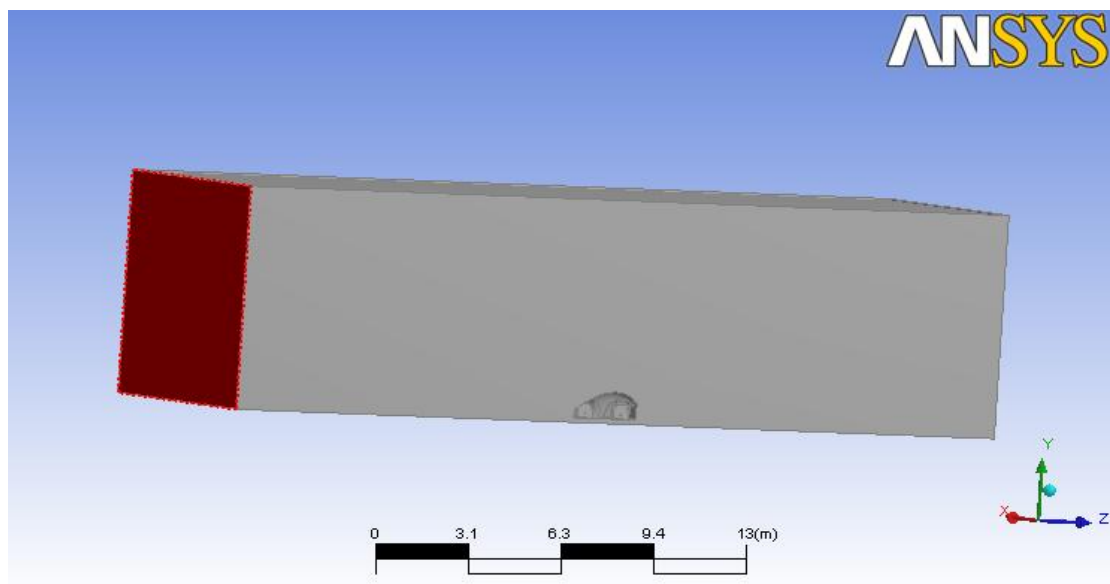


Figure 5.10: The "Inlet" surface of the flow domain

- Outlet: the outlet region where the outlet boundary conditions will be applied (Figure 5.11).

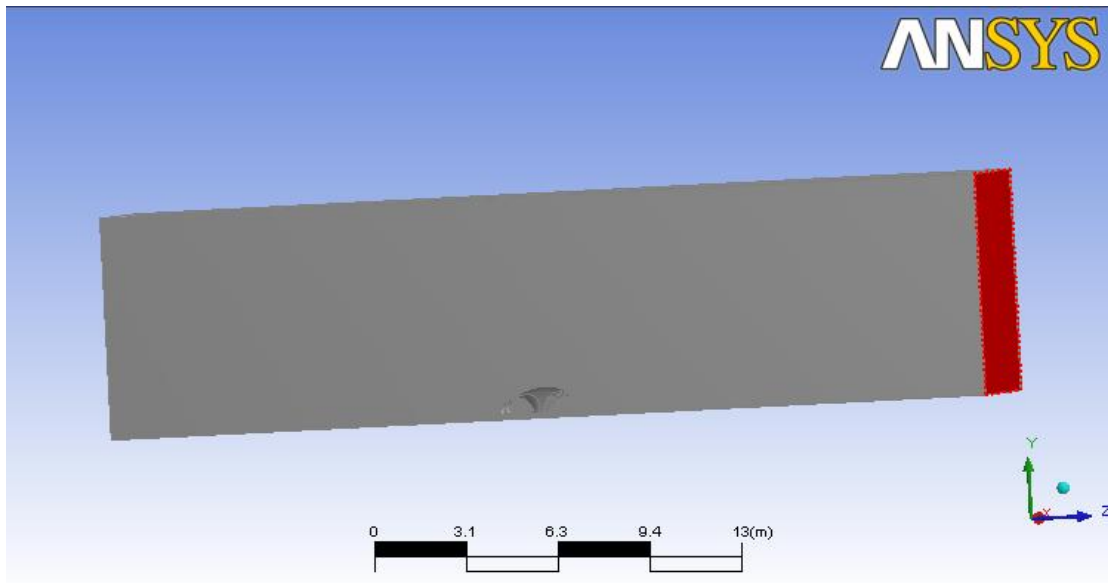


Figure 5.11: The “Outlet” surface of the flow domain

- Symmetry: The symmetry plane of the flow domain, where symmetry boundary conditions will be defined (Figure 5.12).

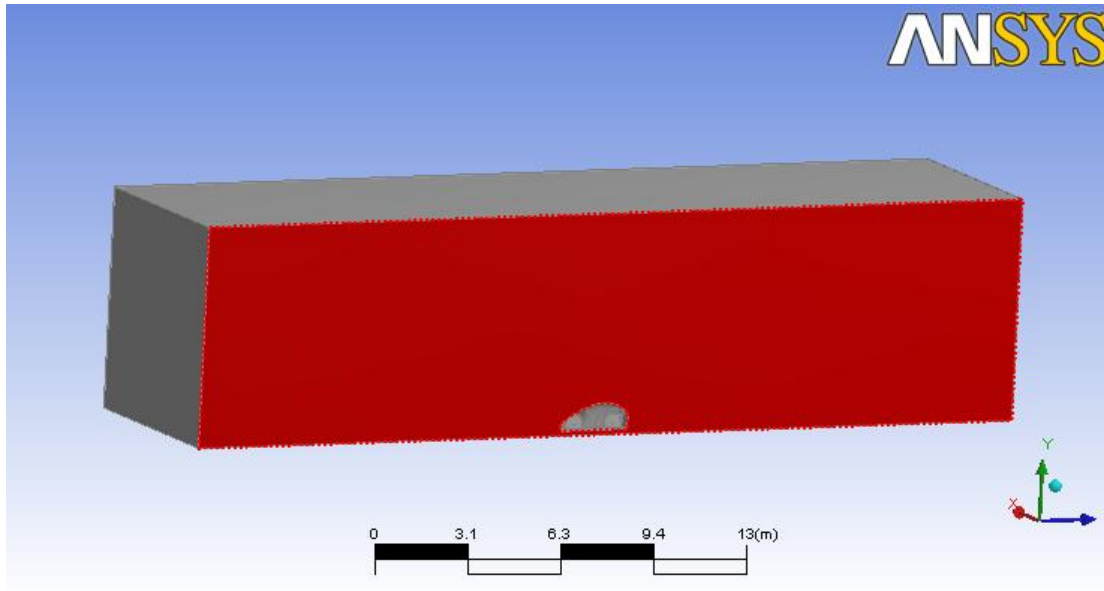


Figure 5.12: The “Symmetry” plane of the flow domain

- Side: The left side of the flow domain (Figure 5.13).

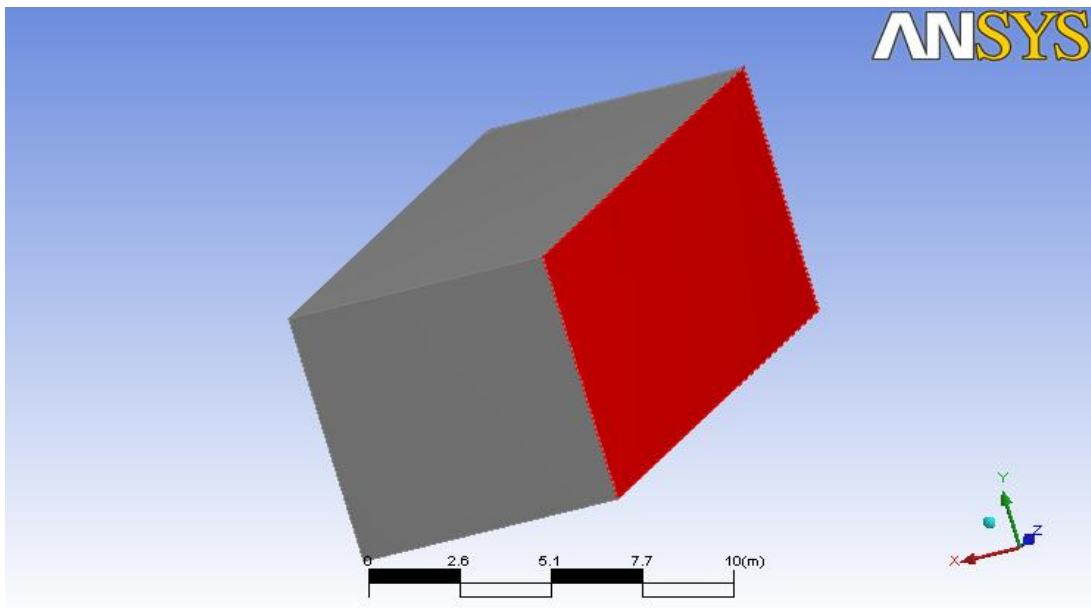


Figure 5.13: The "Side" surface of the flow domain

1. Spacing definition

The "spacing" determines the mesh length scale either on faces or inside the volume, or on edges, for the description of mesh density at different regions [25]. In Figure 5.14 two surfaces have been selected to define on them the mesh spacing.

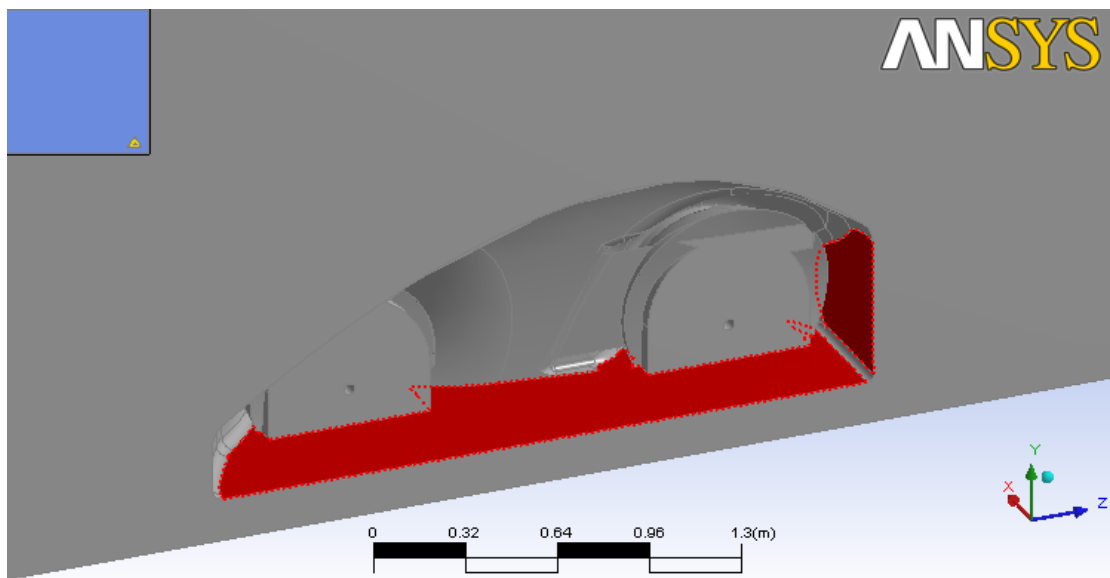


Figure 5.14: Face spacing definition

To define face spacing the following information should be specified [25]:

- **Face Spacing Type** - This can be set to one of the following four types:
 - Angular Resolution
 - Relative Error
 - Constant - Set a Constant Edge Length for the faces, overriding the Body Spacing. This length scale cannot be set to be larger than the Maximum Spacing specified in the Default Body Spacing.
 - Volume Spacing - Use the same spacing on the face as the Maximum Spacing specified for the Body on the faces selected.
- **Radius of Influence** - Specification of the extent of the Face Spacing influence. If, for example, a Radius of Influence of 2 cm is specified then the region of space within 2 cm of the Face Spacing is filled with mesh with the same length scale as on the face itself. Beyond the Radius of Influence, the size of the elements expands as we move away from the faces, in accordance with the Expansion Factor. This parameter does not apply when the Face Spacing Type is set to Volume Spacing [25].
- **Expansion Factor** - It specifies how fast the mesh length scale returns to its background value away from a region where it has been constrained by a Face Spacing. Each successive element as we move away from the face (outside the Radius of Influence specified above) is approximately one Expansion Factor larger than the previous one. Hence large values tend to coarsen the mesh rapidly away from the face. This parameter also governs how fast a local surface length scale that has been overridden near a curve (because of its curvature) expands back to its global value. It therefore controls both the rate of growth of volume elements away from faces and the rate of growth of surface elements away from curved boundaries into the middle of a flat face. It does not apply when the Face Spacing Type is set to Volume Spacing. Expansion Factors should be between 1.0 and 1.5 (Figure 5.15) [25].

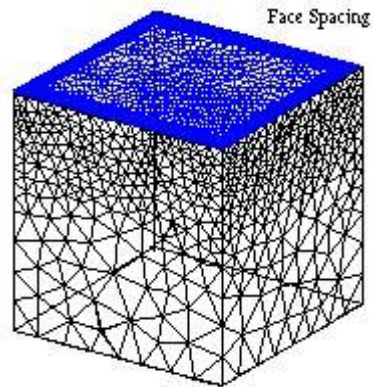


Figure 5.15: Face Spacing on a 1 m cube, with a Constant Edge Length of 0.05 m, Radius of Influence 0.2 m, and Expansion Factor 1.2 [25].

2. Inflation

In near-wall regions, boundary layer effects give rise to velocity gradients which are greatest normal to the face. Computationally-efficient meshes in these regions require that the elements have high aspect ratios. If tetrahedral elements are used, then a prohibitively fine surface mesh may be required to avoid generating highly distorted tetrahedral elements at the face (Figure 5.16) [25].

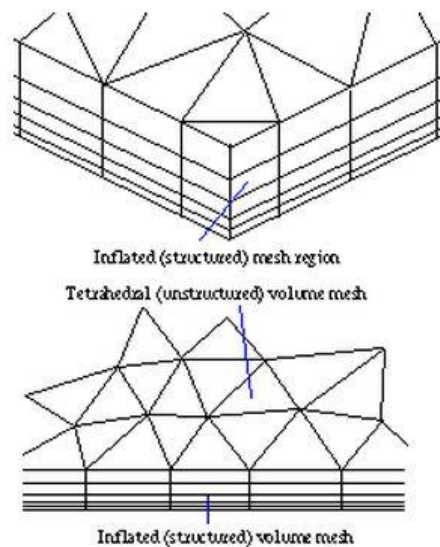


Figure 5.16: Inflated mesh region and the transition between the inflation mesh and the tetrahedral mesh [25].

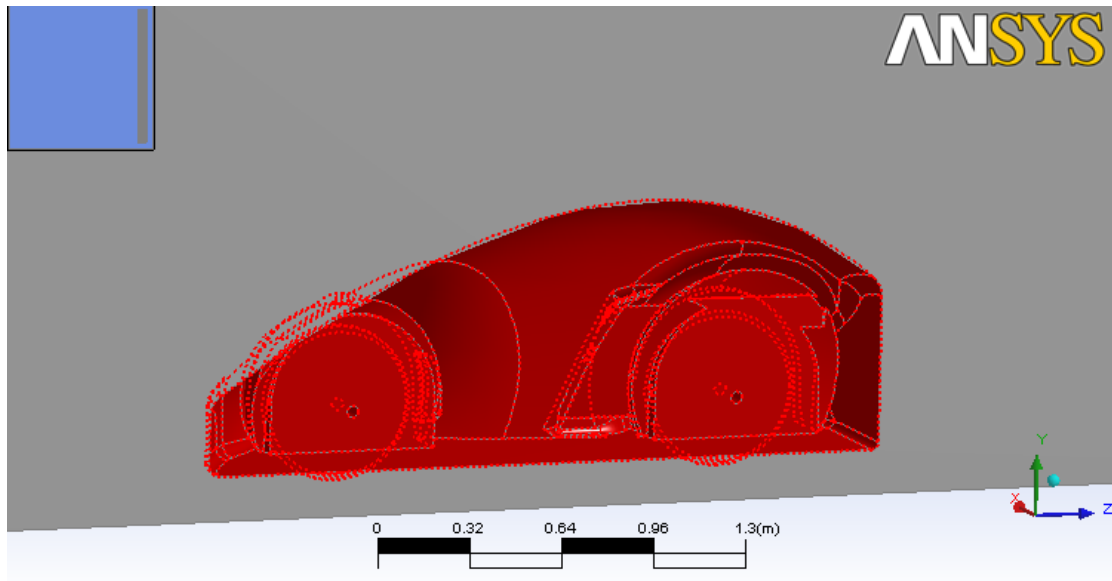


Figure 5.17: Reference area for “Inflated Boundary”

The following parameters are available for Inflation and provide global control over all Inflated Boundaries [25]. The surface for the application of inflation is defined by the user (Figure 5.17). The inflation parameters used here are given in Figure 5.18.

- **Number of Inflated Layers** - This controls the number of inflation layers. If **First Layer Thickness** is used to specify the thickness of the inflation layer, then this is a maximum number of inflation layers. Otherwise, it will be the actual Number of inflation layers, except in places where layers are removed locally for reasons of improving mesh quality (e.g., where inflation layers would otherwise collide with each other). The Number of Inflated Layers is restricted to be no more than 100 and the default is 5 layers.
- **Expansion Factor** - The relative thickness of adjacent inflation layers is determined by a geometric expansion factor. Each successive layer, as we move away from the face to which the Inflation is applied, is approximately one Expansion Factor thicker than the previous one. Expansion Factors must be set to between 1.0 and 1.5.
- **Number of Spreading Iterations** - This governs how far the effects of deleted elements propagate.
- **Minimum Internal Angle**- This governs the minimum angle that is allowed in the triangular face of a prism nearest to the surface before it is deemed to be of unacceptable quality and marked for deletion.
- **Minimum External Angle**- This governs the minimum angle that is allowed in the triangular face of a prism farthest from the surface, before it is deemed to be of unacceptable quality and marked for deletion.

| | |
|-------------------------|-----------------|
| Inflation | |
| Number of Inflated L... | 8 |
| Expansion Factor | 1.2 |
| Number of Spreading ... | 0 |
| Minimum Internal Ang... | 2.5 |
| Minimum External An... | 10.0 |
| Inflation Option | |
| Option | Total Thickness |
| Thickness Multiplier | 1 |

Figure 5.18: Inflation parameters used in this project

The mesh constructed for the ER11 vehicle is presented in Figures 5.19 - 5.21.

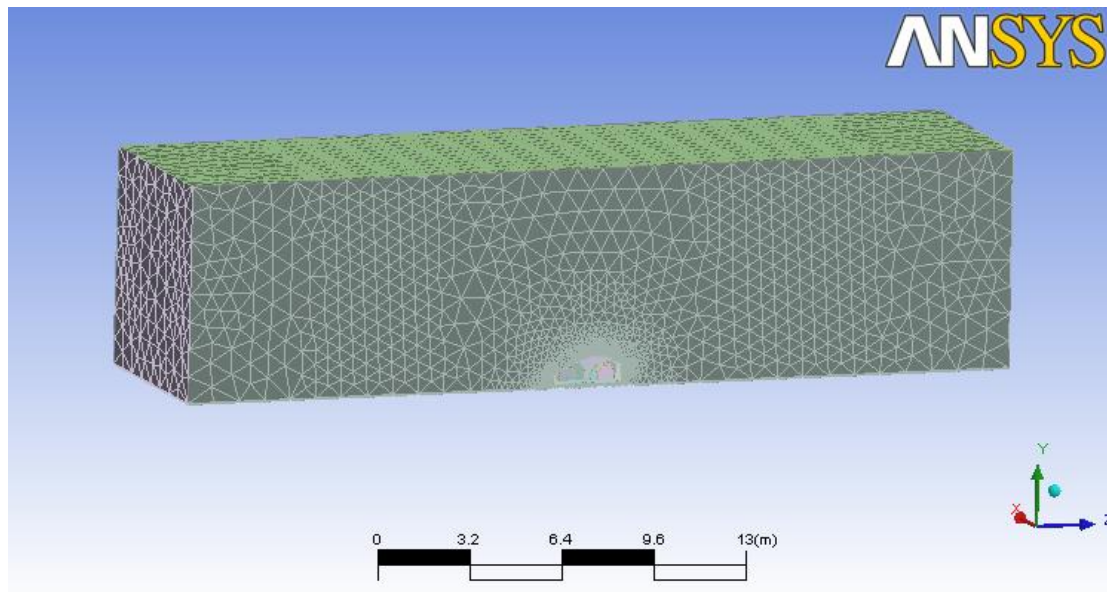


Figure 5.19: Final mesh for the ER11 vehicle

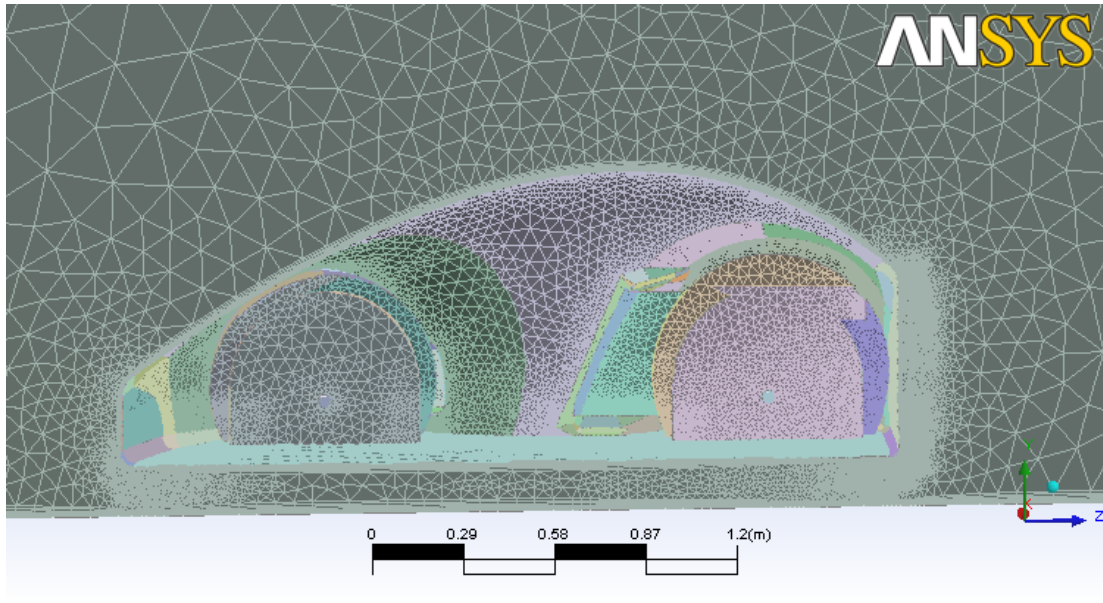


Figure 5.20: close-up of the final mesh at the vehicle region (ER11)

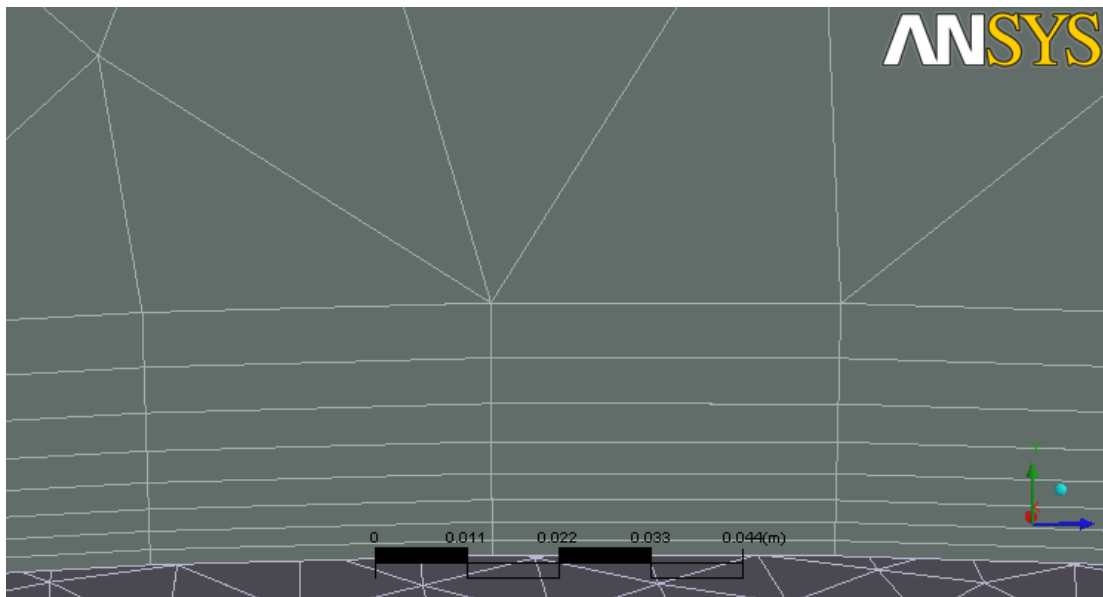


Figure 5.21: Detail of the inflation layer at the solid boundary

The final mesh around the vehicle includes the following characteristics:

- **Total number of nodes: 1,278,563**
- **Total number of tetrahedral elements: 5,374,948**
- **Total number of pyramids: 9,364**
- **Total number of prisms: 650,192**
- **Total number of elements: 6,034,504**

5.3 Boundary Conditions

The boundary conditions were specified on ANSYS CFX-PRE, after importing the mesh. ANSYS CFX-Pre allows for multiple meshes to be imported, allowing each section of complex geometries to use the most appropriate mesh. A full range of boundary conditions, including inlets, outlets and openings, together with boundary conditions for heat transfer models and periodicity, are all available in ANSYS CFX through ANSYS CFX-Pre [25]. ANSYS CFX-Pre uses the concept of domains to define the type, properties and regions of the fluid, porous or solid. Domains are regions of space in which the equations of fluid flow or heat transfer are solved (Figure 5.22) [25].

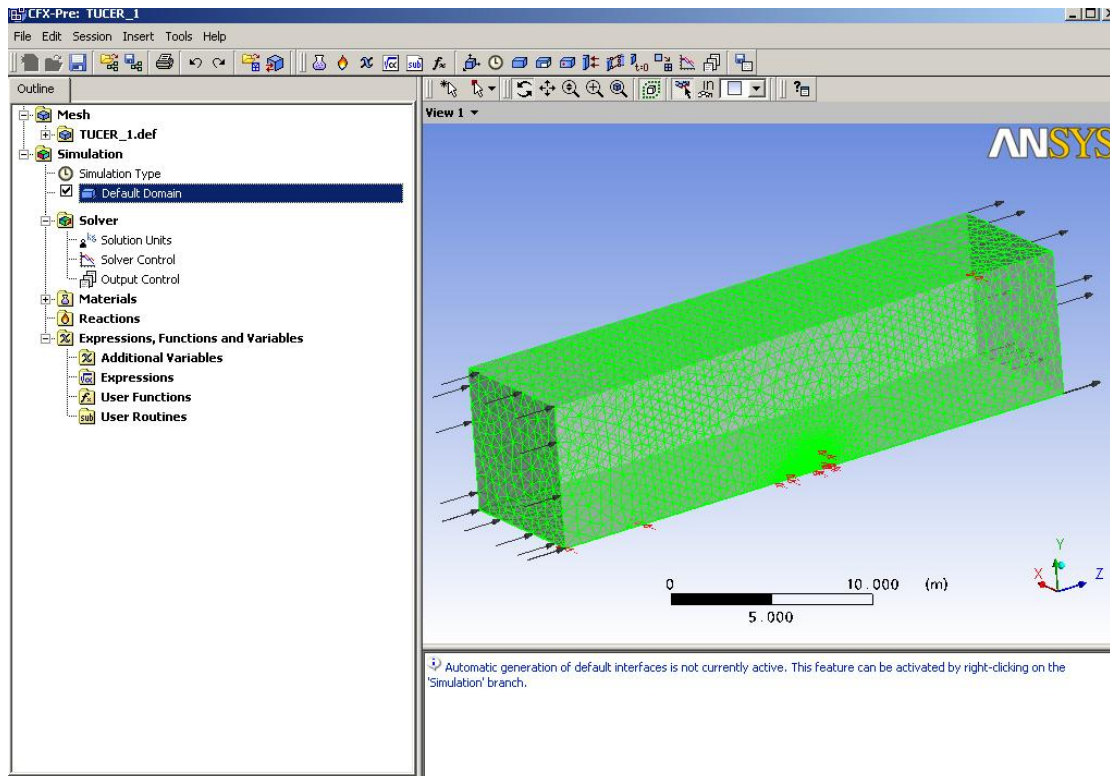


Figure 5.22: View of the ANSYS CFX-Pre and the meshed flow domain with the corresponding boundary conditions

Firstly the Default Domain should be edited, defining the general boundary conditions such as the pressure and the temperature of the control volume environment (Figures 5.23, 5.24).

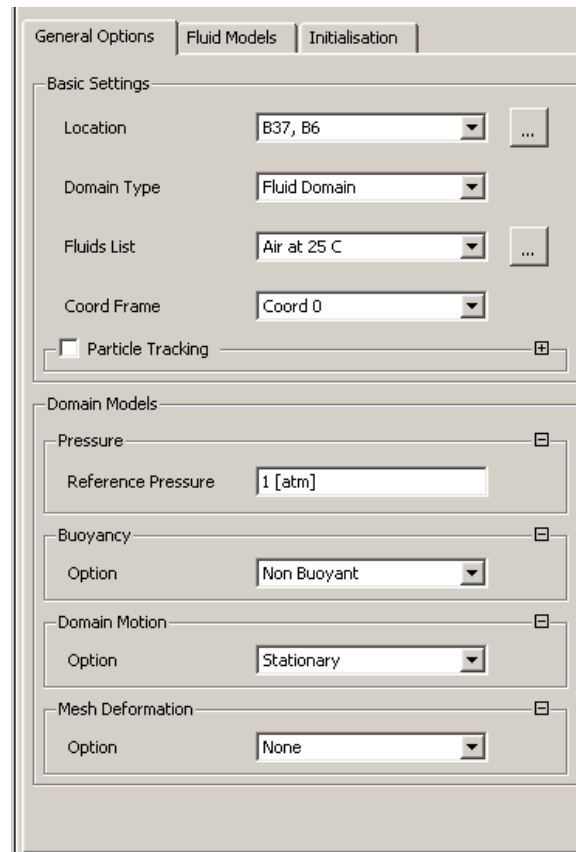


Figure 5.23: General options for the flow domain (Default Domain)

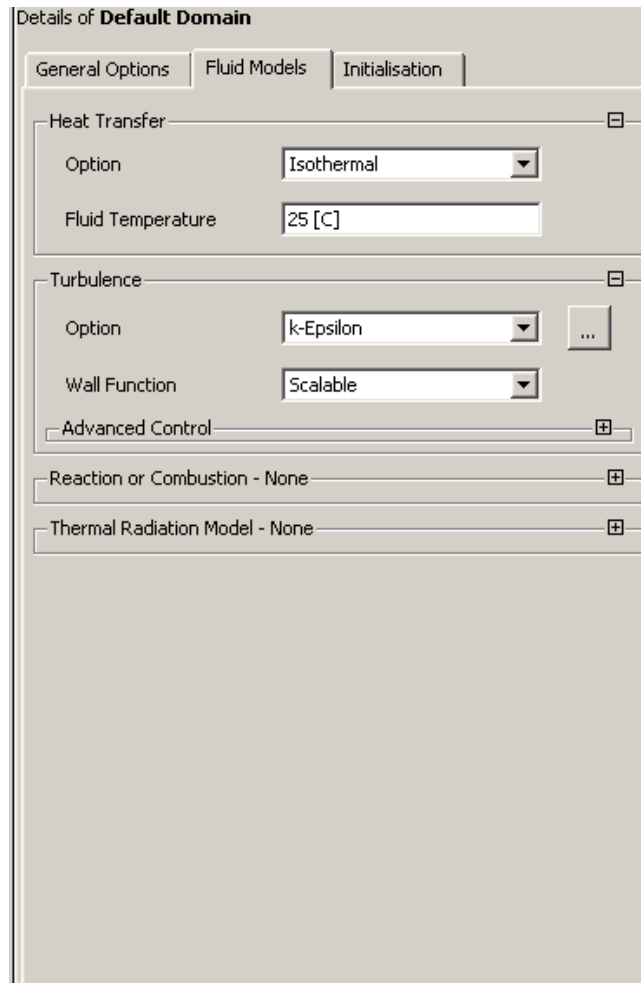


Figure 5.24: Fluid Model parameters of the Default Domain

Using the discrete surfaces defined during the mesh generation procedure the various domains where the different boundary conditions have to be defined are introduced in the corresponding tree (Figure 5.25).

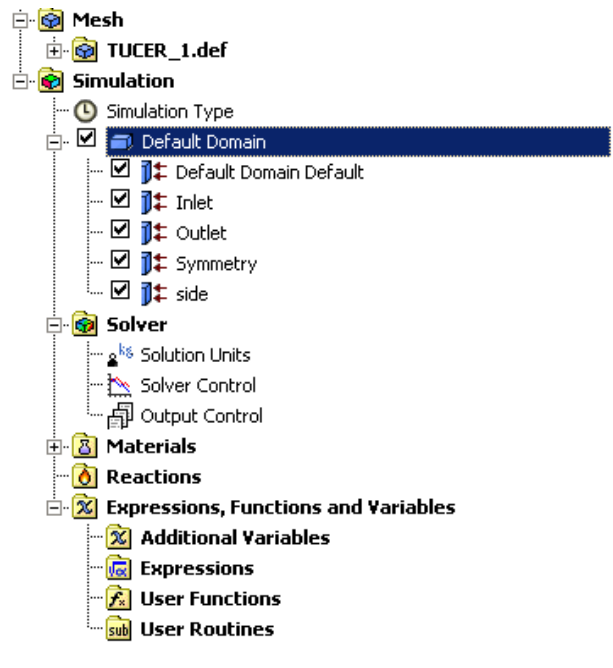


Figure 5.25: The tree of parameters in ANSYS CFX-Pre

1. Default Domain Default (vehicle solid surface)

That domain describes the surface of the vehicle, making easier to set the boundary condition on it. It is necessary to define some additional parameters of the domain, like boundary type as “wall”, which refers to a impenetrable boundary to fluid flow. Furthermore, the wall influence on flow is set as “no slip”, determining that velocity of the fluid at the wall boundary is set to zero (Figures 5.26 - 5.28) [25].

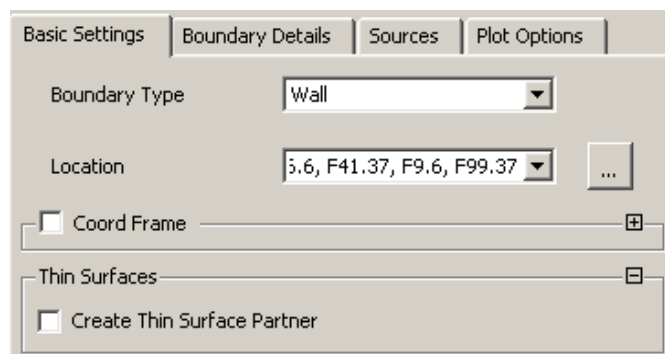


Figure 5.26: Basic Settings on Default Domain Default (vehicle)

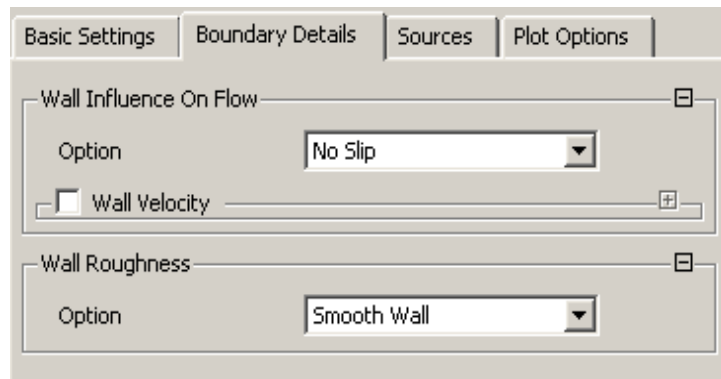


Figure 5.27: Boundary Details of Default Domain Default (vehicle)

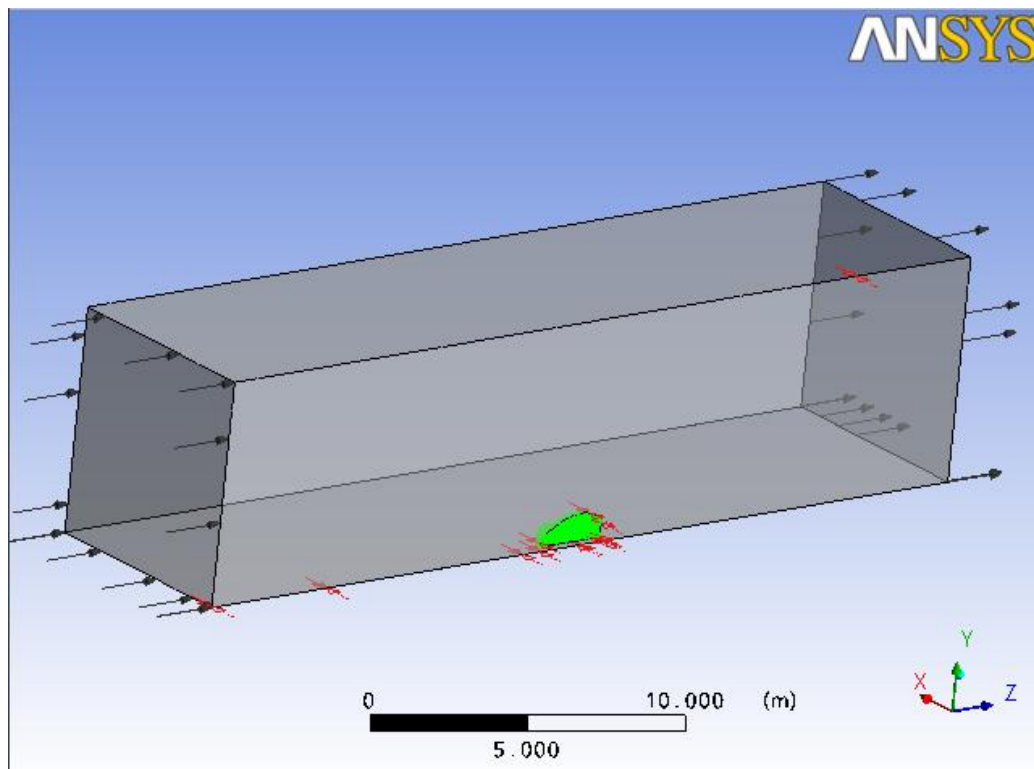


Figure 5.28: The surface that consists the Default Domain Default (vehicle)

1. Inlet

The fluid (air) predominantly flows into the domain. The normal speed of the air entering the flow domain was defined at 6.94 m/s or 25km/h which is the average achieved velocity of the vehicle during the racing. The turbulence intensity was set at 5% at the inlet.

2. Outlet

The fluid (air) predominantly flows out of the domain. The relative pressure of the air has been defined at 0 Pa at the outlet (the reference pressure was set to 1 atm).

3. Side

That domain includes the Bottom, Side and Top regions. Furthermore wall influence on the flow has been set as Free-slip which means that the velocity component parallel to the wall has a finite value (which is computed), but the velocity normal to the wall is zero[25].

4. Symmetry

The last domain defines the symmetrical area of the control volume. The vehicle is divided in two symmetrical parts, in order to reduce the time of the simulation.

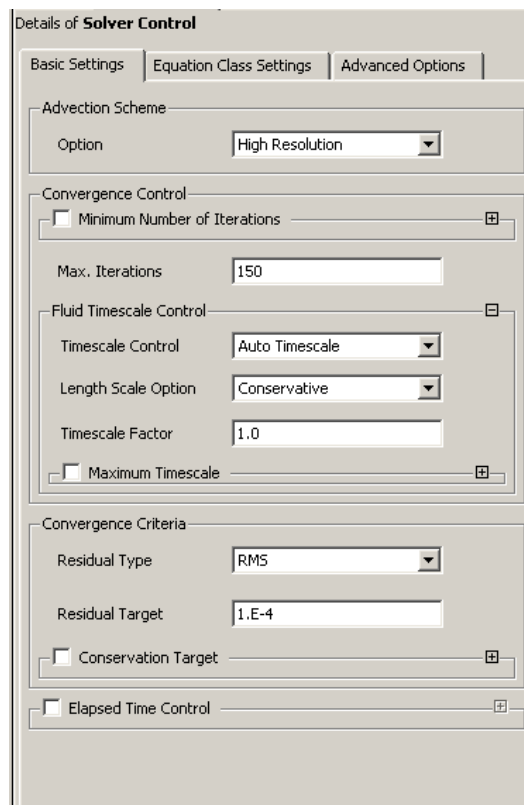


Figure 5.29: Basic setting for the solver control (ANSYS-CFX)

Having already set and edit the boundary conditions, the solver control details should be defined, specifying some parameters like maximum iterations (Figure 5.29).

5.4 Results

Pressure

By completing the first simulation a basis of comparison with the upcoming models is created. In the images below, the results are illustrated for static pressure. The red color corresponds to high pressure regions (as at the stagnation region at the frontal area of the vehicle - Figure 5.25). The main target of this work is drag reduction, which is caused by pressure differential between the front and rear surfaces (as well as the surface friction). The main cause of high drag formation is the high recirculation region at the rear side of the vehicle. The aim of the design work is to decrease this region by very careful redesign of the rear part of the vehicle. Concerning the front side, the variation of pressure that is observed in Figure 5.25 is undesirable and a more smooth pressure distribution should be established by a careful redesign of the corresponding region. As we can see in Figure 5.26 a large variation of pressure is observed at the side of the vehicle at the region between the front and rear wheel. This strong variation is connected with deceleration and acceleration of the flow, which adds to the drag formation. This should be taken into account to the redesign procedure of the vehicle. In Figure 5.28 the pressure field at the symmetry plane is presented and the distorted field at the rear of the vehicle is connected with the presence of a recirculation region.

Streamlines are a family of curves that are instantaneously tangent to the velocity vector of the flow. These show the direction a fluid element will travel in at any point in time [18]. In that way the airflow around the vehicle is better illustrated, showing flow separations (Figures 5.29-5.30). Figures 5.31 - 5.34 contain iso-velocity surfaces for different levels of velocity. These are used to illustrate the low velocity regions connected with flow separation and recirculation. The recirculation and flow separation is evident not only at the rear of the vehicle but also behind the front wheels.

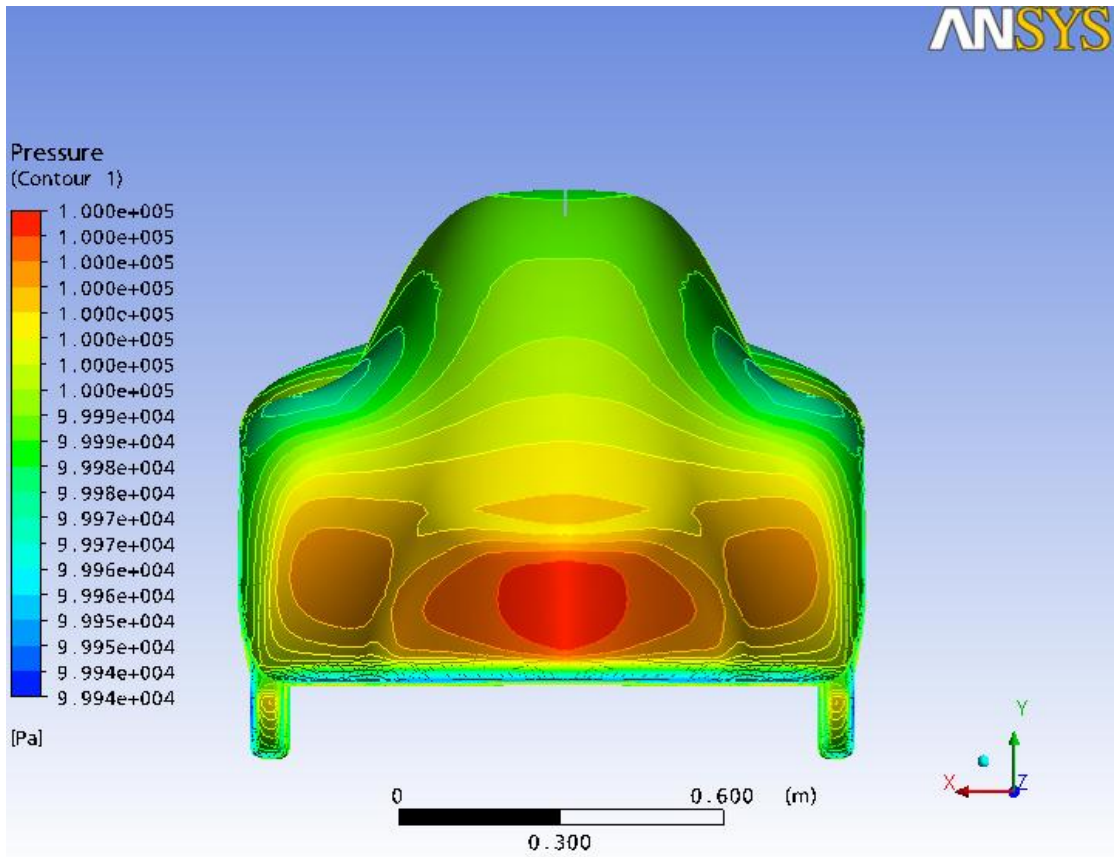


Figure 5.30: Surface pressure contours - front view

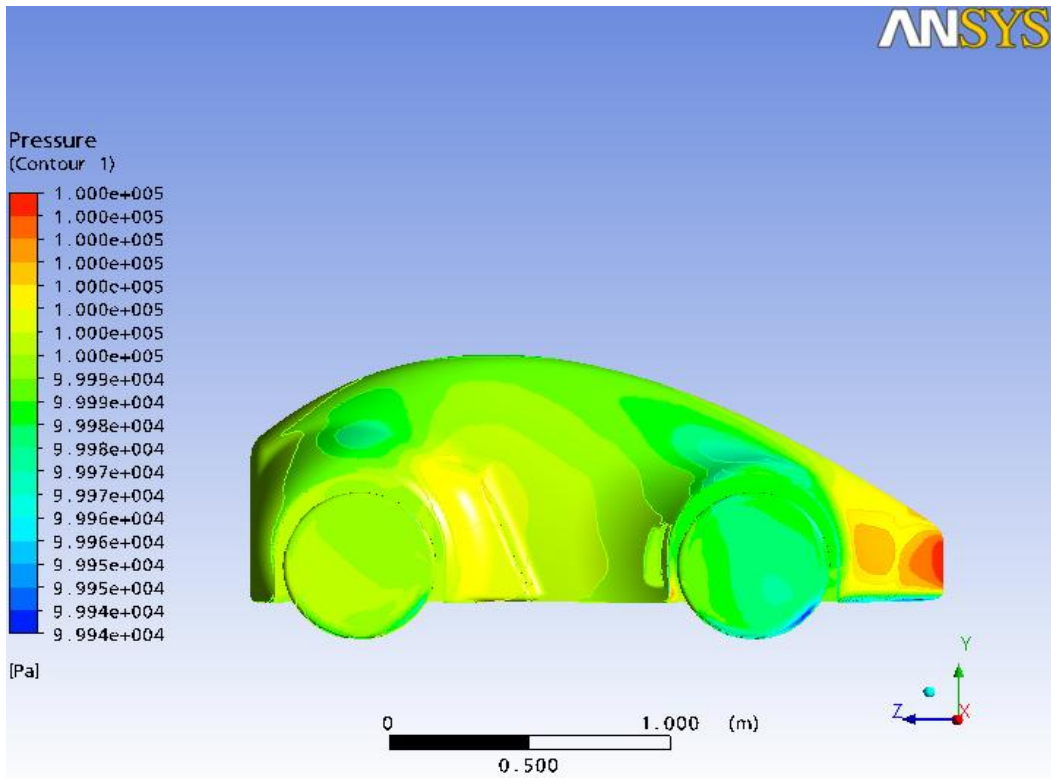


Figure 5.31: Surface pressure contours - side view

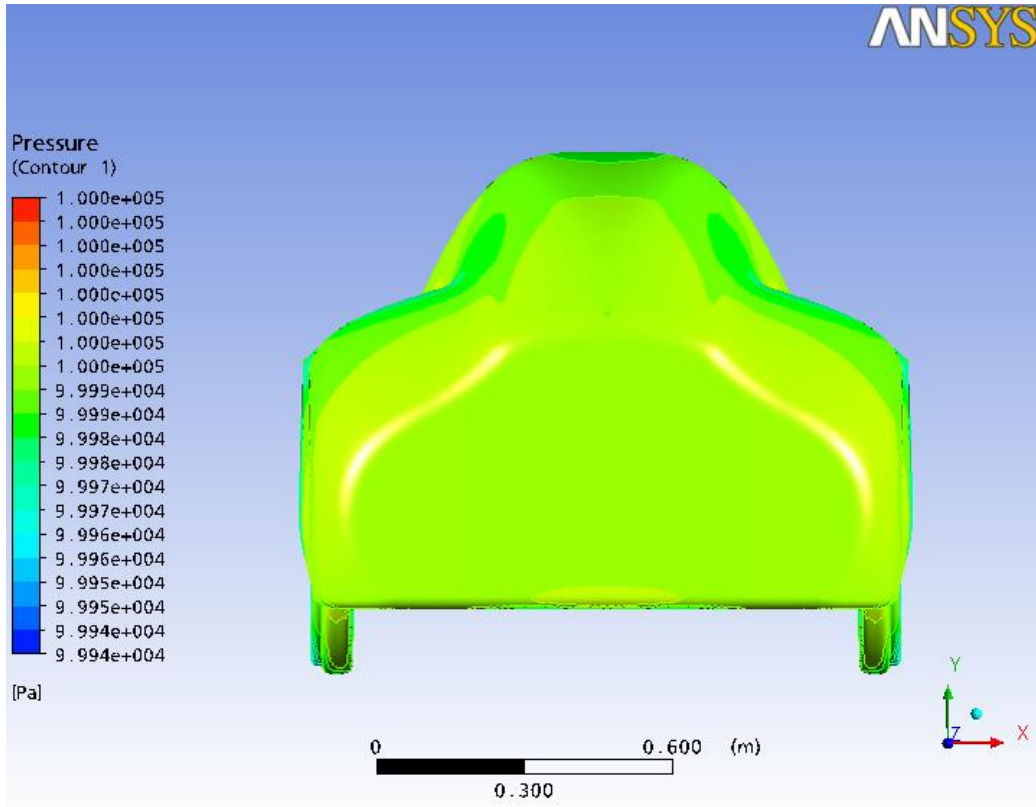


Figure 5.32: Surface pressure contours - rear view

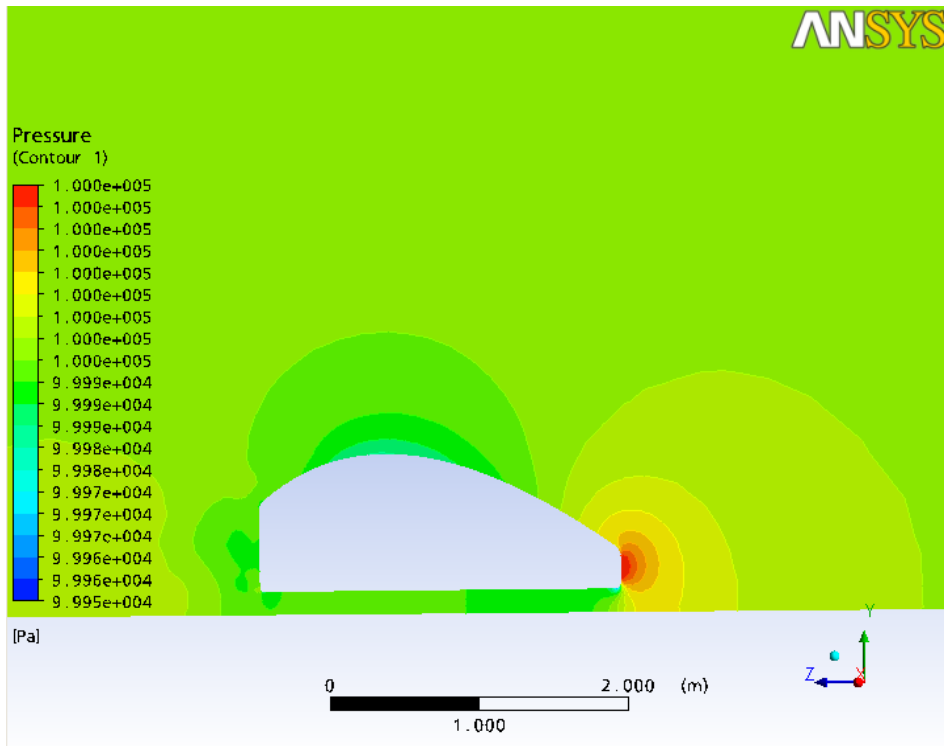


Figure 5.33: Pressure contours at the symmetry plane

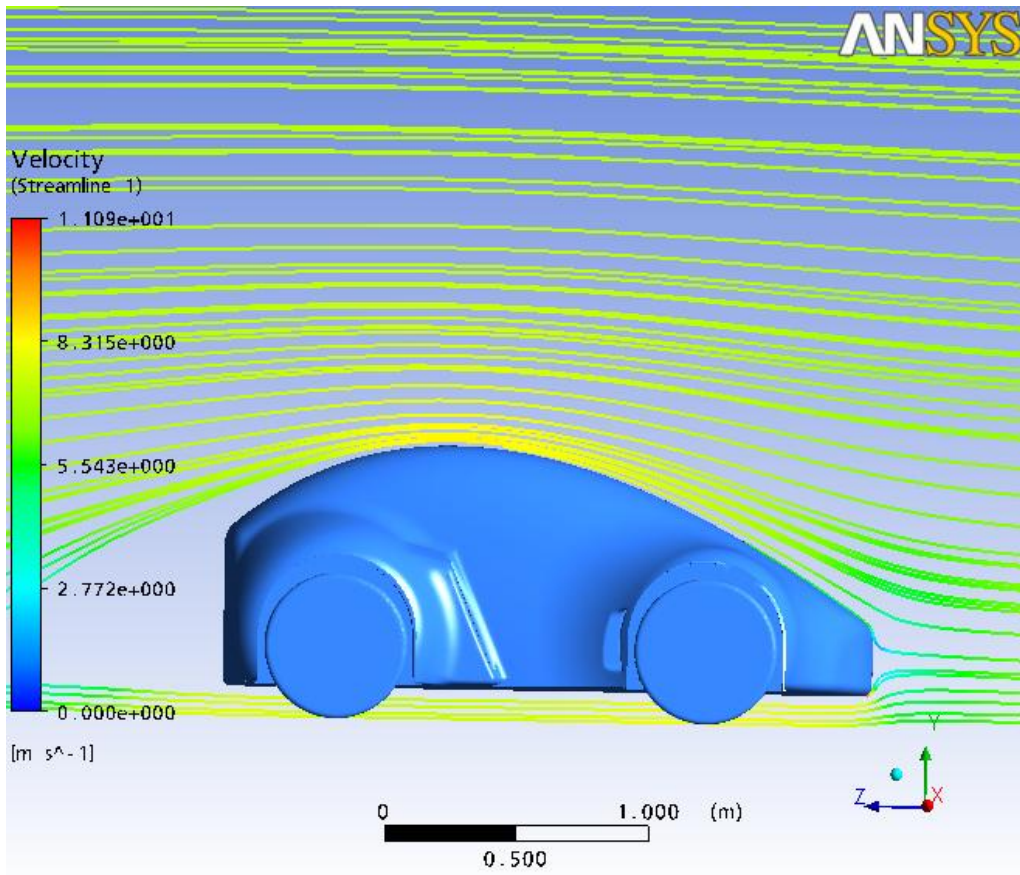


Figure 5.34: Streamlines at the symmetry plane

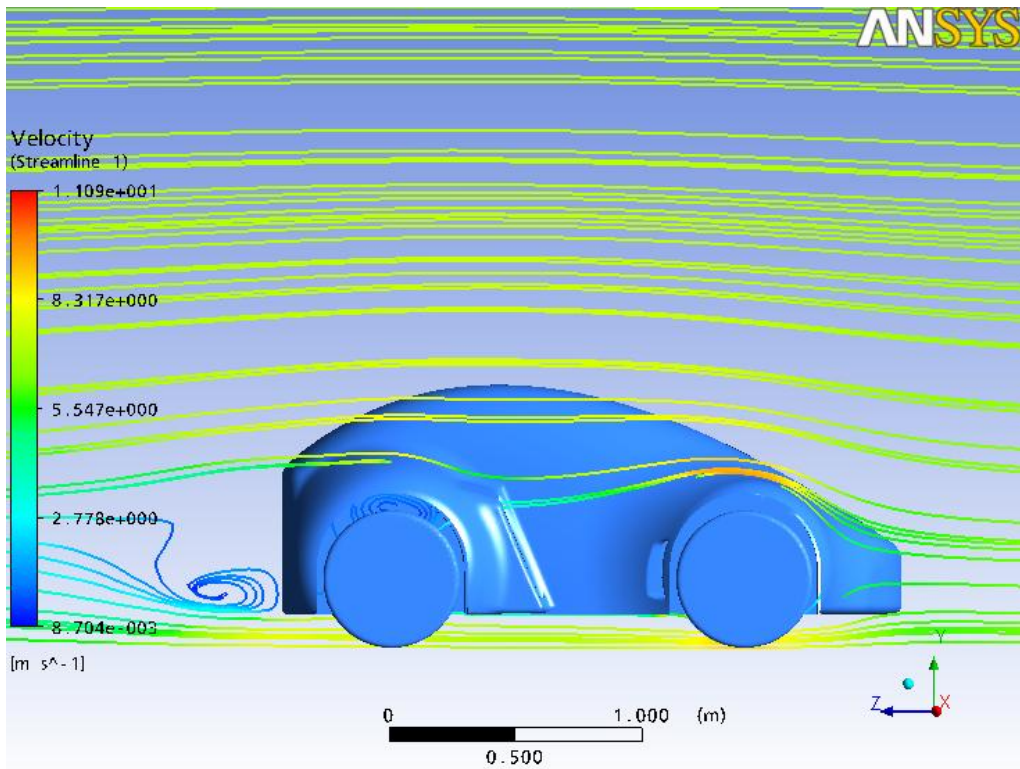


Figure 5.35: Streamlines at a plane 0.35m away from the symmetry plane

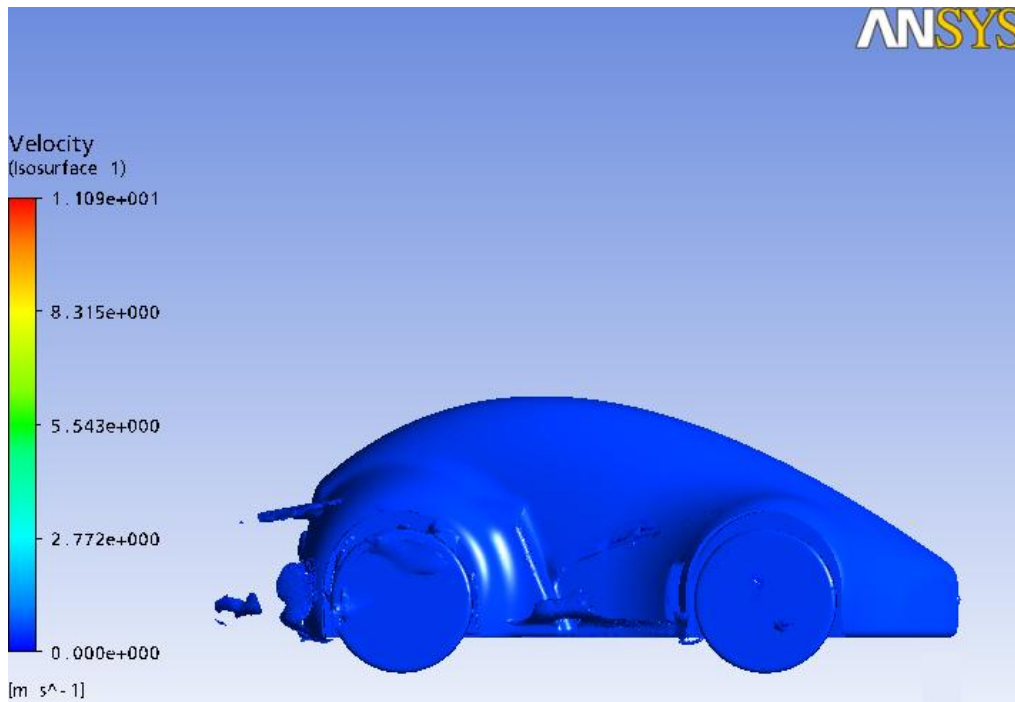


Figure 5.36: Equal-velocity surface for 0.5m/s

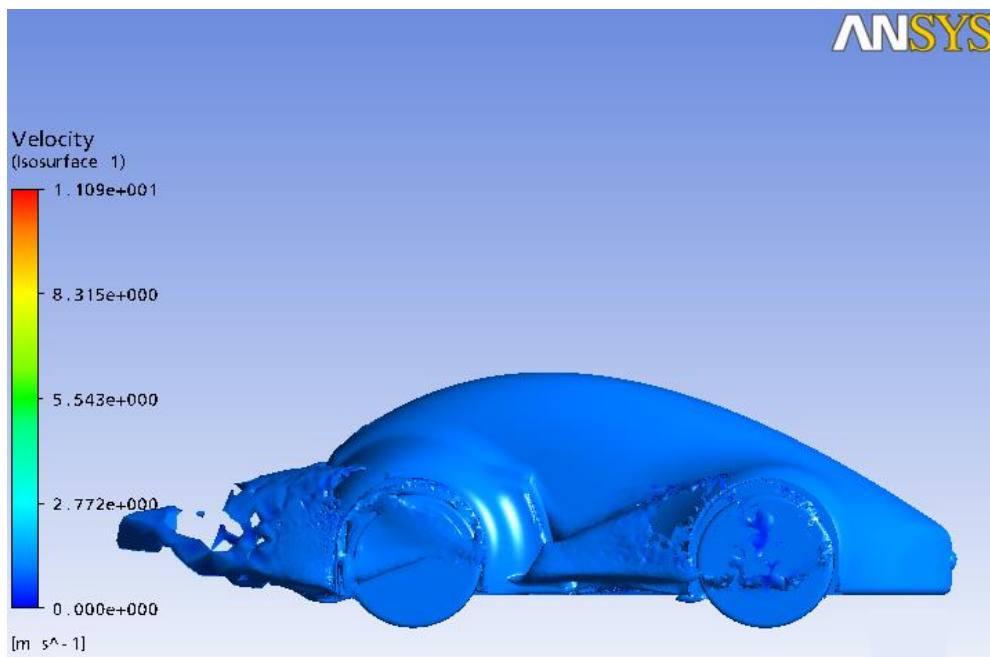


Figure 5.37: Equal-velocity surface for 1m/s

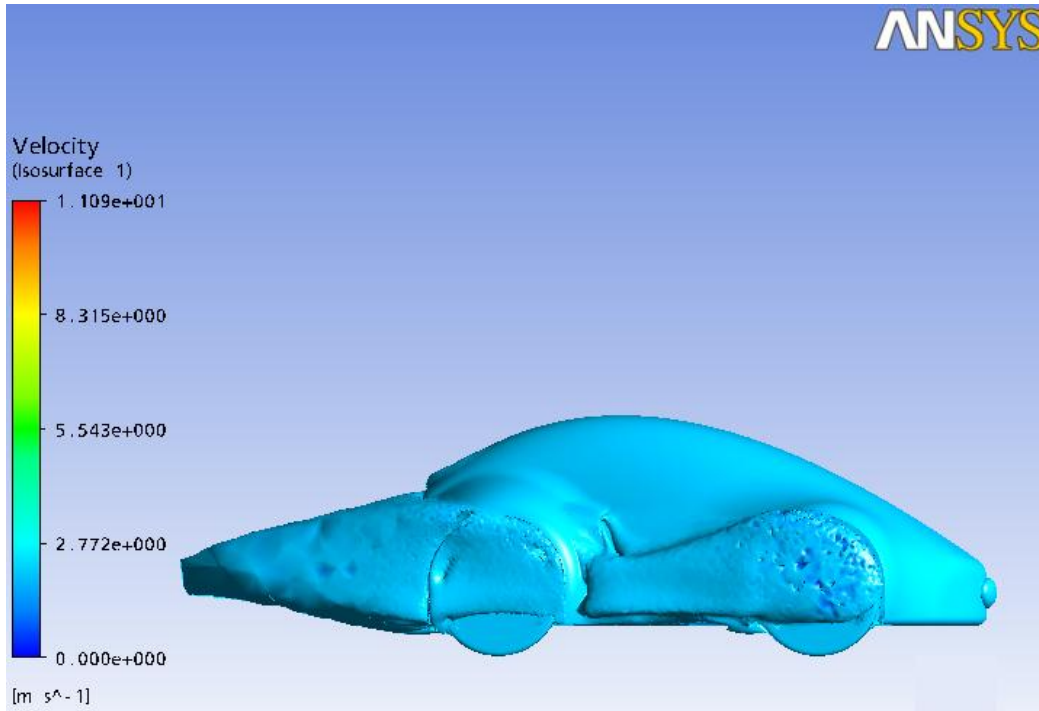


Figure 5.38: Equal-velocity surface for 2 m/s

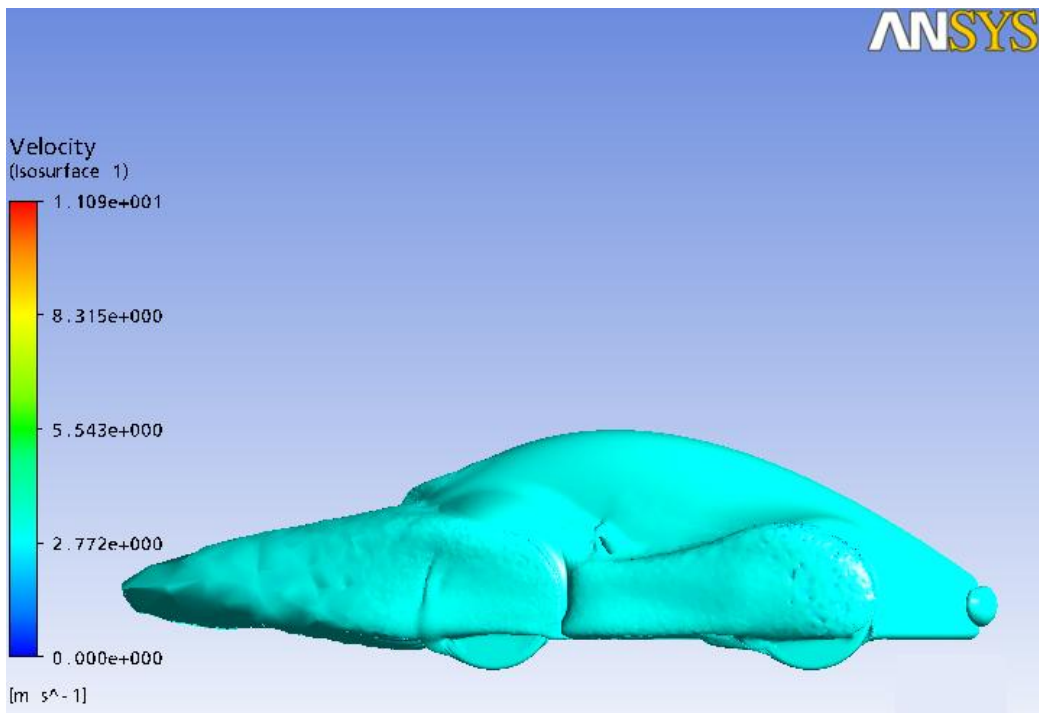


Figure 5.39: Equal-velocity surface for 3 m/s

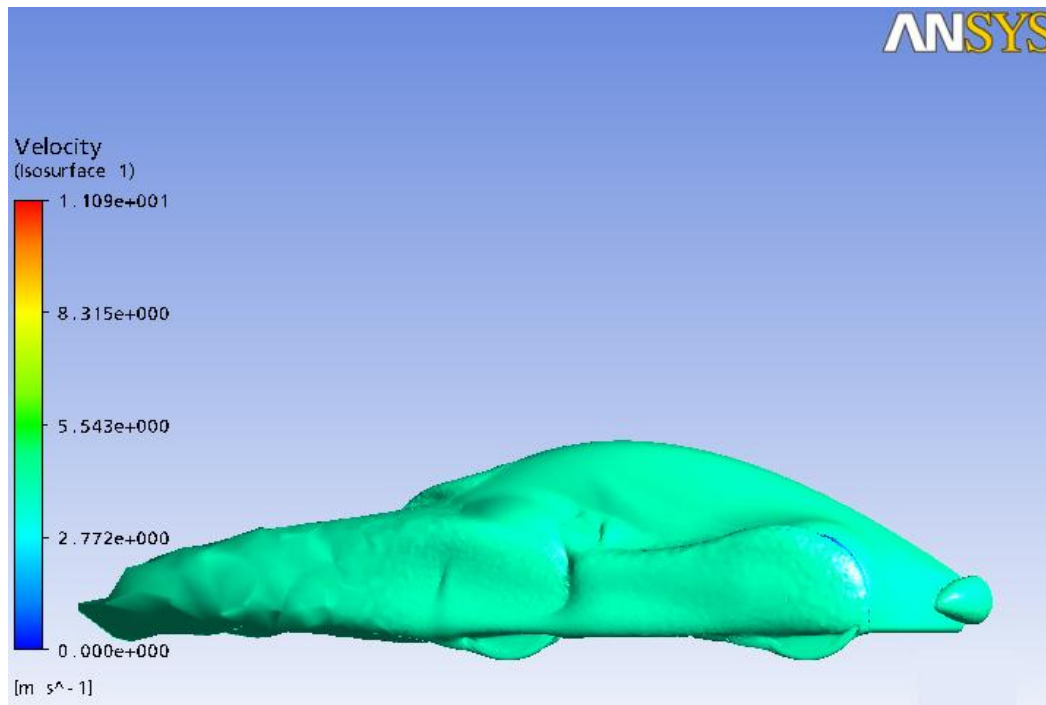


Figure 5.40: Equal-velocity surface for 4 m/s

The drag force is calculated equal to 5.86 Nt for the half vehicle, so for the whole vehicle is equal to 11.72 Nt. That means that the vehicle demands almost 82 Watts to maintain its velocity (25 km/h) (for the aerodynamic force). The drag Coefficient C_d is computed equal to 0.33.

By simulating the flow around the old vehicle (ER11) the aerodynamic problems were identified and it was realized that its drag coefficient is high for a racing vehicle. A major reshaping of the vehicle was decided, including a more rounded frontal area, removing totally the front and back air ducts, extending the rear side of the vehicle and providing a constant area between the wheels.

5.5 Design specifications

5.5.1 Rules

The vehicle (ER12) participates in urban concept category of the Shell Eco Marathon Completion in Urban concept category which is close in appearance to today's production type passenger cars. ER12 is designed having as a main aim to be more efficient than the previous one complying with the specific rules of that category. The rules are described below[28].

5.5.2 Vehicle Design

- a) During vehicle design, construction and competition planning, participating Teams must pay particular attention to all aspects of safety, i.e. Driver safety, the safety of other Team members and spectator safety.
 - Prototype vehicles must have three or four running wheels, which under normal running conditions must be all in continuous contact with the road.
 - Urban Concept vehicles must have exactly four wheels, which under normal running conditions must be all in continuous contact with the road. A fifth wheel for any purpose is forbidden.
- a) Aerodynamic appendages, which adjust or are prone to changing shape due to wind whilst the vehicle is in motion, are forbidden.
- b) Vehicle bodies must not be prone to changing shape due to wind and must not include any external appendages that might be dangerous to other Team members; e.g. sharp points must have a radius of 5 cm or greater, alternatively they should be made of foam or similar deformable material.
- c) The vehicle interior must not contain any objects that might injure the Driver during a collision.
- d) Windows must not be made of any material which may shatter into sharp shards. (m.g. Lexan)

5.5.3 Visibility

- a) The Driver must have access to a direct arc of visibility ahead, and to 90° on each side of the longitudinal axis of the vehicle. This field of vision must be achieved without aid of any optical (or electronic) devices such as mirrors, prisms, periscopes, etc. Movement of the Driver's head within the confines of the vehicle body to achieve a complete arc of vision is allowed.
- b) The vehicle must be equipped with a rear-view mirror on each side of the vehicle, each with a minimum surface area of 25 cm² (e.g. 5 cm x 5 cm). The visibility

- provided by these mirrors, and their proper attachment, will be subject to inspection. An electronic device must not replace a rear-view mirror.
- c) An Inspector will check visibility in each of the vehicles in order to assess on-track safety. This Inspector will check good visibility with 60 cm high blocks spread out every 30° in a half-circle, with a 5 m radius in front of the vehicle.
 - d) For Urban Concept vehicles wet weather visibility is also mandatory

5.5.4 Vehicle Access

- a) It is imperative for Drivers, fully harnessed, to be able to vacate their vehicles at any time without assistance in less than 10 seconds.
- b) Concept vehicles, the opening release mechanism must be easily and intuitively operable from the inside and the outside of the vehicle. The method of opening from the outside must be clearly marked by a red arrow and must not require any tools.

5.5.5 Dimensions

- a) The total vehicle height must be between 100 cm and 130 cm.
- b) The total body width, excluding rear view mirrors, must be between 120 cm and 130 cm.
- c) The total vehicle length must be between 220 cm and 350 cm.
- d) The track width must be at least 100 cm for the front axle and 80 cm for the rear axle, measured between the midpoints where the tyres touch the ground.
- e) The wheelbase must be at least 120 cm.
- f) The Driver's compartment must have a minimum height of 88 cm and a minimum width of 70 cm at the Driver's shoulders.
- g) The ground clearance must be at least 10 cm.
- h) The maximum vehicle weight (excluding the Driver) must be 205 kg.

5.5.6 Wheels

- a) The rims must be between 13 to 17 inches in diameter.
- b) The wheels located inside the vehicle body must be made inaccessible to the Driver by a bulkhead. Any handling or manipulation of the wheels is forbidden from the moment the vehicle arrives at the starting line until it crosses the finish line.

6. Design and CFD Simulation

Having as a base the central drawing line of the old model, many different models were constructed using CATIA V5R19 and simulated in ANSYS CFX v.11 for aerodynamic purposes. Moreover, the final model was chosen having two criteria, the achievement of the lower drag in combination with the aesthetic acceptance of the modeling, taking also into account the project deadlines as well.

In comparison with ER11 , the design of the new vehicle aims at:

- Rounding the frontal area of the vehicle.
- Reducing the sectional area which is one of the factors to improve the aerodynamic efficiency.
- Changing the sides of the vehicles, removing air ducts and designing smoother surfaces, in order to improve air flow on the surface.
- Extending the rear of the vehicle in order to eliminate the flow separation.

6.1 TUCER ER12 1st Model

6.1.1 Design

The 1st model was based on the idea that the vehicle would look like an inverted airfoil, with a long curved rear side, maintaining a constant airflow on the side boundaries. The wheelbase remained the same as the previous model, at 1400mm but a totally new vehicle was presented. The existing 3D model of ER11 vehicle was cut in six sections (Figure 6.1), where definition points were set. Using splines and additional points, wireframes were created consisting the basis of the new drawing (Figure 6.2). This procedure was adopted in order to make a new model that will not be very different from the previous one, in order to simplify the construction of the new mold. Using the spline curves as a basis, we proceeded in their reshaping by moving their control points in new positions, according to our goals (Figures 6.3, 6.4).

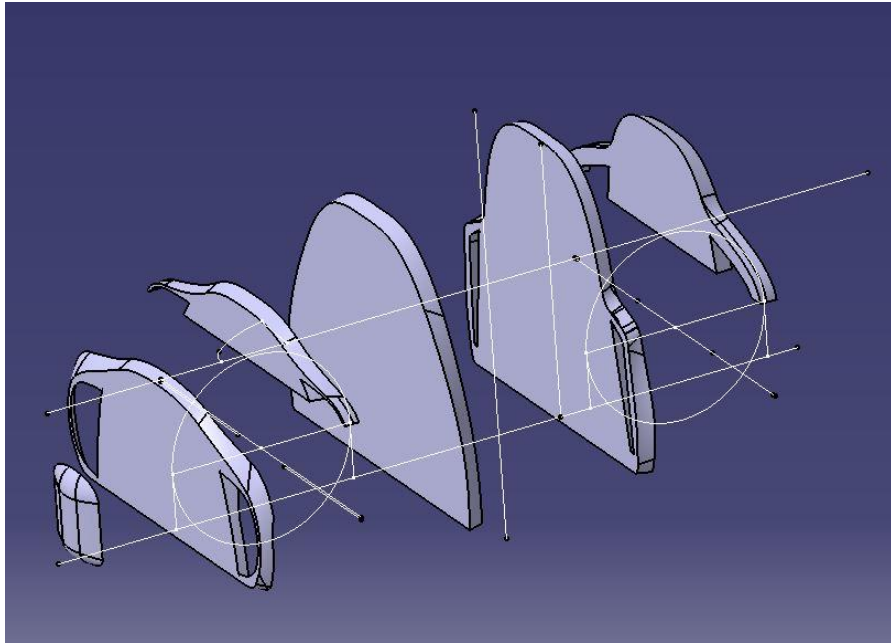


Figure 6.1: Six sections produced from the 3D model of the old vehicle (ER11)

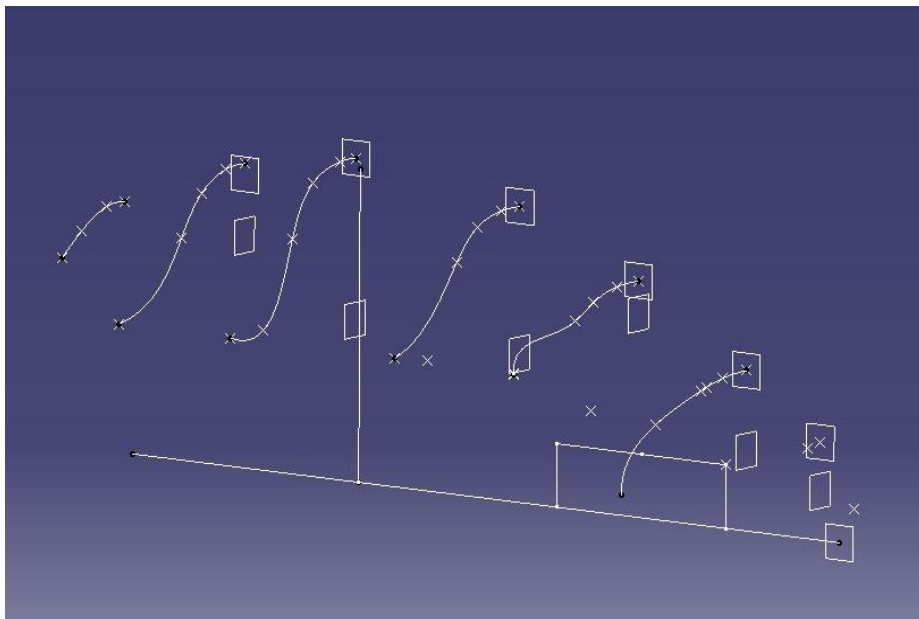


Figure 6.2: The wireframes resulted from the sections

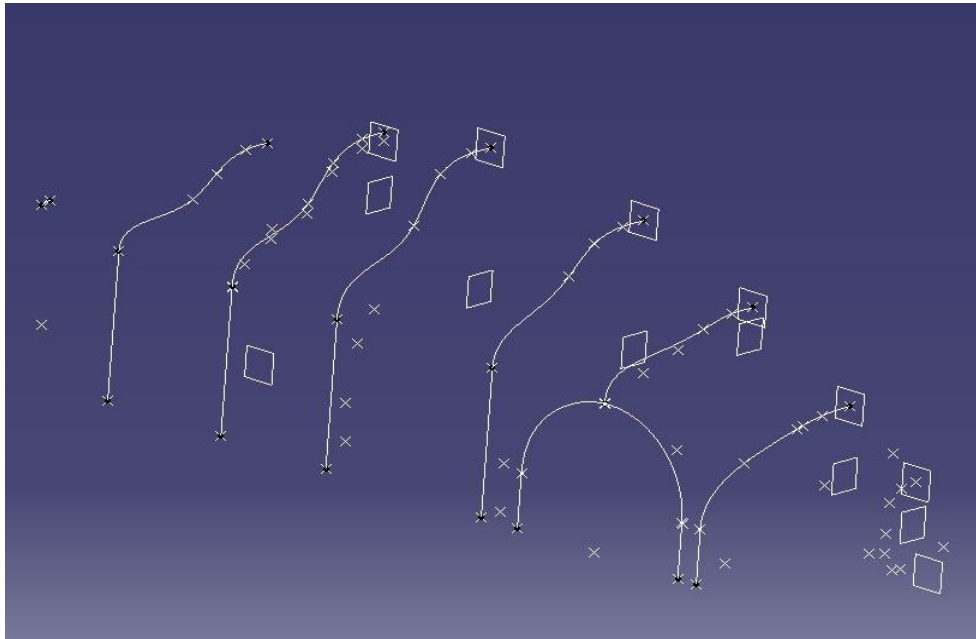


Figure 6.3: Reshaping the vehicle using the wireframes

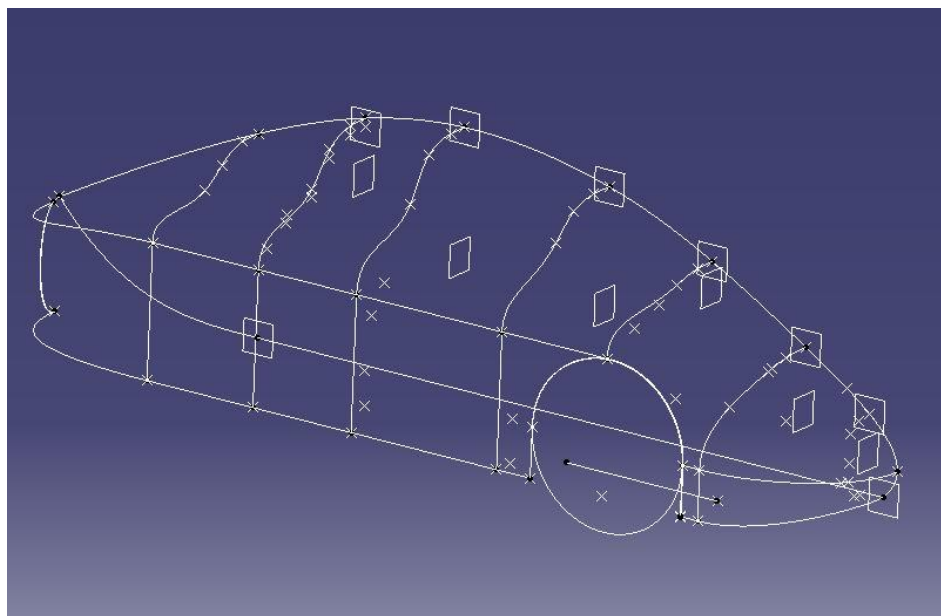


Figure 6.4: The final shape of the 1st model using wireframes

The final surface was created using “Multi-Sections surface” command choosing as “Sections” the wireframes and as a “Guide” the line at the symmetry plane (Figure 6.5).

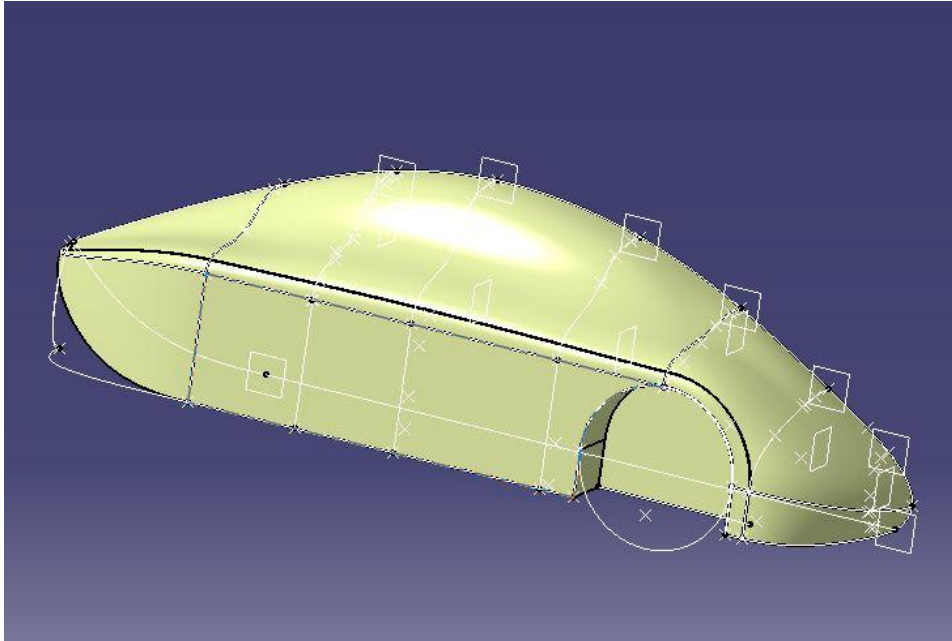


Figure 6.5: The final surface for the 1st model

As it was presented in the previous chapter, a solid volume of the vehicle should be created in order to be simulated; this was accomplished through the command "close surface". In Figures 6.6 to 6.9 various view of the solid model are presented. Figure 6.10 contains a 2D drawing of the vehicle.

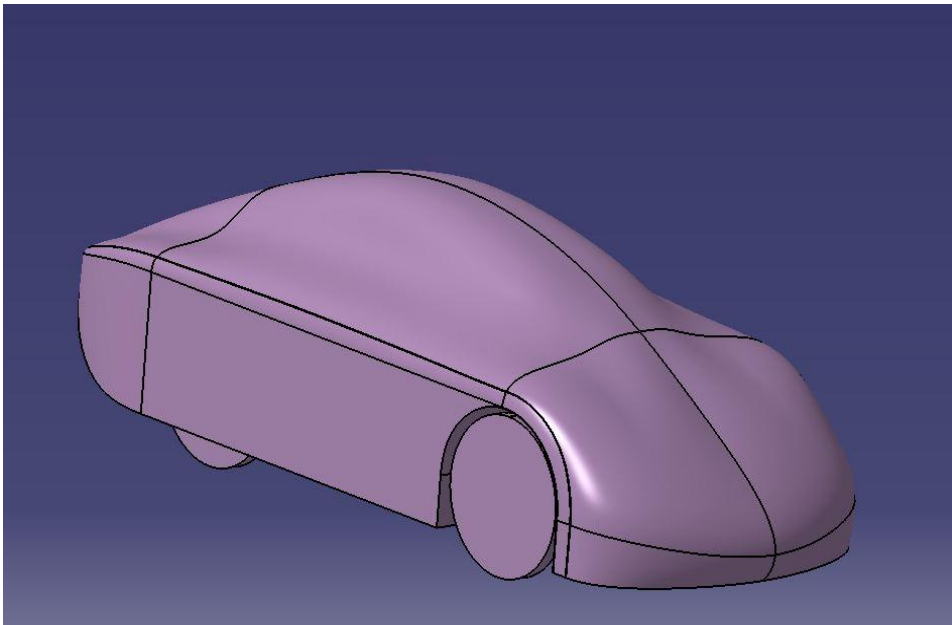


Figure 6.6: Front - side view of the 1st model

The wheel base remained the same with the one in the old vehicle. The height of the vehicle is approaching the minimum racing requirements, having as a goal to reduce the frontal area.

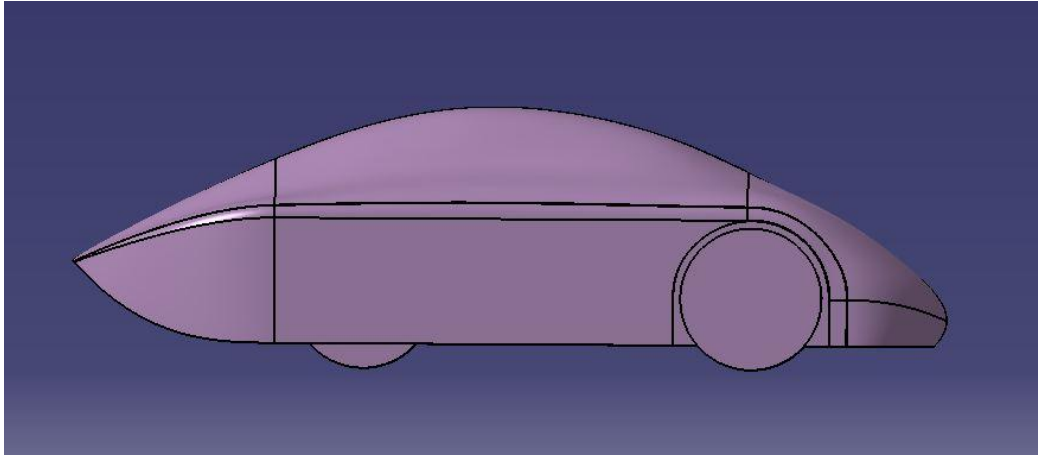


Figure 6.7: Side view of the 1st model

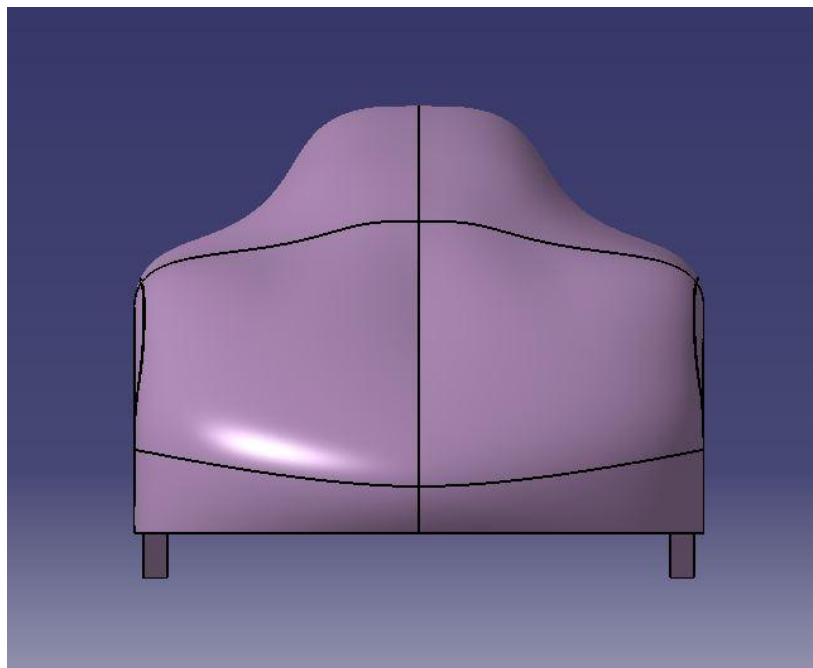


Figure 6.8: Front view of the 1st model

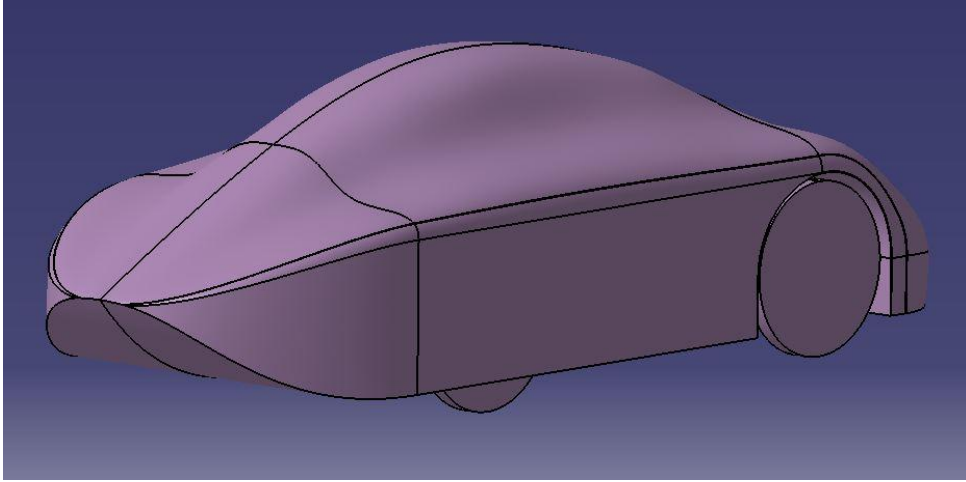


Figure 6.9: Back-side view of the 1st model

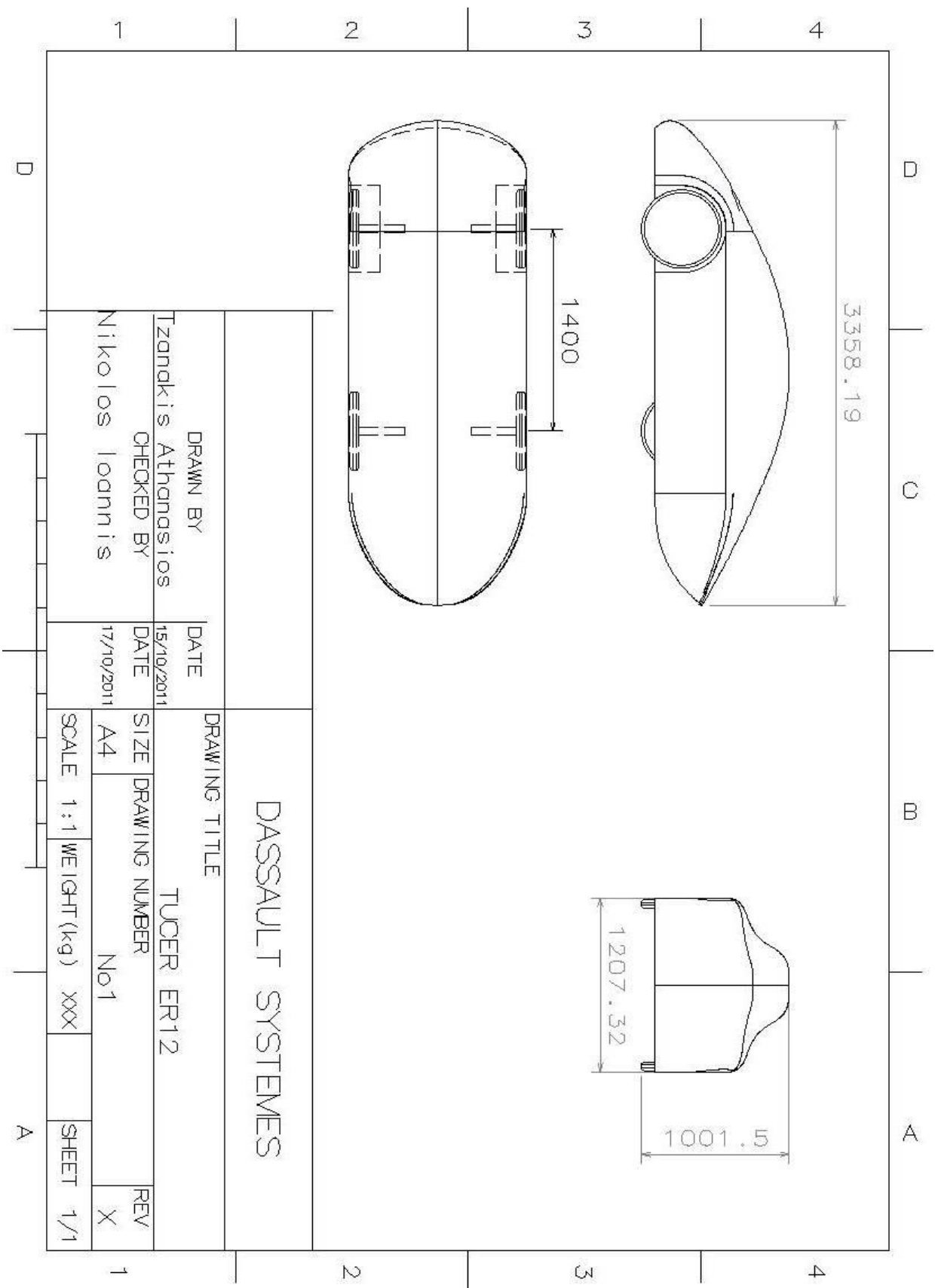


Figure 6.10: 2D drawings of the 1st model

6.1.2 CFD Simulation Results for the 1st model

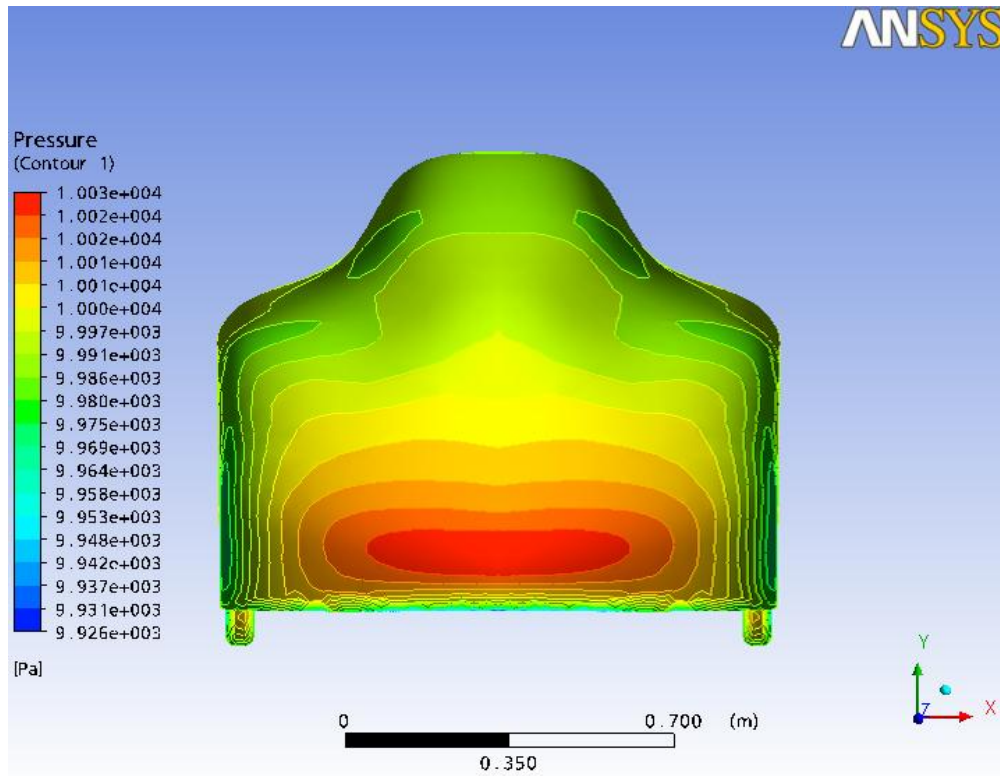


Figure 6.11: Surface pressure contours - front view

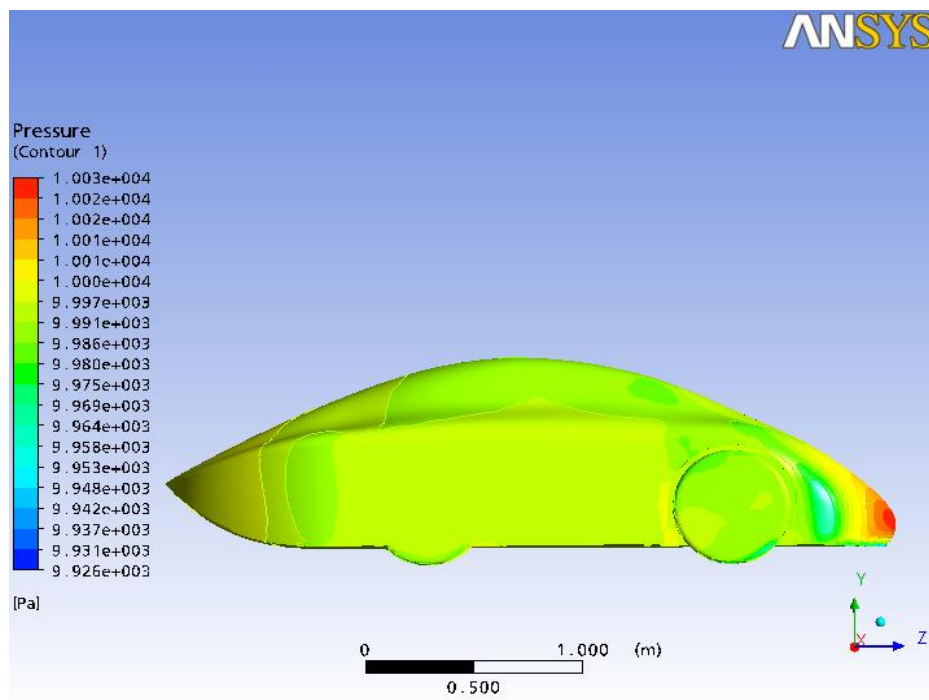


Figure 6.12: Surface pressure contours - side view

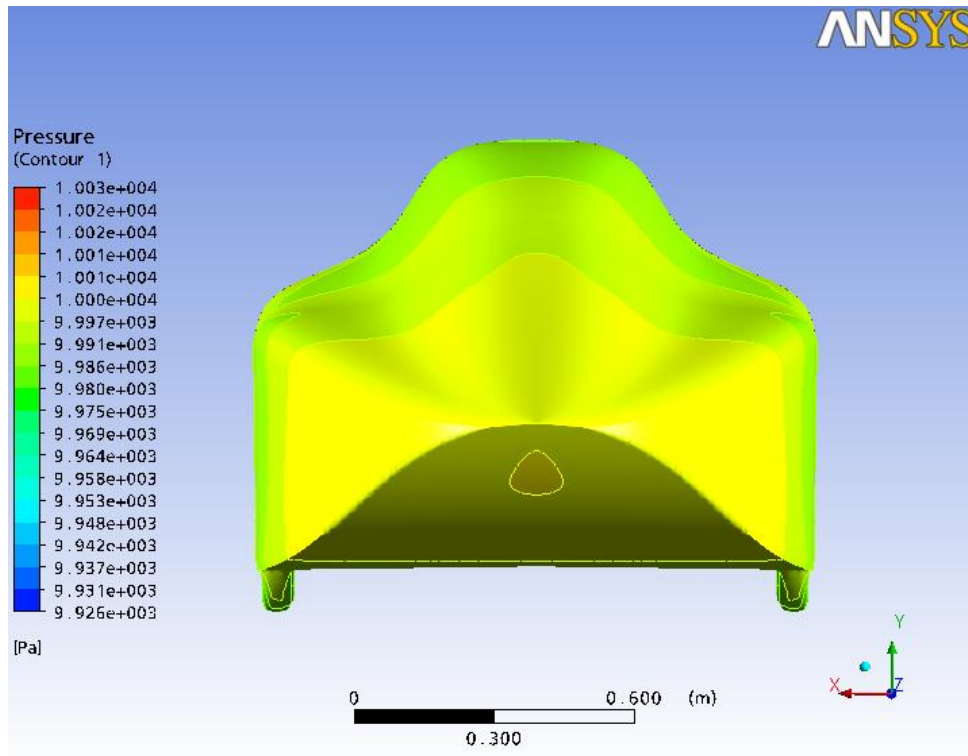


Figure 6.13: Surface Pressure contours - rear view

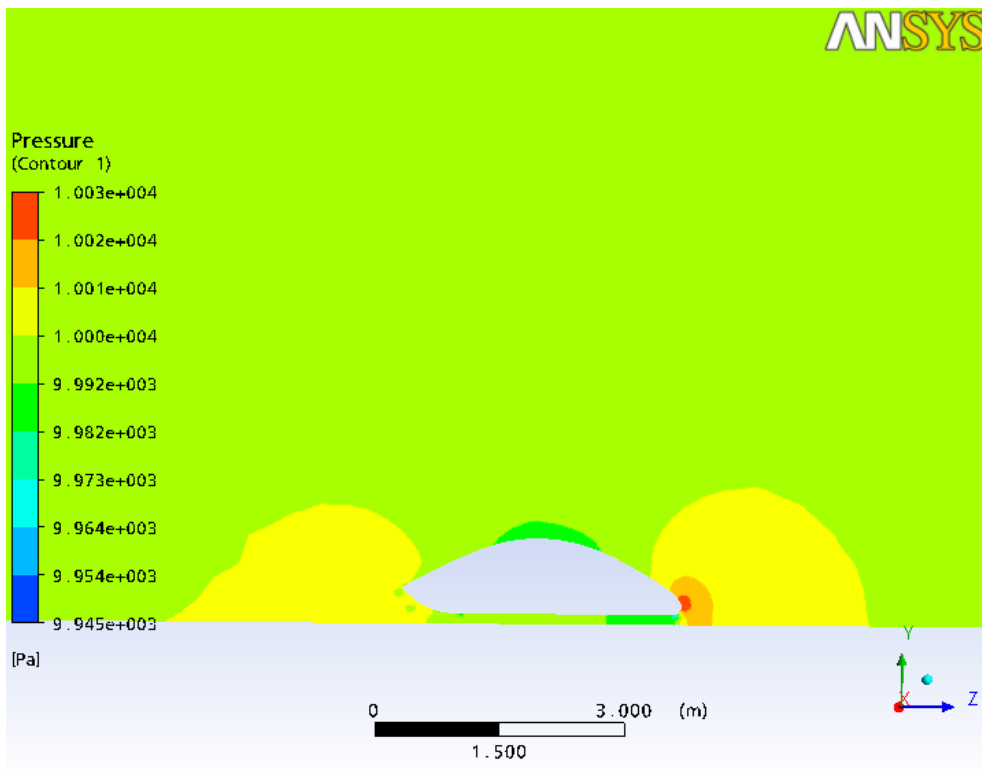


Figure 6.14: Pressure contours at the symmetry plane

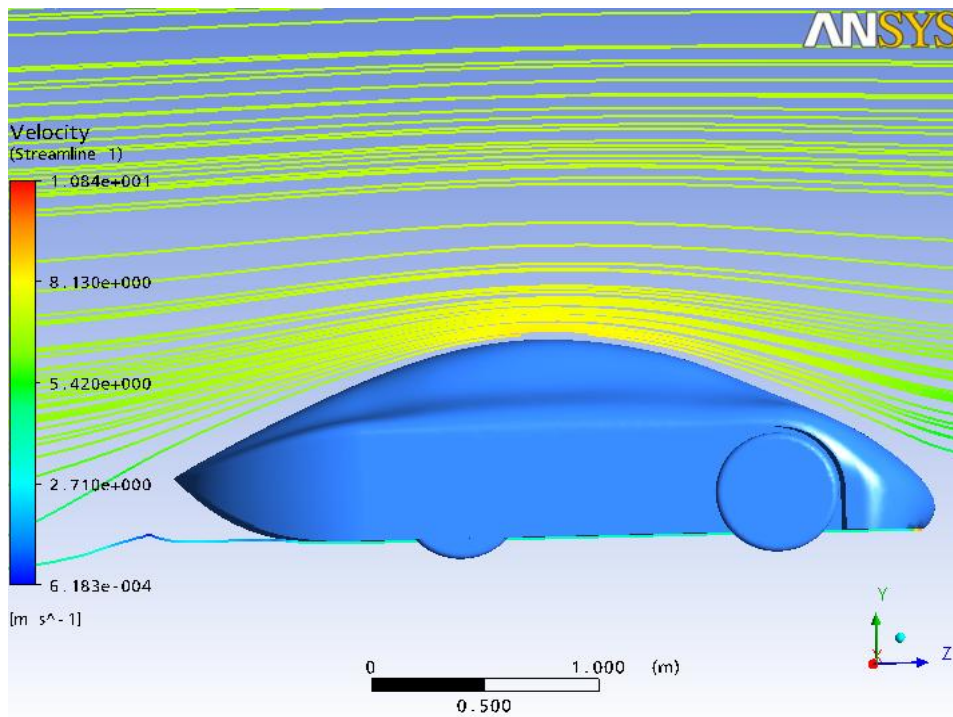


Figure 6.15: Streamlines on the symmetry plane

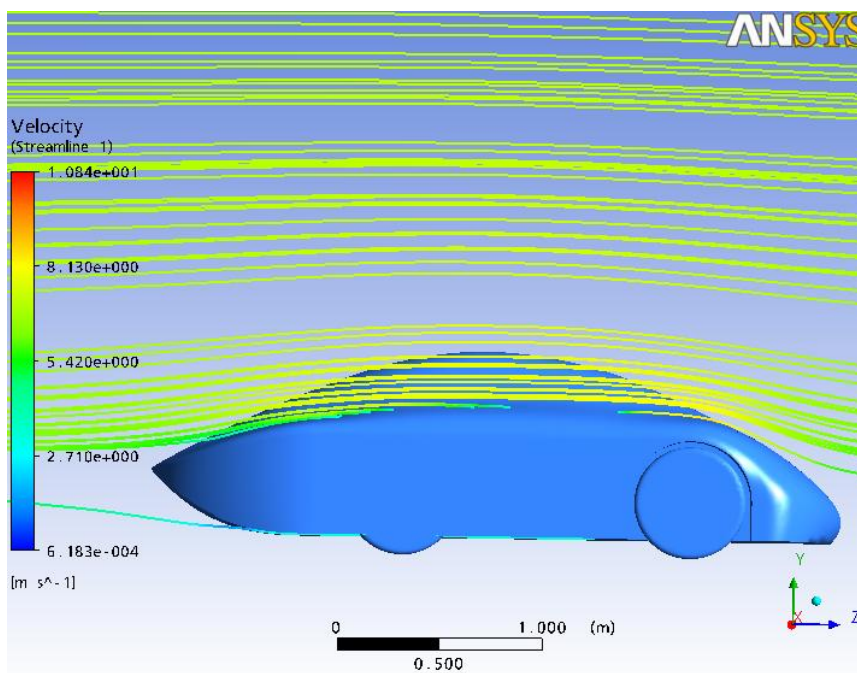


Figure 6.16: Streamlines on a plane 0.35m away from the symmetry plane

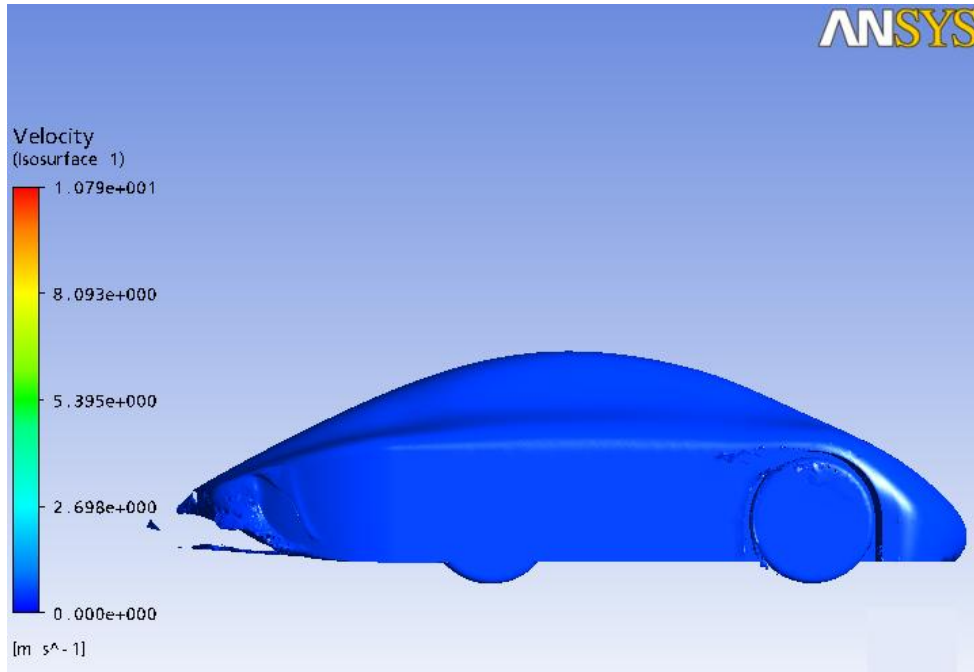


Figure 6.17: Equal-velocity surface for 0.5m/s

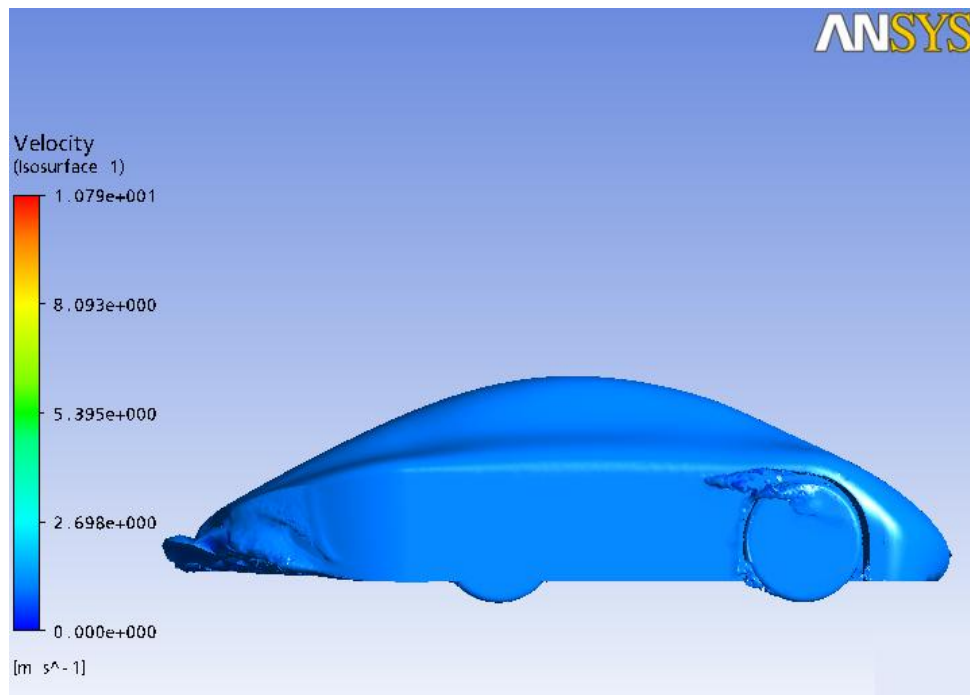


Figure 6.18: Equal-velocity surface for 1m/s

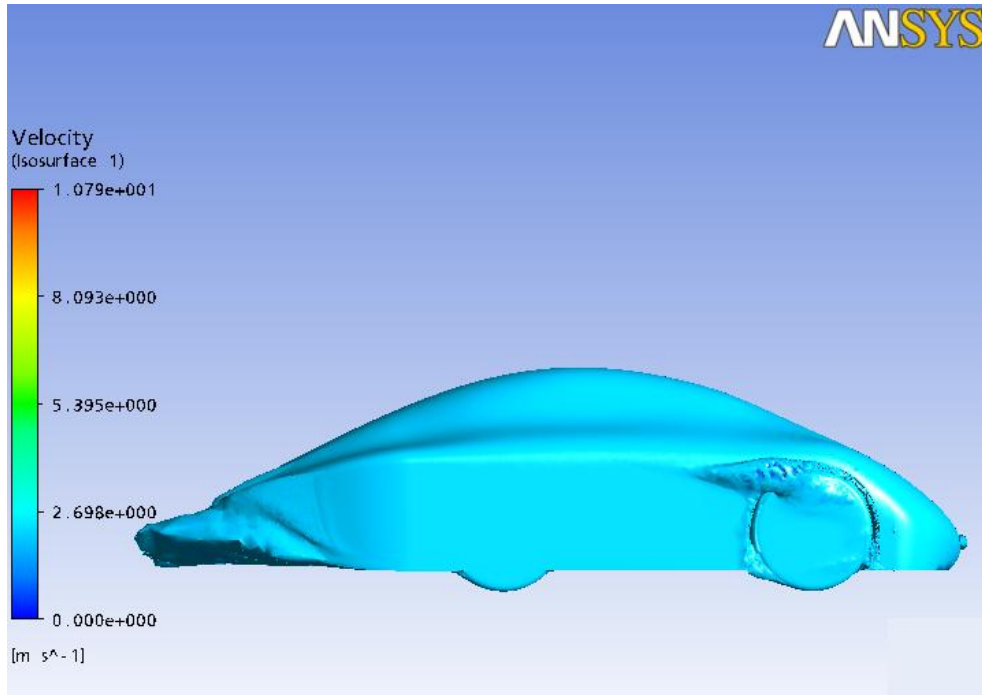


Figure 6.19: Equal-velocity surface for 2m/s

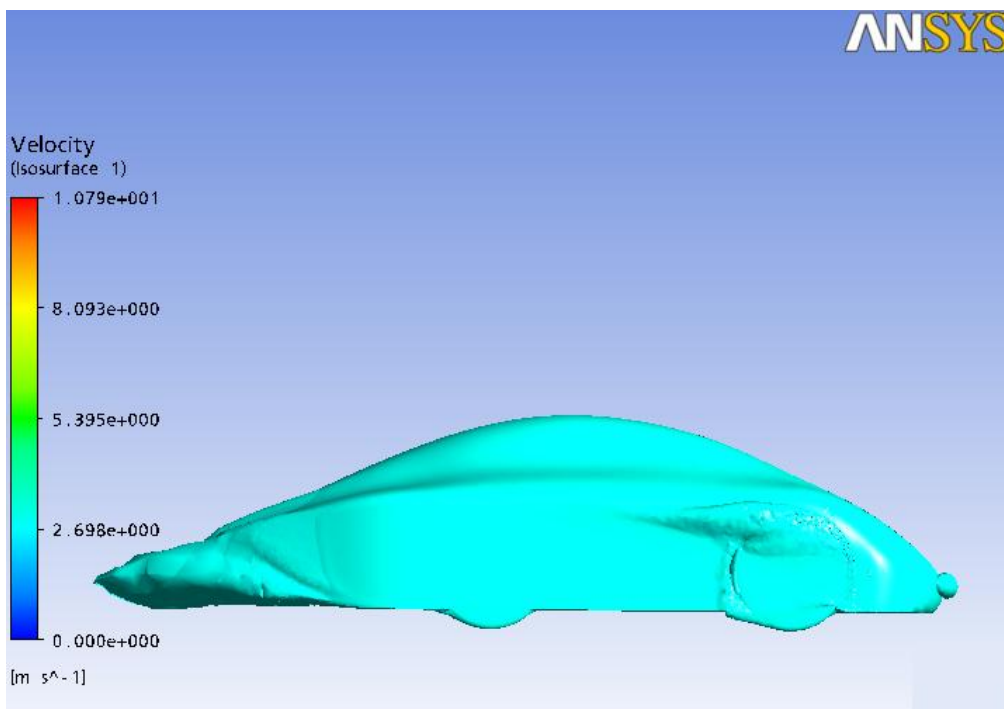


Figure 6.20: Equal-velocity surface for 3m/s

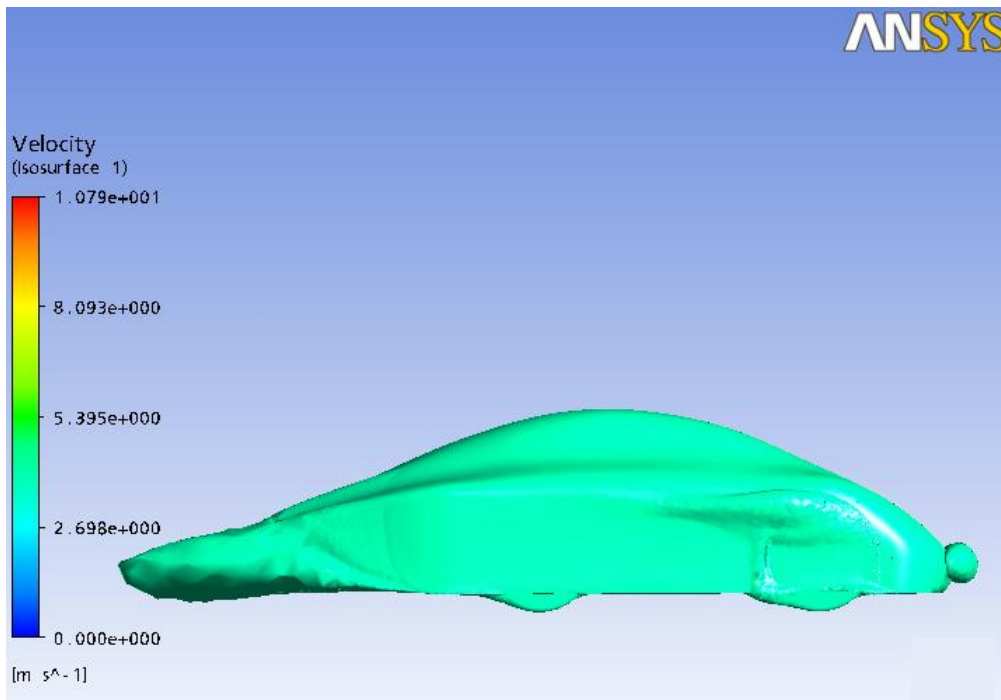


Figure 6.21: Equal-velocity surface for 4m/s

Figures 6.11 to 6.14 present static pressure contours for the 1st model. Figures 6.15 to 6.16 present the streamlines at two parallel planes, while Figures 6.17 to 6.21 present iso-velocity surfaces. Comparing with the corresponding illustrations for the ER11 vehicle, it can be easily seen that the separation region behind the front wheels has been eliminated and the separation region at the rear of the car was considerably decreased. This has a significant result on the drag force, which is now equal to 2.51 Nt for half the vehicle (5.02 Nt for the whole vehicle), **while the required power to withstand the aerodynamic drag was reduced by 56%, at only 34 Watts, compared to 82 Watts of ER11 vehicle.**

6.2 TUCER ER12 2nd Model

6.2.1 Design

The second model is not as long as the 1st model, considering the cost of construction and the area of the surface, which adds weight to the vehicle. Moreover it was a prerequisite that the vehicle should look like a regular commercial vehicle. However, the same simple

design lines have been maintained, having as a target a better aerodynamic efficiency. Figures 6.22 to 6.25 demonstrate the shape of the 2nd model.

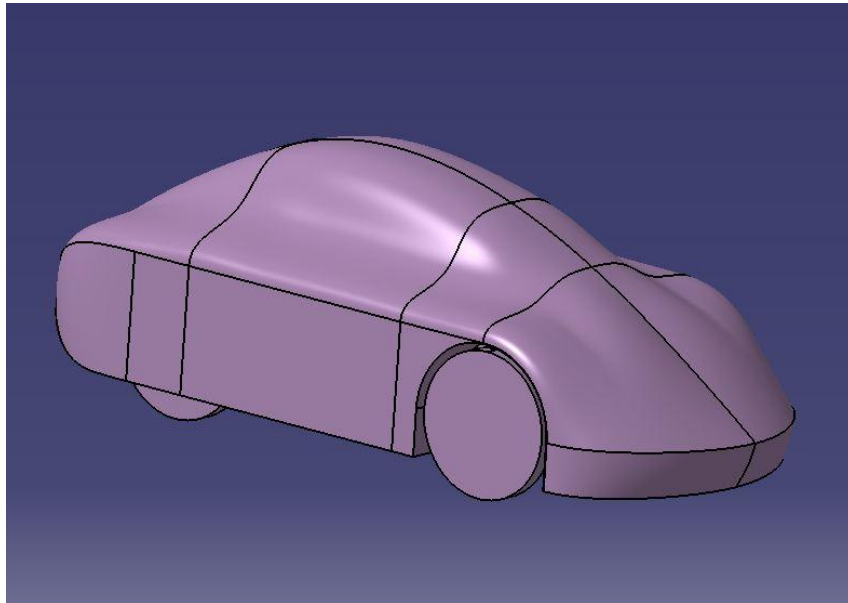


Figure 6.22: Front-side view of the 2nd model

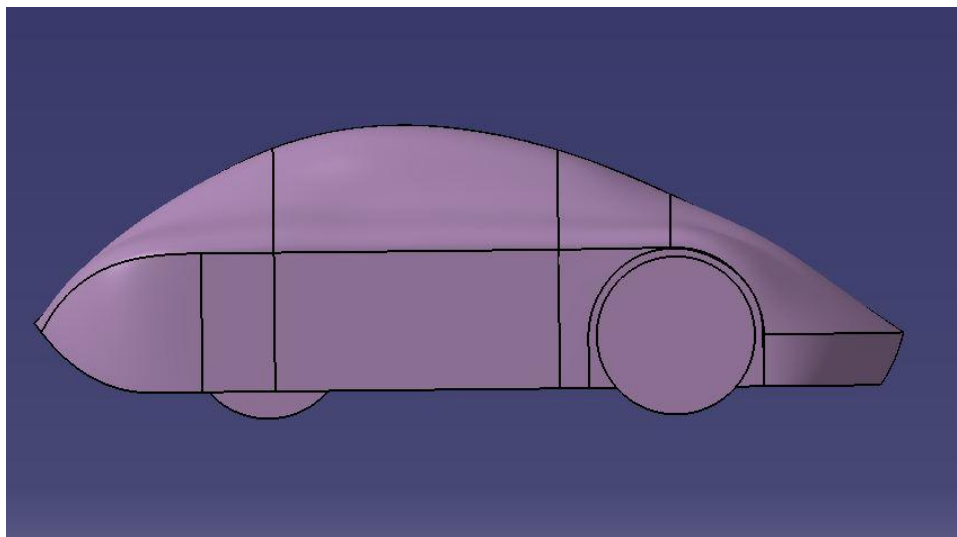


Figure 6.22: Side view of the 2nd model

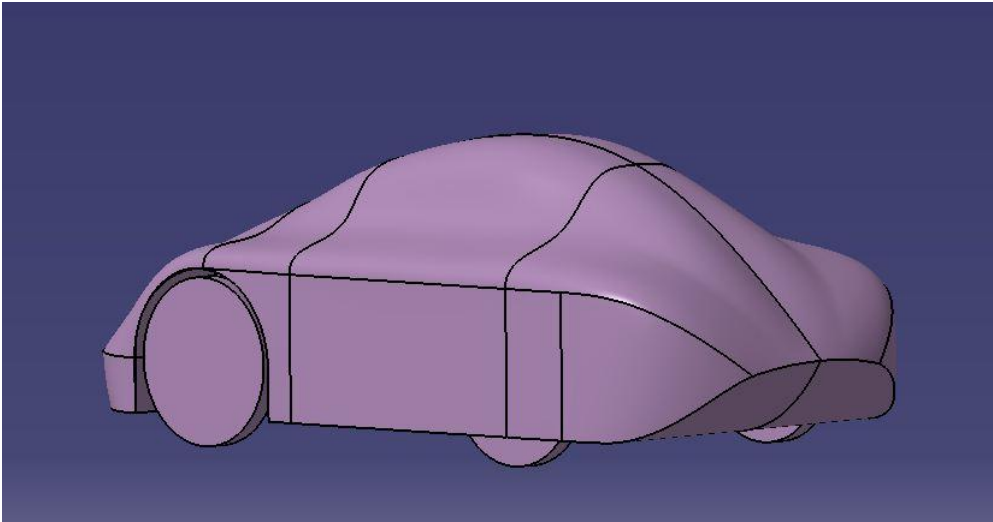


Figure 6.23: Rear-side view of the 2nd model

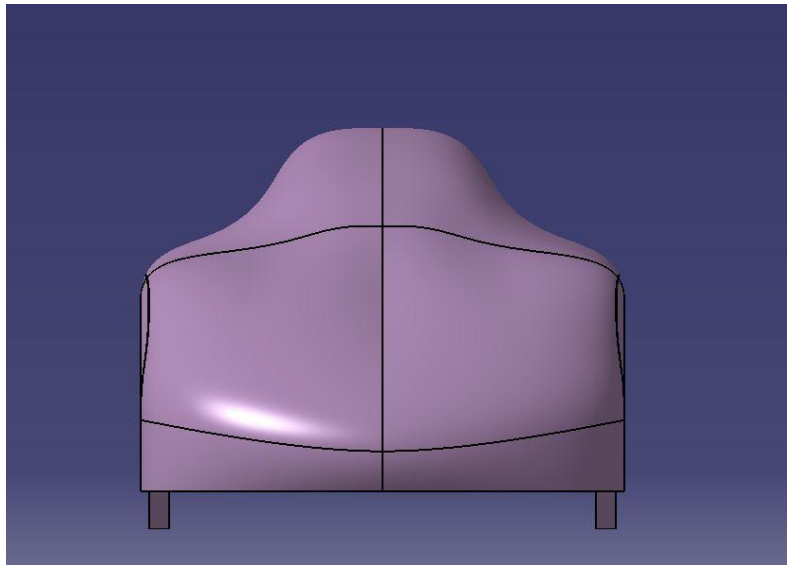


Figure 6.24: Front View of the 2nd model

The 2nd model was not simulated with ANSYS-CFX because the cost of its construction was predicted to be high and its shape was not accepted by the members of the racing team for aesthetic reasons. The following models were designed with the aim of producing a shorter vehicle, with smaller surface, which would result in less weight, a crucial factor for the vehicle's efficiency, which covers smaller surface. The second model has 1400mm wheelbase and 2980mm total length. The 2D drawings of the 2nd model are included in Figure 6.26.

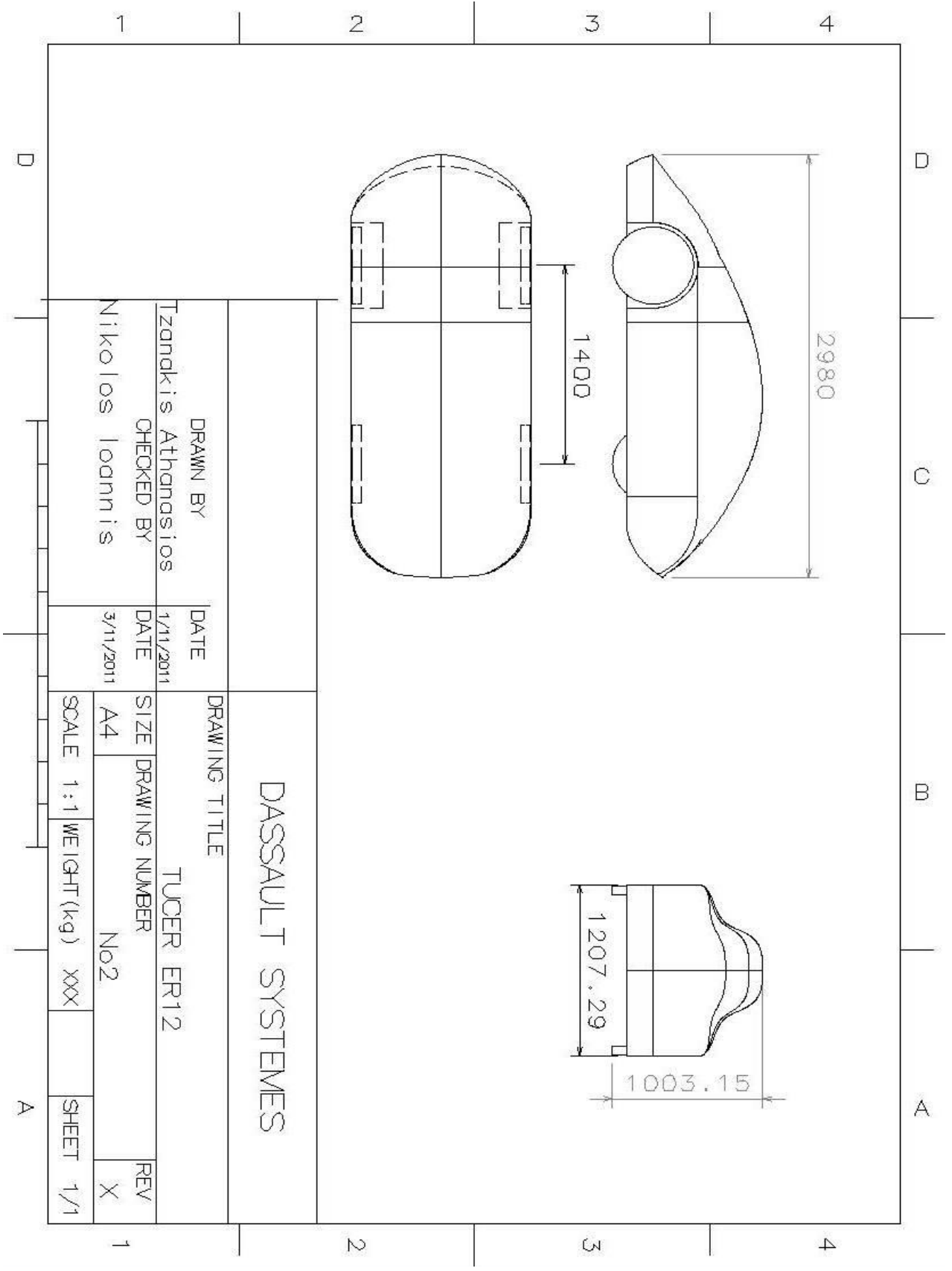


Figure 6.25: 2D drawings of the 2nd model

6.3 TUCER ER12 3rd Model

6.3.1 Design

The design objective of the 3rd model was focused on the length reduction of the vehicle, having as a result a smaller surface, so less air friction, lower construction cost and lower weight. There are two main changes in comparison with the previous mockups, shorter wheel base and a totally different rear side as Figures 6.27 to 6.30 illustrate.

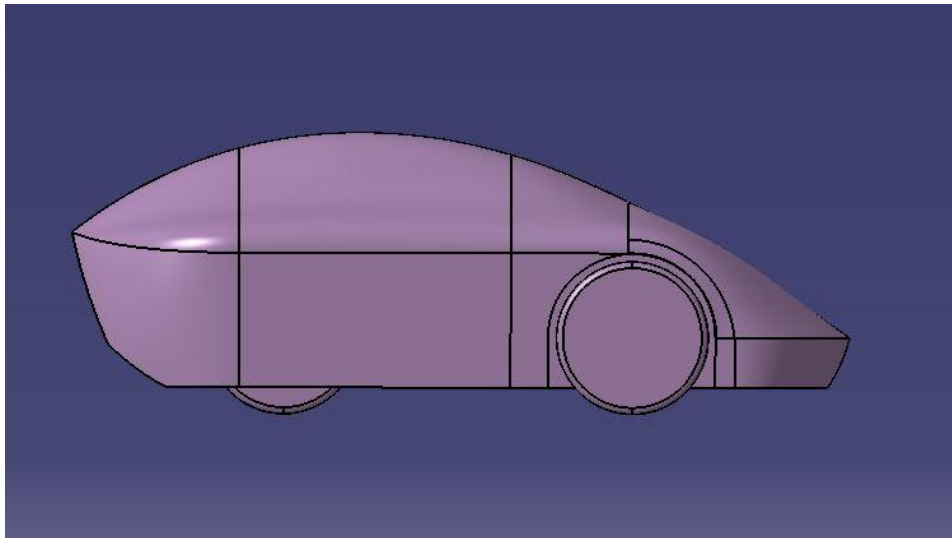


Figure 6.26: Side view of the 3rd model

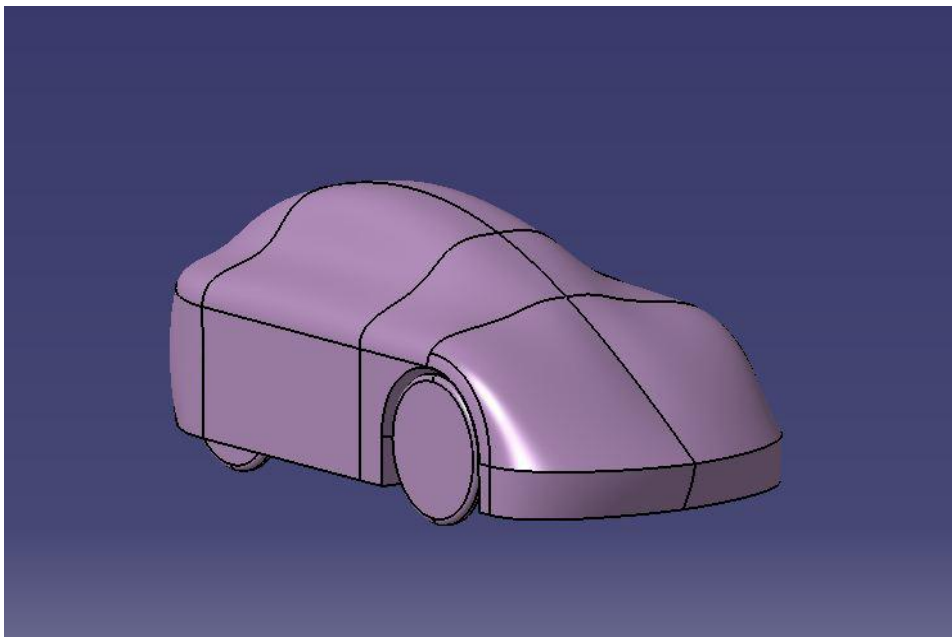


Figure 6.27: Front-side view of the 3rd model

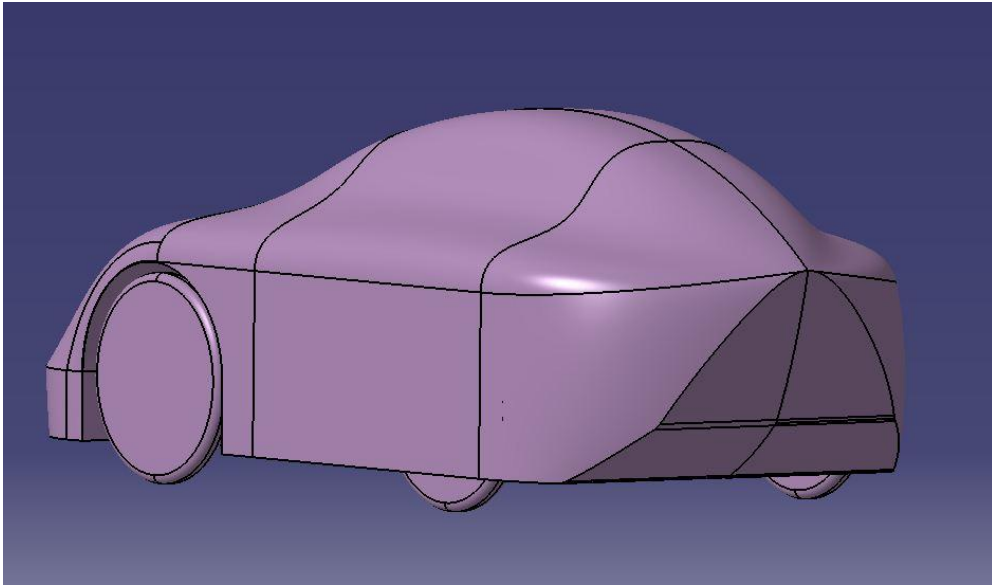


Figure 6.28: Rear-side view of the 3rd model

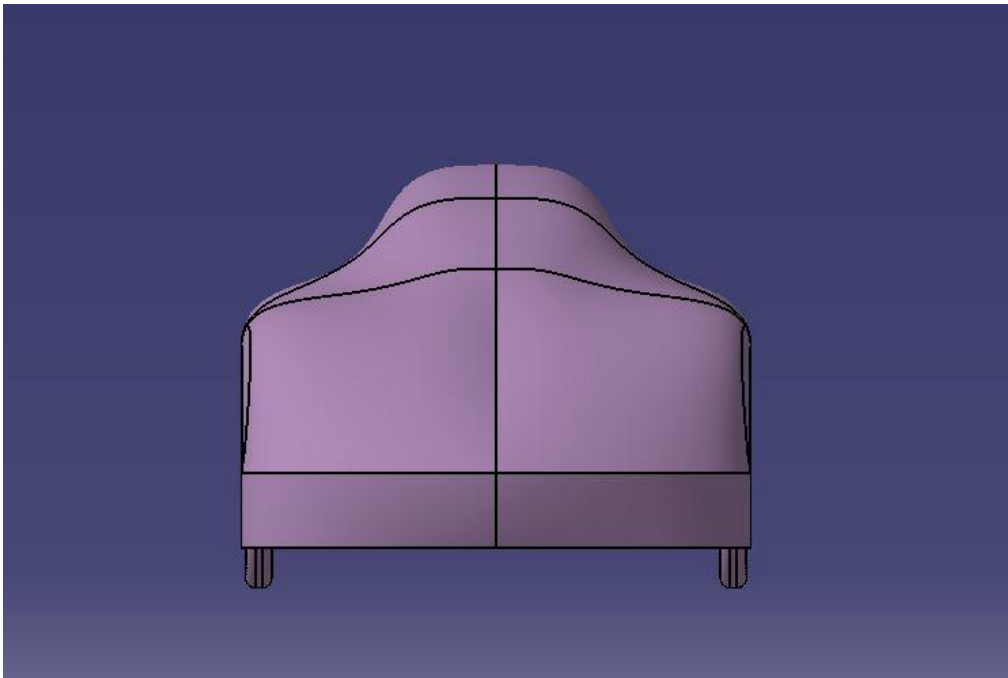


Figure 6.29: Front view of the 3rd model

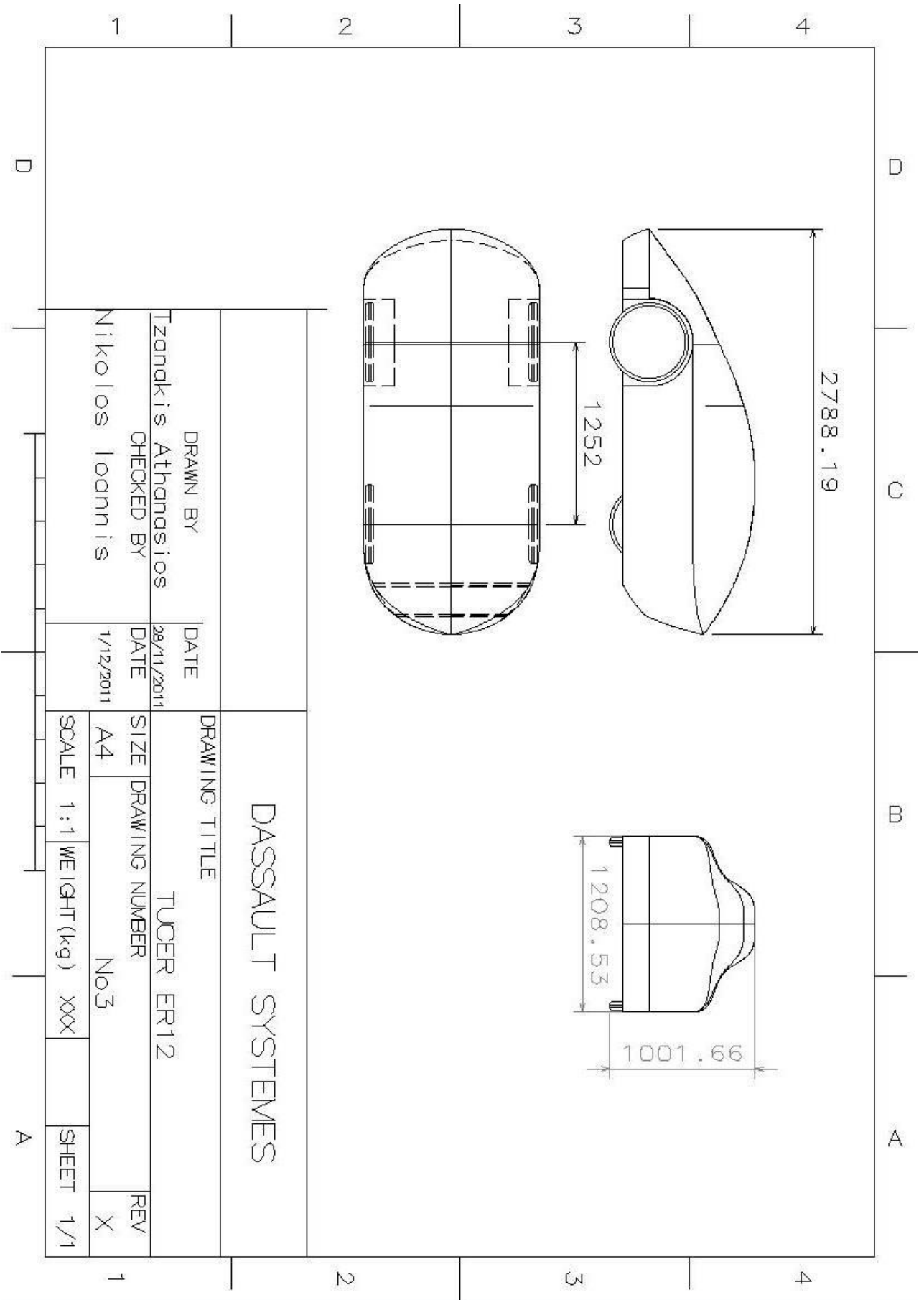


Figure 6.30: 2D drawings of the 3rd model

6.3.2 CFD Simulation Results for the 3rd model

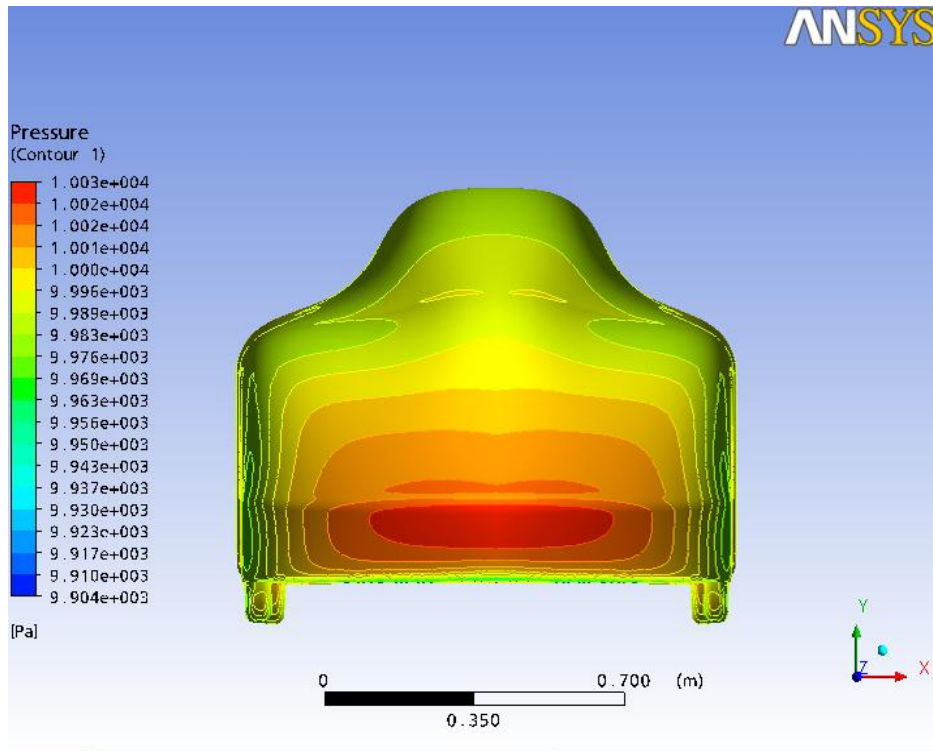


Figure 6.31: Surface Pressure contours - front view - 3rd model

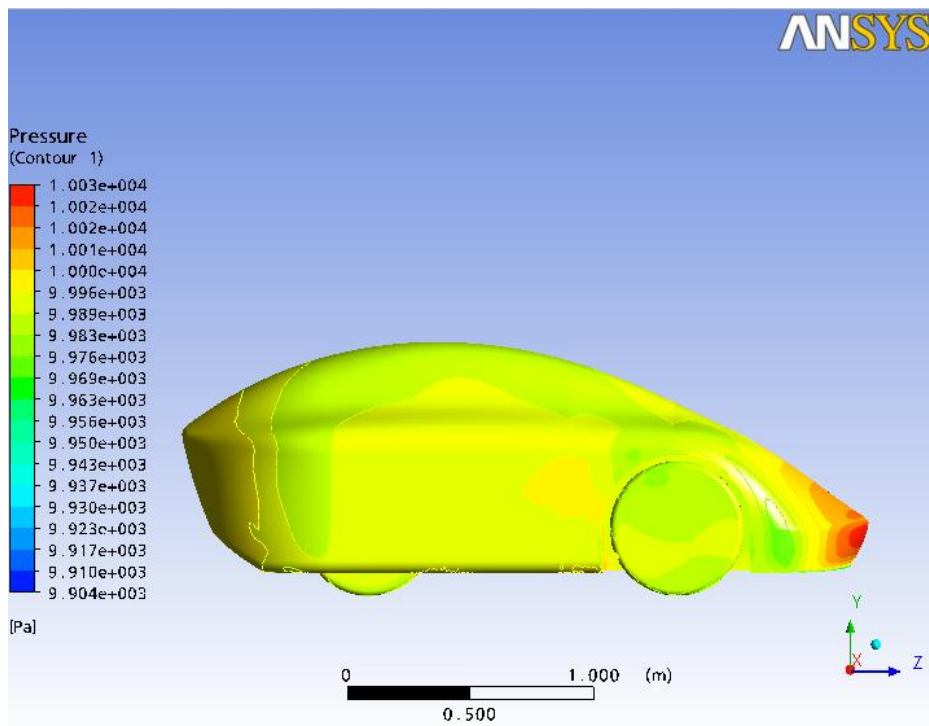


Figure 6.32: Surface Pressure contours - side view - 3rd model

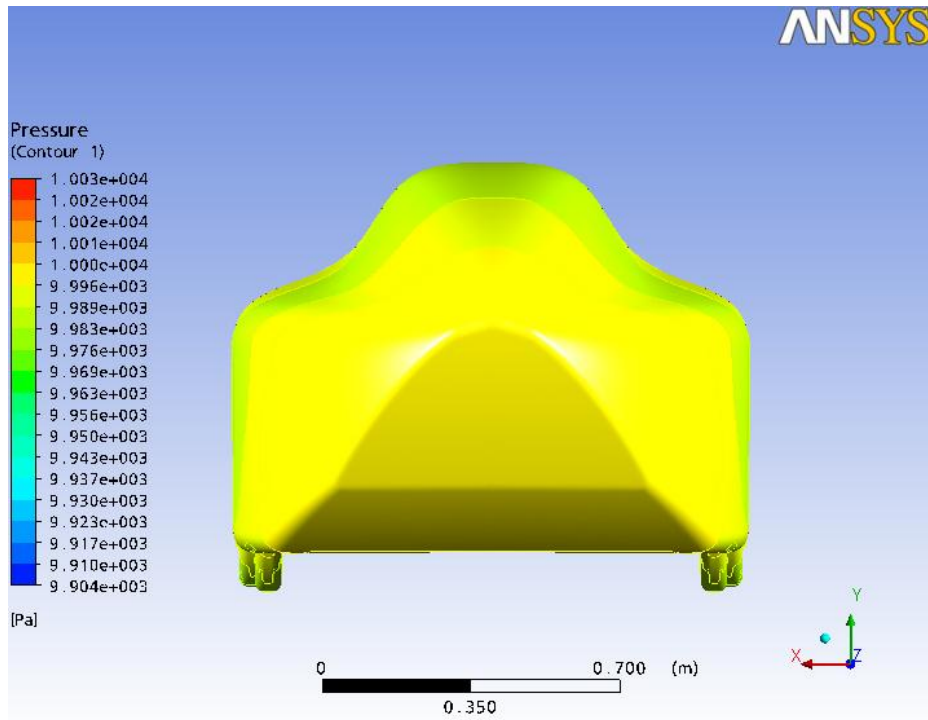


Figure 6.33: Surface pressure contours - Rear View - 3rd model

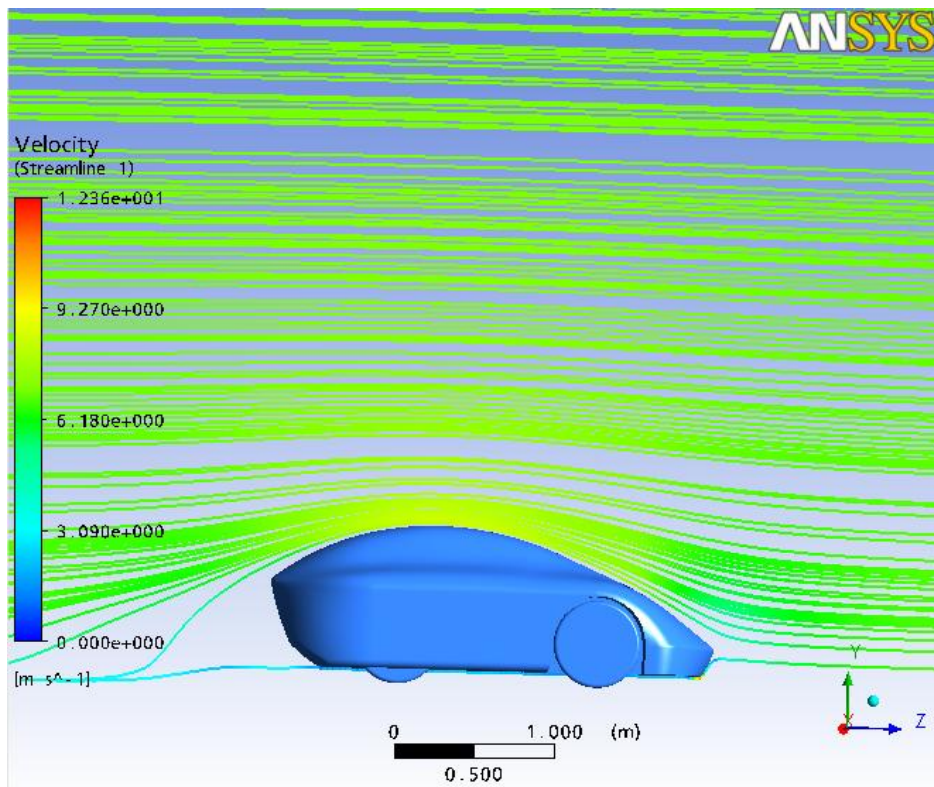


Figure 6.34: Streamlines - symmetry plain - 3rd model

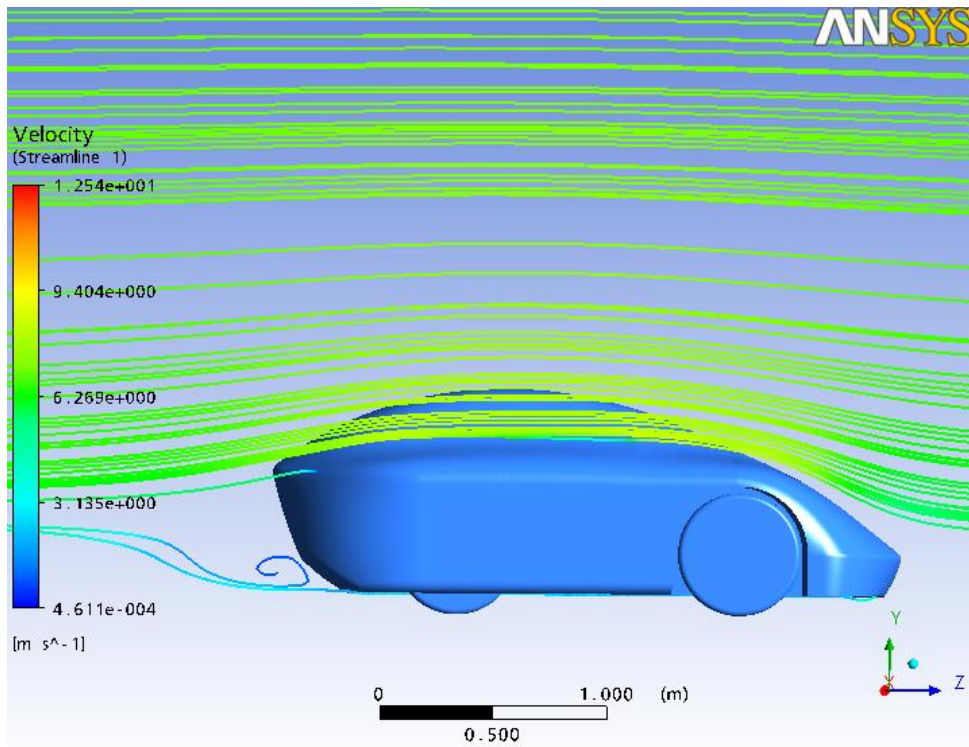


Figure 6.35: Streamlines at a plane 0.35m away from the symmetry plain - 3rd model

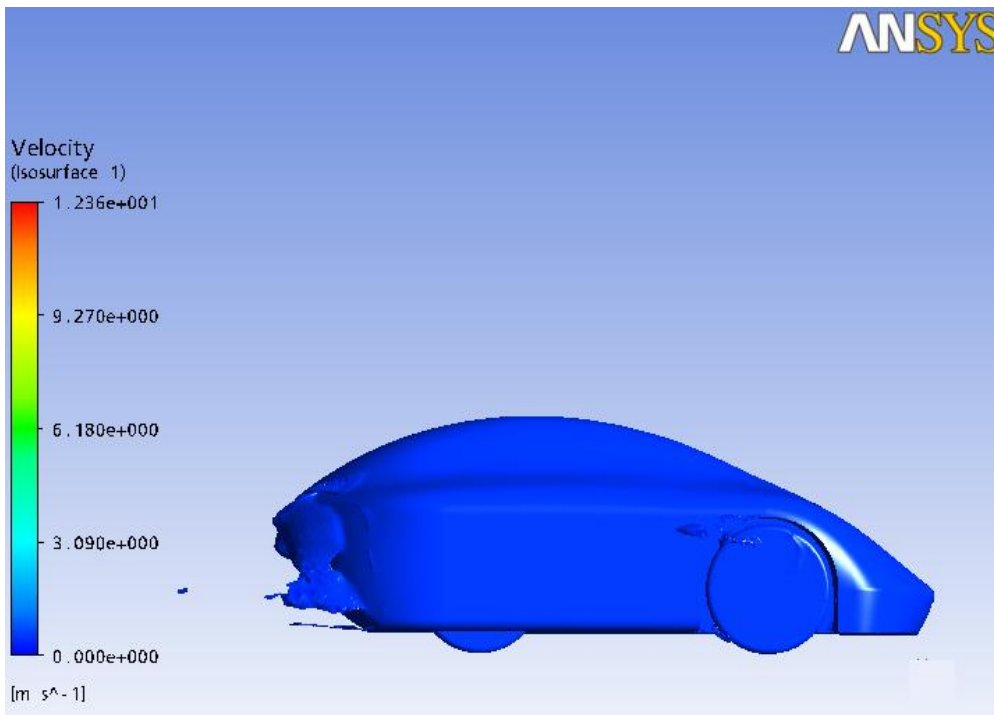


Figure 6.36: Equal-velocity surface for 0.5m/s - 3rd model

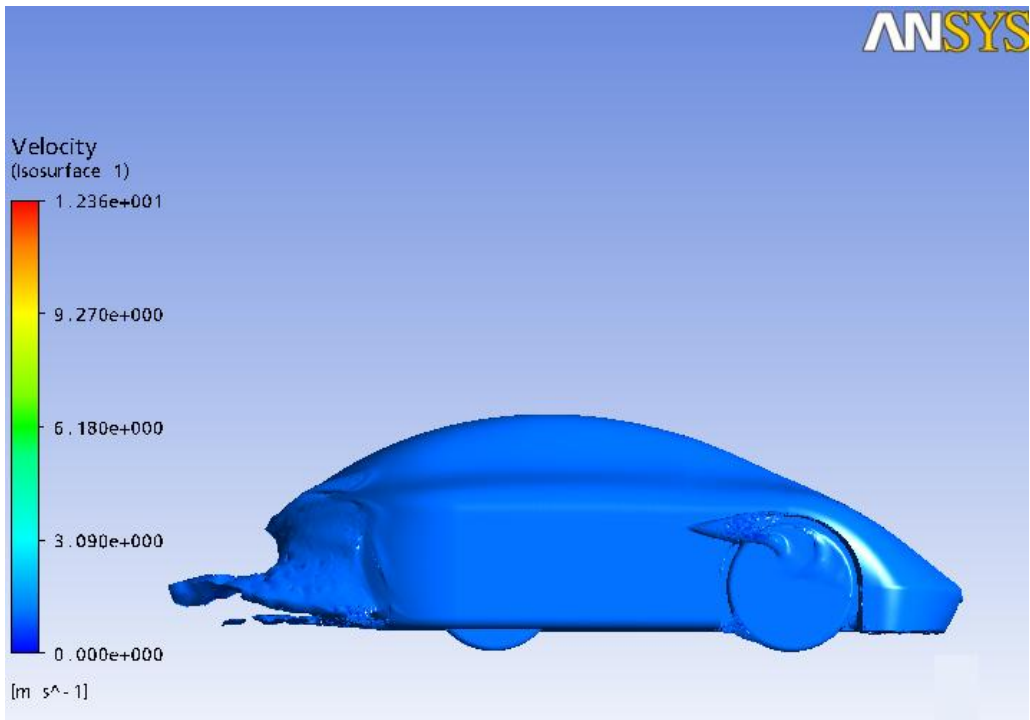


Figure 6.37: Equal-velocity surface for 1 m/s - 3rd model

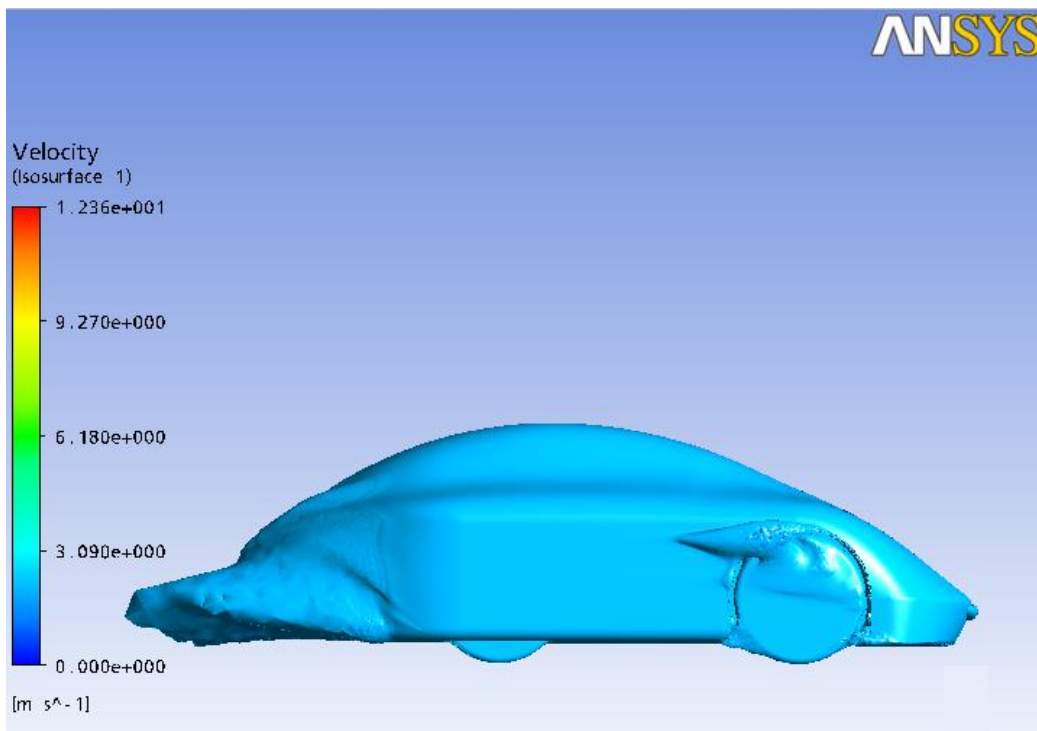


Figure 6.38: Equal-velocity surface for 2 m/s - 3rd model

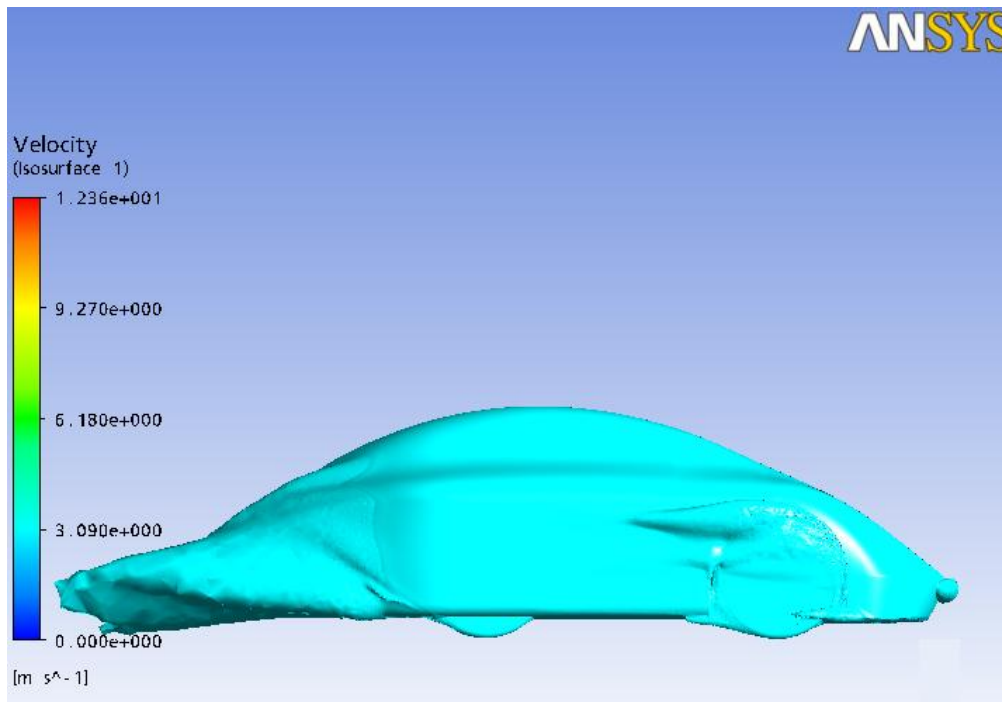


Figure 6.39: Equal-velocity surface for 3 m/s - 3rd model

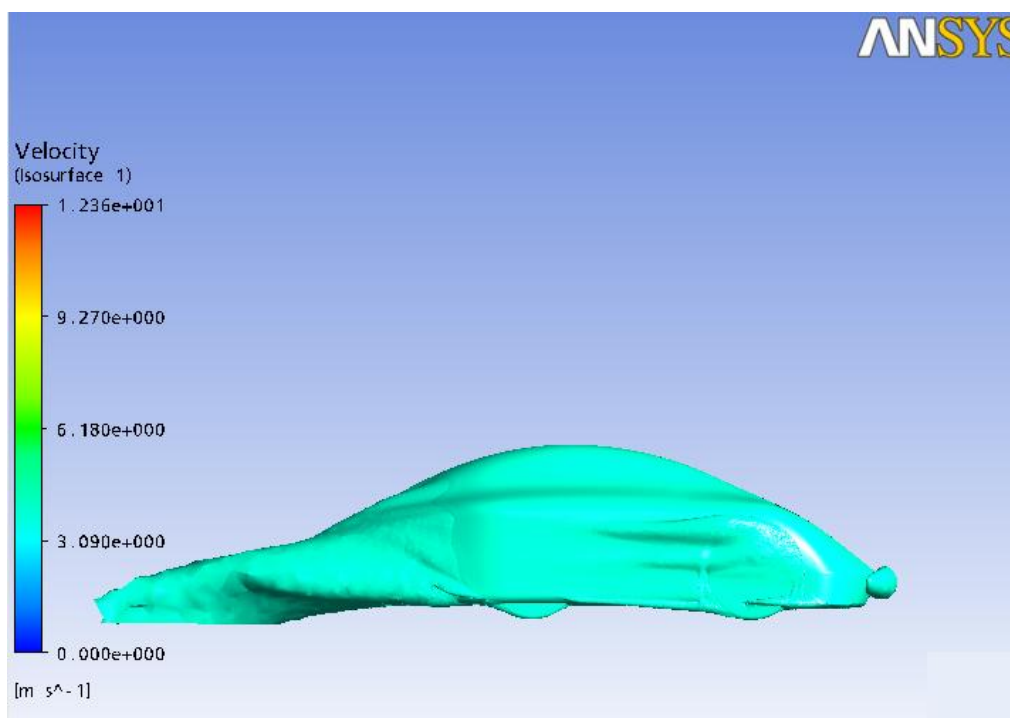


Figure 6.40: Equal-velocity surface for 4 m/s - 3rd model

Figures 6.31 to 6.33 contain static pressure contours for the 3rd model. Figure 6.34, 6.35 contain the stream lines at two different parallel planes. Figures 6.36 to 6.40 contain iso-velocity surfaces for the 3rd model. Compared to the 1st model it is evident that the

separation and recirculation region is larger for the 3rd model, as it was expected from its rear shape. Consistently, the drag force was computed equal to 6.085 Nt, while the power connected to aerodynamic drag was computed equal to 42 Watts.

6.4 TUCER ER12 4th Model

6.4.1 Design

For the 4th model smaller frontal and rear areas were achieved, with a narrower driver cabin and a more curved rear side, respectively. The rear wheels were located closer to each other, the width between the front wheels is 1230mm and 1000mm for the rear ones, having as a result the size reduction of the vehicle (especially at the rear) and at the same time improving the turning cycle of the vehicle. In addition, better aerodynamic efficiency is expected (compared to the 3rd model) due to the smaller frontal area and the more streamlined rear part. Figures 6.43 to 6.46 illustrate the shape of the 4th model. A serious criterion for its design was also the aesthetic acceptance of its shape by the team members. Figure 2.47 contains the 2D drawings of the 4th model.

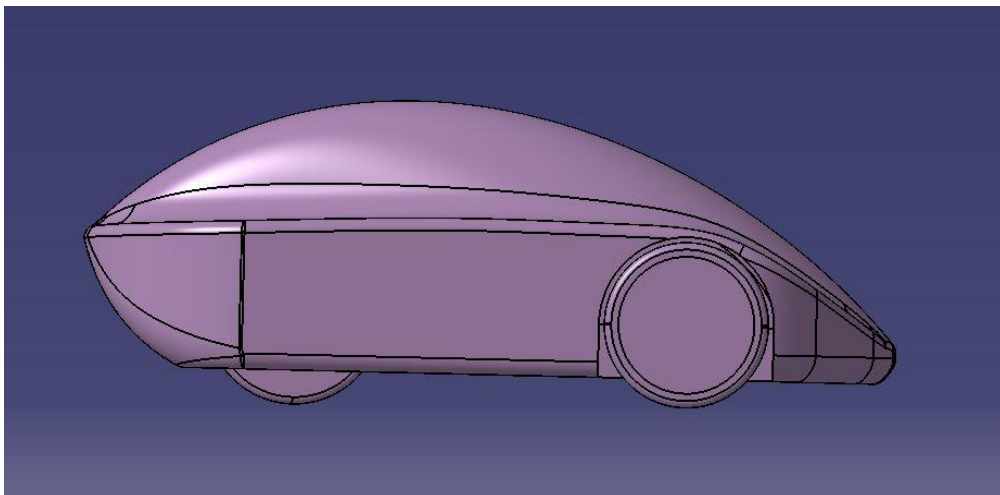


Figure 6.41: Side view of the 4th model

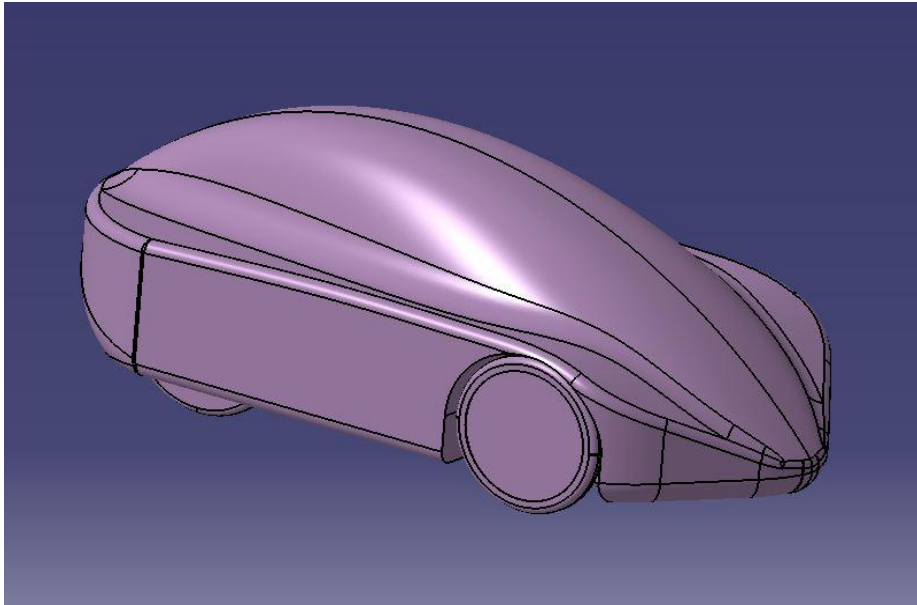


Figure 6.42: Front-side view of the 4th model

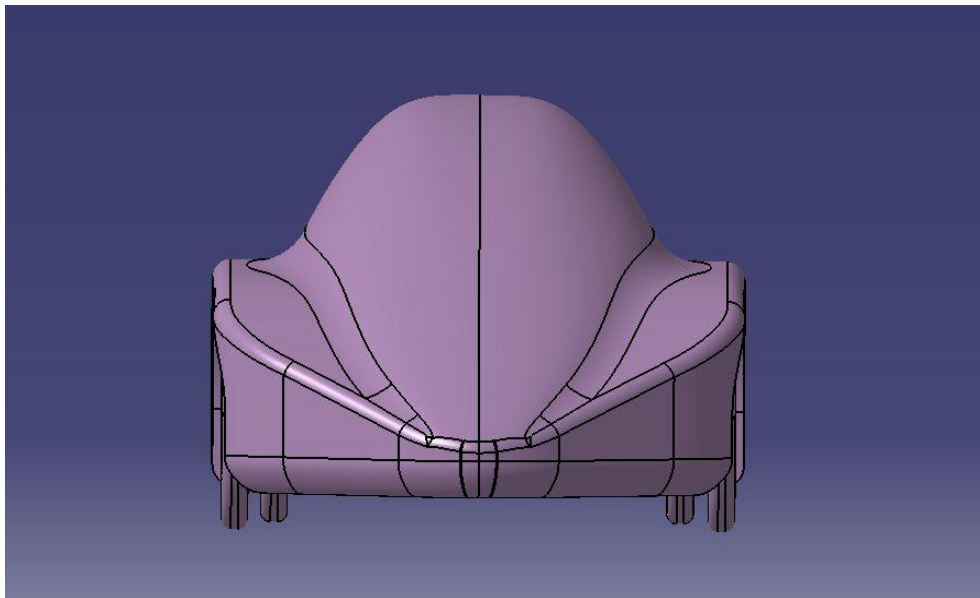


Figure 6.43: Front View of the 4th model

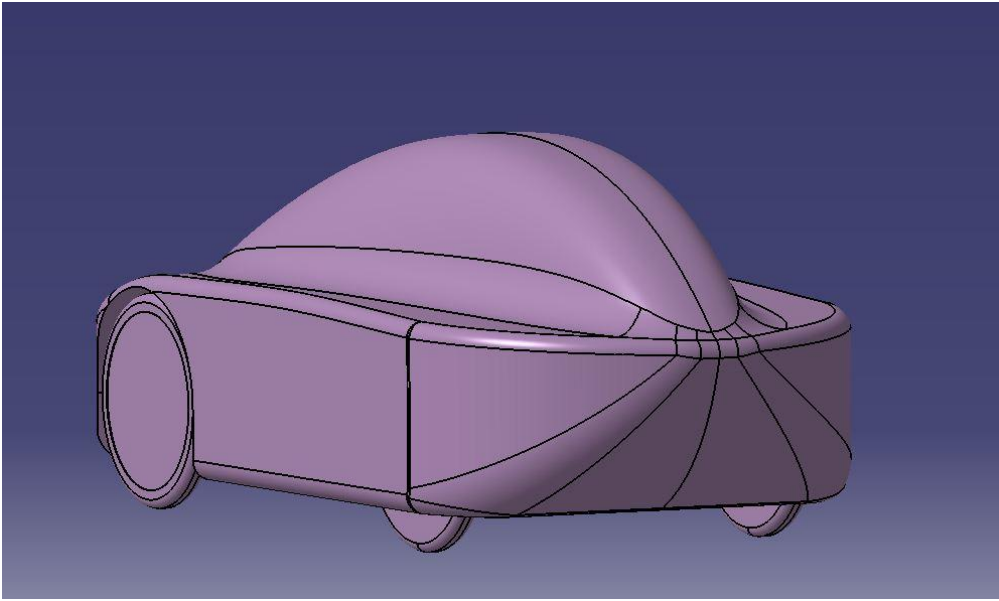


Figure 6.44: Rear Side - 4th model

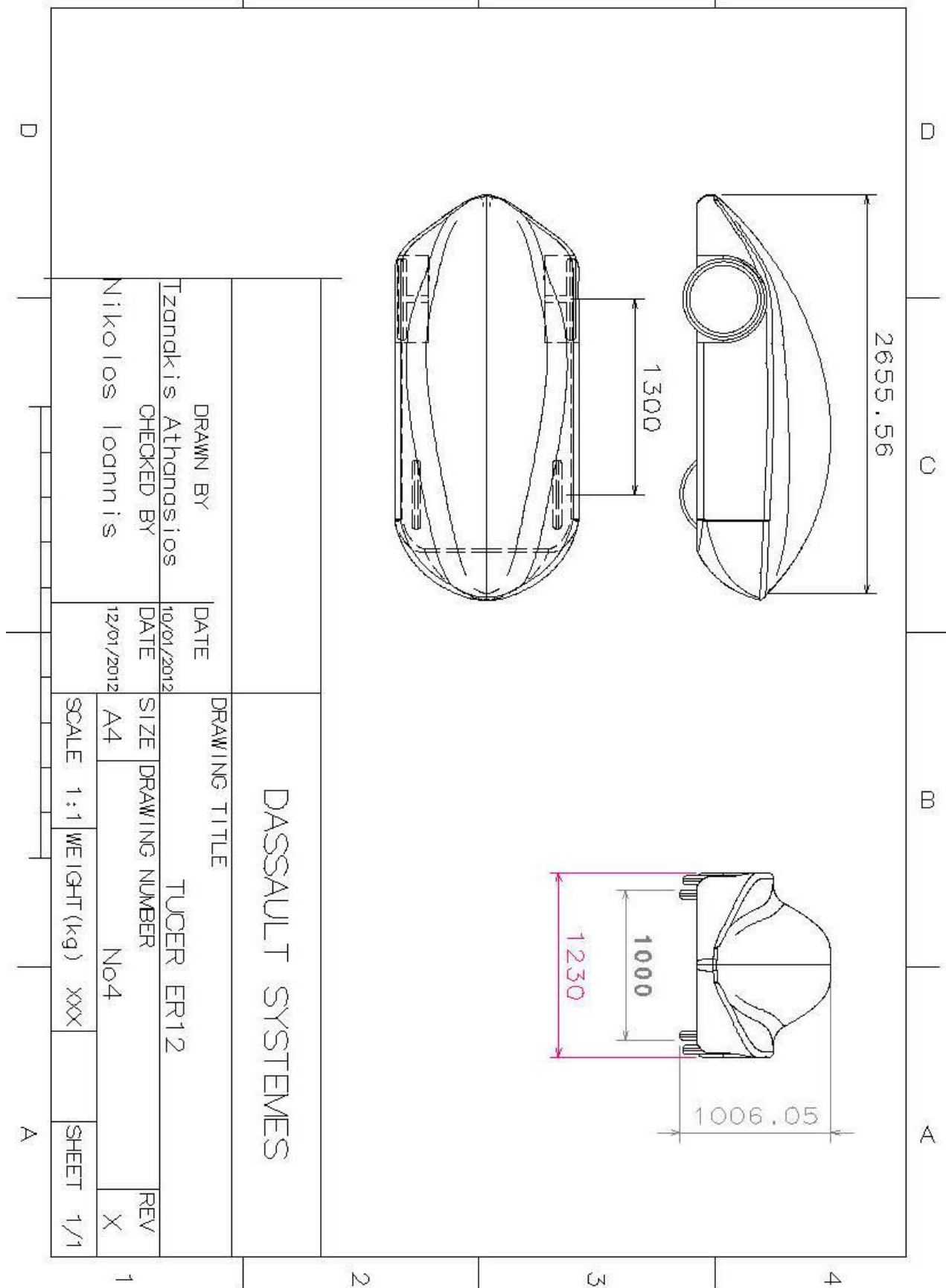


Figure 6.45: 2D drawing of the 4th model

6.4.2 CFD Simulation Results

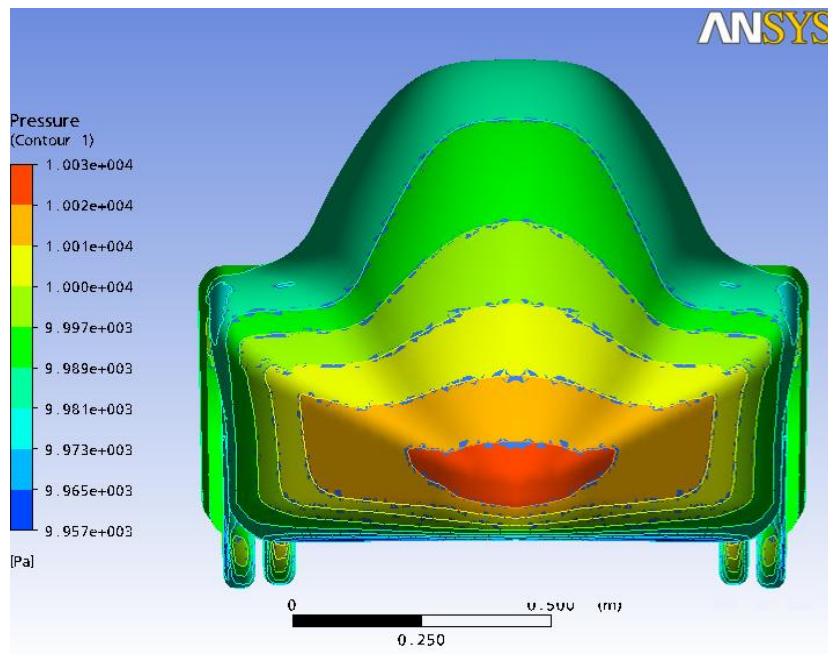


Figure 6.46: Surface pressure contours - Front View - 4th model

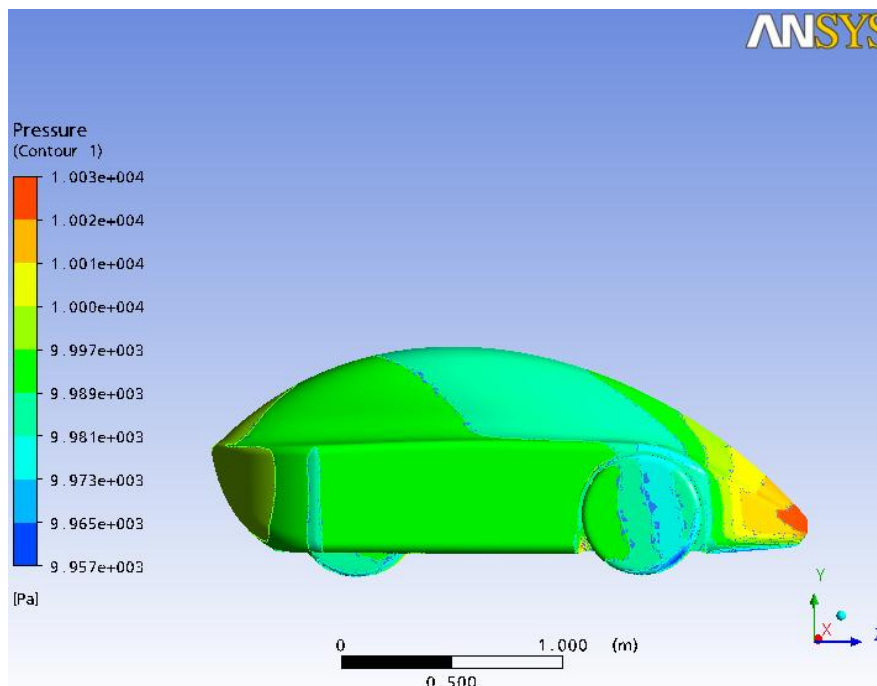


Figure 6.47: Surface pressure contours - Side View - 4th model

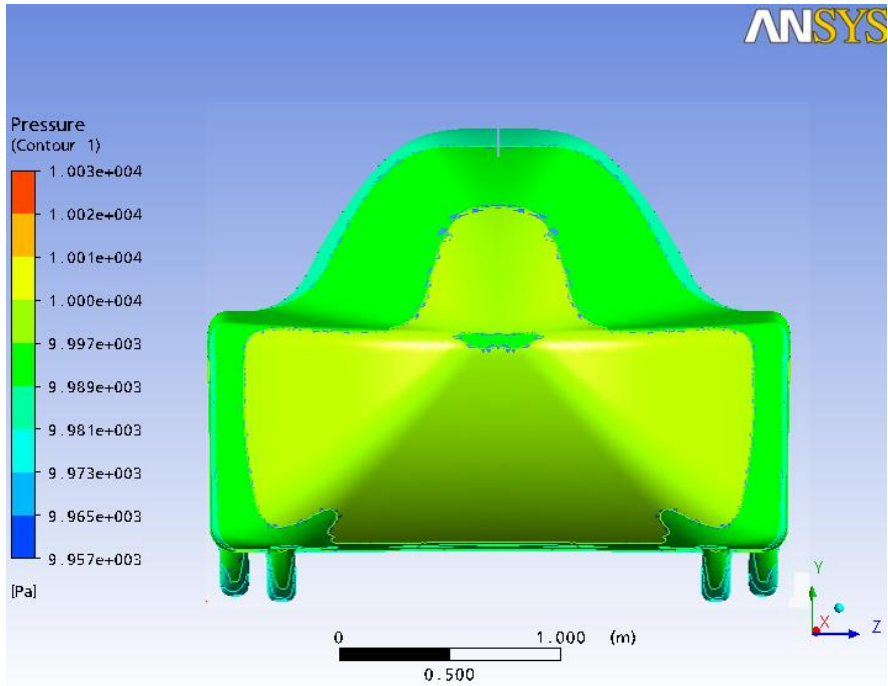


Figure 6.48: Surface pressure contours - Rear View - 4th model

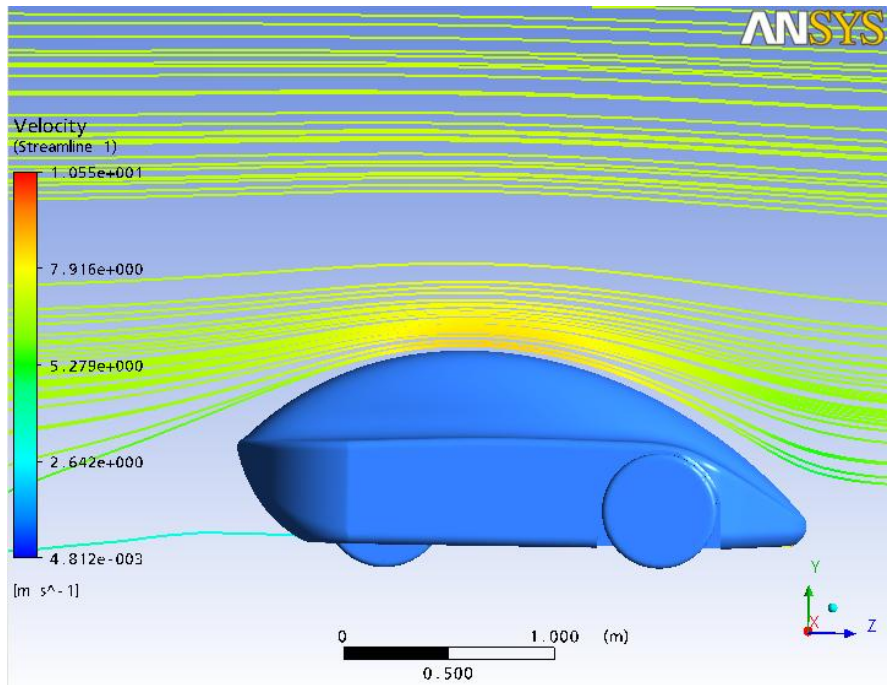


Figure 6.49: Streamlines at symmetry plane - 4th model

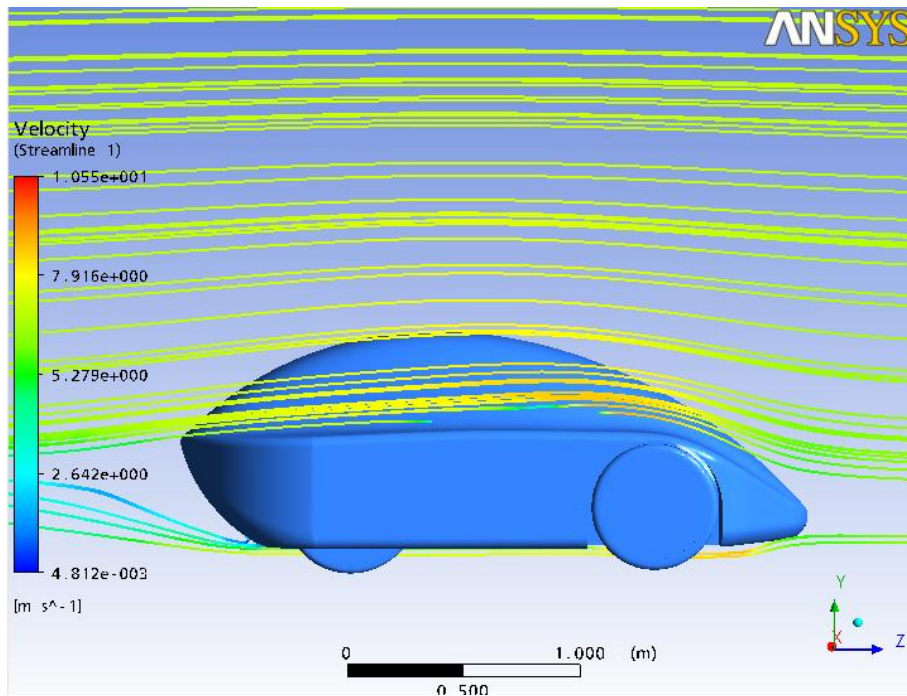


Figure 6.50: Streamlines at a plane 0.35m away from symmetry plane - 4th model

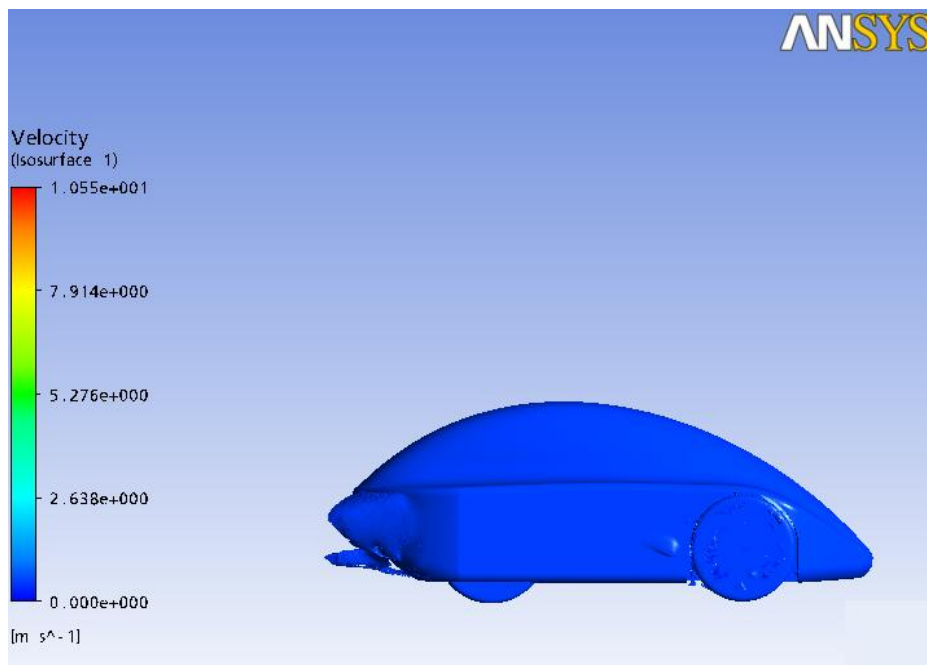


Figure 6.51: Equal-velocity surface for 0.5m/s - 4th model

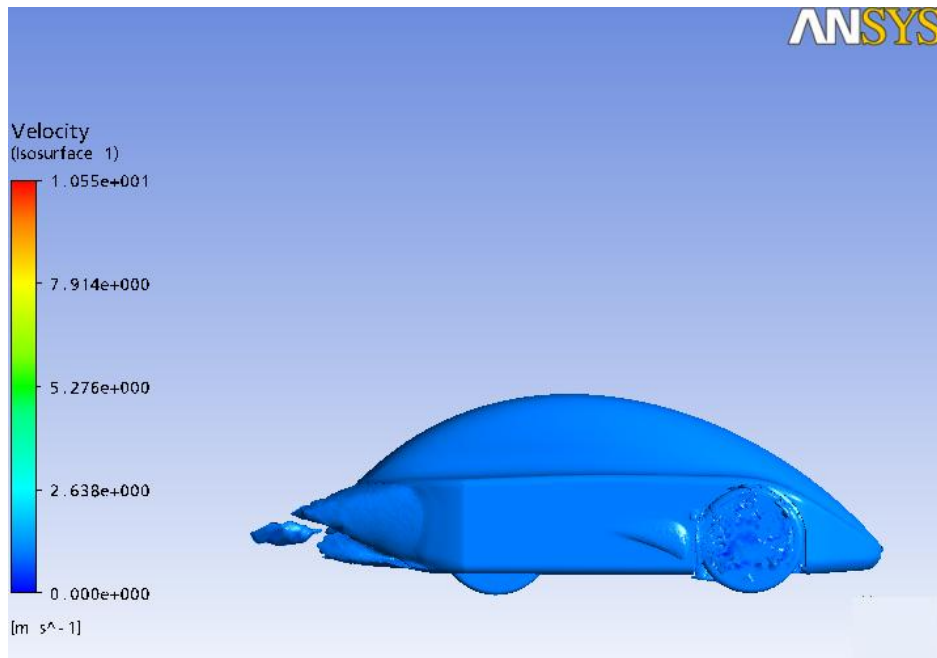


Figure 6.52: Equal-velocity surface for 1 m/s - 4th model

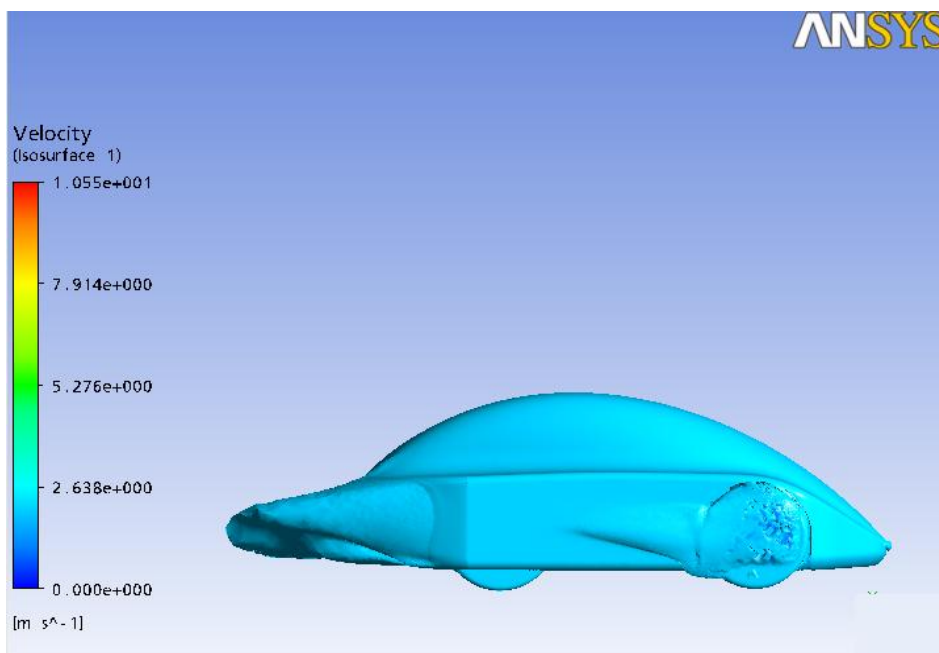


Figure 6.53: Equal-velocity surface for 2 m/s - 4th model

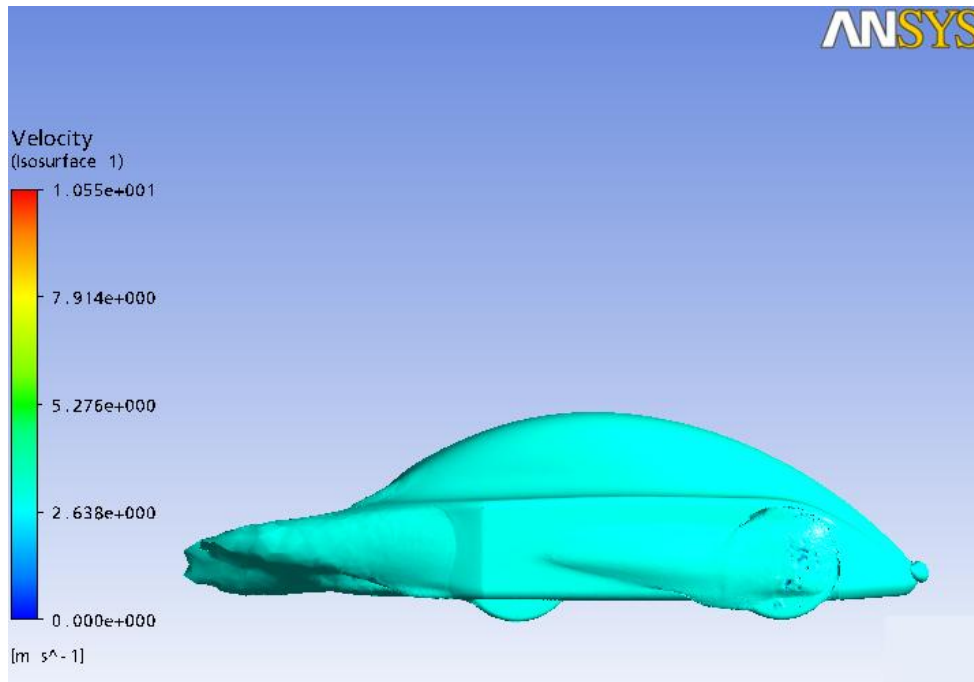


Figure 6.54: Equal-velocity surface for 3m/s - 4th model

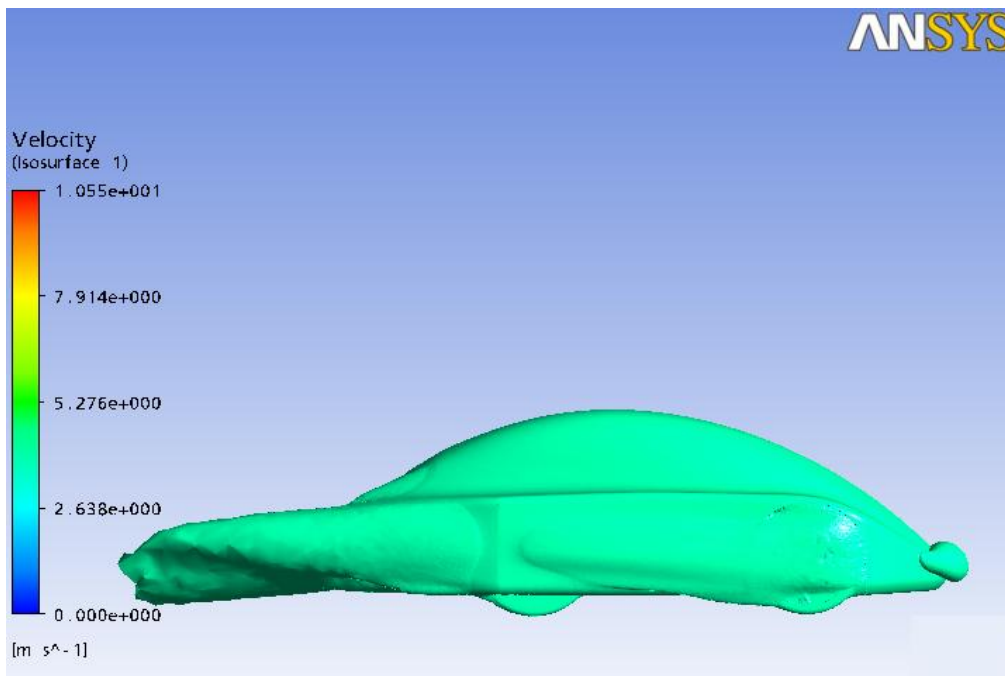


Figure 6.55: Equal-velocity surface for 4 m/s - 4th model

Figures 6.46 to 6.48 contain static pressure contours for the 4th model. Figures 6.49 and 6.50 contain the streamlines at two parallel plains, while Figures 6.51 to 6.55 contain iso-velocity surfaces for different velocity levels. Even though the rear side of the 4th model was very similar to the previous one (3rd model), by decreasing the frontal area of vehicle the drag force decreased to 5,407 Nt, approaching the number of the 1st model, but with a much lower area of its surface(6,5 m^2), which results in a lower weight of the vehicle. The required power is computed to be equal to 37.5 Watts.

7. Final Decision

Having designed already four different models and conducting aerodynamic analysis in three of them, the first phase of the work was completed. The criteria of selection of the best design are aerodynamic efficiency, the weight, the cost and the aesthetic acceptance of the vehicle. The new vehicle will be ultra light and made of carbon-fiber composites. However, the cost of that material is really high, so all the criteria should be analyzed carefully achieving a good combination of them.

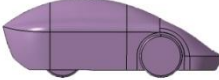
| |  |  |  |
|------------------------------------|--|---|--|
| Drag Coefficient(C_d) | 0.19 | 0.23 | 0.21 |
| Weight(kg) (4 Carbon fiber layers) | 10kg | 9kg | 8.2 |
| Cost (€)(of carbon fiber) | €984 | €852 | €780 |
| Aesthetic | ★ | ★★ | ★★★ |

Table 7.1: Comparison of the alternative designs

The 4th model was finally chosen as the best solution for the new vehicle ER12. The construction started according to the final detailed drawings with weekly supervision from the team; some stages of construction are illustrated in the pictures below (Figures 7.1 to 7.8). **A lighter, more aerodynamic, with a totally new appearance vehicle was presented in Rotterdam during the European Shell Eco Marathon 2012, taking part in the most**

competitive category of the completion, the Hydrogen Urban category, and achieving the 4th position.



Figure 7.1: Using the old vehicle to construct the initial mockup



Figure 7.2: The Final male-mold



Figure 7.3: The constructed female-mold



Figure 7.4: The rear side of the female-mold



Figure 7.5: The rear carbon-fiber surface



Figure 7.6: The final carbon-fiber surface of ER12 (4th model)



Figure 7.7: ER12 at European Shell Eco Marathon 2012



Figure 7.8: Technical University of Crete Eco Racing Team in front of ER12

References

[1]European Commision. *A sustainable future for transport*. Luxembourg: Puplications office of the European Union.

[2]Giuliano, S. H. (2004). *The Geography of Urban Transportation*.

[3]U.S. Department of Transportation, Federal Highway Administration, 1990 Nationwide Personal Transportation Survey: Summary of Travel Trends, FHWA-PL-92027, Washington, DC, March 1992, Figure 6. Data from 2009 NHTS were generated from the Internet site nhts.ornl.gov, March 2011. (Additional resources: www.fhwa.dot.gov, nhts.ornl.gov)

[4] Yizhou Wu, College of Logistics and Transport Guangdong Communication Polytechnic Guangzhou, P.R.China, Analysis of Present Status and Prediction of Future Demand on Parking in the Central Area of Medium and Small City

[5] Christian Thiel, Adolfo Perujo, Arnaud Mercier, Cost and CO2 aspects of future vehicle options in Europe under new energy policy scenarios

[6] Report of the European Union expert group on future transport fuels, January 2011

[7] Feng An, Amanda Sauer, COMPARISON OF PASSENGER VEHICLE FUEL ECONOMY AND GREENHOUSE GAS EMISSIONSTANDARDS AROUND THE WORLD, December 2004

[8] SILENCE ,An Integrated Project co-funded by the European Commission under the Sixth Framework Programme for R&D, Priority 6 Sustainable Development, Global Change and Ecosystems

[9][*Well-to-Wheels Analysis of Advanced Fuel/Vehicle Systems— A North American Study of Energy Use, Greenhouse Gas Emissions, and Criteria Pollutant Emissions* Norman Brinkman, General Motors Corporation Michael Wang, Argonne National Laboratory Trudy Weber, General Motors Corporation Thomas Darlington, Air Improvement Resource, Inc.,2005]

[10] Antoine Delorme, Sylvain Pagerit, Phil Sharer, Aymeric Rousseau, Cost Benefit Analysis of Advanced Powertrains from 2010 to 2045, *Stavanger, Norway, May 13-16, 2009*

[11] [REPORT FROM THE COMMISSION TO THE EUROPEAN PARLIAMENT, THE COUNCIL, AND THE EUROPEAN ECONOMIC AND SOCIAL COMMITTEE. Progress report on implementation of the Community's integrated approach to reduce CO2 emissions from light-duty vehicles, 2010.

[12] On the road in 2020, Energy Laboratory, Massachusetts Institute of Technology Cambridge, Massachusetts, 2000.

[13] Modern Electric, Hybrid Electric and Fuel Cell Vehicles, Mehrdad Ehsani, Yimin Gao, Sebastien E. Gay, Ali Emadi, Muhammad H. Rashid, Series Editor *University of West Florida*

[14] Electric Vehicle Technology Explained, James Larminie, John Lowry

British Library Cataloguing in Publication Data

[15] Development of an In-Wheel Motor Axle Unit, NTN TECHNICAL REVIEW No.75②2007②

[16] Polaris generator (http://www.dtic.mil/ndia/2011power/Session23_12836Stewart.pdf)

[17] Automotive Handbook, Bosch, 4th edition, 1996.

[18] (Batchelor, G. (2000). *Introduction to Fluid Mechanics*).

[19] The estimates for the overall alternative powertrain market use estimates from the McKinsey (2009) industry report. Estimates for hybrid sales are based on industry reports by McKinsey (2009), Deutsche Bank (2008), Credit Suisse (2008), and J.D. Power (2008).

[20] Senator für Bau, Umwelt und Verkehr, 2007.

[21] Future of transport, Conducted by The Gallup Organisation, Hungary upon the request of Directorate General Mobility and Transport

[22] Stavanger, Norway, May 13-16, 2009

[23] "[Rechargeable Li-Ion OEM Battery Products](#)". Panasonic.com. Retrieved 23 April 2010.

[24] <http://delphi.com/shared/pdf/ppd/pwrelec/universal-battery-charger.pdf>

Delphi Universal On-board Battery Charger.

[25] ANSYS CFX- Solver Modeling Guide

[26] Berglund et al 1999, p. iii

[27] <http://www.mitsubishi-cars.co.uk/imiev/>

[28] http://ecomarathon.shell.com/registration/documents/2012_SEM_Rules.pdf